Title
Coactivator regulation of active site chemistry in the mRNA decapping enzyme Dcp2

Author
Aglietti, Robin

Publication Date
2014

Peer reviewed|Thesis/dissertation

Coactivator regulation of active site chemistry in the mRNA decapping enzyme Dcp2

By

Robin A. Aglietti

DISSERTATION

Submitted in partial satisfaction of the requirements for the degree of

DOCTOR OF PHILOSOPHY

in

Chemistry and Chemical Biology

in the

GRADUATE DIVISION

of the

UNIVERSITY OF CALIFORNIA, SAN FRANCISCO

[redacted]

ACKNOWLEDGEMENTS

You can't do science in a box. This simple statement was my guiding principle in choosing my graduate institution - I was looking for an environment where people recognized the potential of different scientific disciplines to enhance each other. While I most certainly did find that at UCSF (right down to the physical design of the buildings), through my time here I have come to appreciate the broader implications of this statement: the course of my graduate studies has been shaped by individuals too numerous to count.

My advisor, Dr. John Gross, has been a limitless source of scientific ideas, enthusiasm, and knowledge, and I consider myself very fortunate to have worked for someone who was always available to answer my questions or discuss my ideas. In addition, my thesis committee members Dr. Geeta Narlikar and Dr. Nevan Krogan have been extremely helpful and I thank them for their keen insights and feedback, as well as their unwavering support as my project focus evolved and changed.

Our lab has expanded and contracted many times throughout my graduate studies, but it has consistently been home to exceptional colleagues, all of whom have contributed to this work. I would like to especially thank Linda Yen, whose support, levity, and caffeine helped me find my way through the late-night trenches of Upf1. David Stanley has been my constant lab-mate for the entirety of my time in the Gross lab, and I am extremely grateful for his scientific support

and many thought-provoking discussions about the world at large. Nathalie Caretta Cartozo has not only kept the lab running smoothly, but has been an invaluable source of encouragement and perspective. I thank Stephen Floor for his guidance during my rotation and early Gross lab career, as well as a fruitful collaboration. Brittnee Jones and Mark Borja introduced me to the world of enzyme kinetics and decapping, skills that have served me well and certainly will continue to do so. More recently, Jeff Mugridge and David Paquette have given very useful feedback and suggestions as I completed my graduate work.

It has also been my privilege to be an honorary member of the Craik lab and the Andino lab, and I thank the members of both labs for their generosity in expertise and reagents alike. I am especially indebted to Greg Lee, who has helped me troubleshoot NMR issues and the FPLC machine countless times, and Arabinda Nayak, who has been an invaluable resource for my RNA work. I would also like to especially thank Cheryl Tajon, who has been a tireless source of reassurance, encouragement, and understanding during my graduate work.

This thesis would not be what it is without Chris Bohlen, and I am deeply grateful for his companionship, encouragement, counsel and humor. It is a rare person with whom you can have rewarding intellectual conversations regardless of topic; even rarer still is the person with whom you can just as easily pretend to be robots. He keeps me grounded while continually encouraging me to explore my

passions, and I could not ask for a more perfect companion of mutual weirdness as I navigate through life.

Finally, my family has always been a constant source of strength and support, and my journey through graduate school has been no exception. They've had many roles as I've grown as a person and scientist: cheerleaders, sounding boards, fellow adventurers, guidance counselors, playmates, navigators, chefs, and teachers - but always a light in dim times and the punctuation as I write my story. They have fully embraced both my "engineer brain" and my artistic pursuits with equal enthusiasm, and have always honored my belief that science and creative endeavors enhance and complement each other. It is from this foundation that I continue to explore the beauty in the world around us.

ABSTRACT:

Regulation of mRNA half-life is a crucial control point of gene expression. Removal of the protective 5' methylguanosine cap is a committed step in the 5'-3' decay pathway, which is carried out by the decapping enzyme Dpc2. Although Dcp2 is sufficient for decapping *in vitro*, its activity is greatly increased by coactivators; here the activation of Dcp2 is explored through several means. A thorough study of the chemistry of decapping is presented: multiple crystal structures implicate specific active site residues of Dcp2 in catalysis metal binding and enzyme kinetics identify key residues involved in the acid/base chemistry of decapping. Further, a metal binding loop is implicated in conformational changes coupled to Dcp2's catalytic cycle using pH-dependent NMR spectroscopy and molecular dynamics simulations. In addition we hypothesized and tested direct effects of other potential regulators of decapping by *in vitro* assay and binding studies.

In addition, two potential decapping activation pathways are explored. First, a hypothesized interaction between the decapping complex and nonsense-mediated mRNA decay factor Upf1 is explored through GST pull-downs, and enzyme kinetics. Additionally, some evidence suggests the possibility that an extended ribonucleoprotein complex containing mRNA decay factors Pat1/Lsm1-7 and Xrn1 may directly affect the activity of Dcp2; this hypothesis is tested using an *in vitro* decapping assay. However, future experiments are needed to

fully characterize coactivator regulation of Dcp2 within the context of the cell.

TABLE OF CONTENTS

LIST OF FIGURES

LIST OF TABLES

CHAPTER 1

Introduction

Robin Aglietti, John Gross

INTRODUCTION

Central to the life of all organisms, from the simple single-celled yeast to complex organisms such as humans or the giant sequoia, is the ability to control gene expression. This ability allows organisms to account for changing environmental conditions, respond to stimuli, and even differentiate cells with the same genetic makeup into various tissues and organs. The DNA sequence of a gene is transcribed into a molecule of messenger RNA (mRNA), and this mRNA is translated into protein, the machinery that runs a cell. Because a single molecule of mRNA can be translated repeatedly, the regulation of an mRNA's lifespan and stability is a crucial control point for cellular gene expression.

Eukaryotic mRNA molecules are equipped with two protective elements that guard against degradation: the 5' 7-methylguanosine cap, and the 3' poly-A tail. The 5' cap is bound by the eukaryotic translation initiation factor eIF4E within the cap-binding complex to promote translation (Gross et al., 2003; Hodel et al., 1997; Lykke-Andersen, 2002), while the poly(A) binding protein (PABP) binds to the poly(A) tail. Deadenylation of this poly(A) tail is the first step in the majority of mRNA decay pathways, which marks an mRNA for destruction (Chen and Shyu, 2011). In 3'-5' mRNA decay, deadenylation causes loss of PABP followed by degradation of the mRNA via the exosome (Anderson and Parker, 1998; Houseley et al., 2006; Mitchell et al., 1997). In other cases, deadenylation of the mRNA

promotes removal of the 5' cap through a process known as decapping, the committed step in 5'-3' mRNA decay. Cleavage of the cap yields m7GDP and a 5' monophosphate RNA body, which is further degraded by the conserved exonuclease Xrn1 (Stevens and Maupin, 1987).

Decapping was originally thought to be carried out by Dcp1, but it is now well established that Dcp2 is the catalytic subunit of the decapping holoenzyme Dcp1/Dcp2 (Beelman et al., 1996; Dunckley and Parker, 1999). This decapping complex is at the center of a dense network of protein-protein interactions that tune decapping activity in both general and specific manners (Krogan et al., 2006; Li and Kiledjian, 2010). In fact, Dcp2 has been implicated in multiple cellular processes, including transcript quality control (Lykke-Andersen, 2002), immune response (Li et al., 2012), differentiation (Sweet et al., 2012), stress response (Hilgers et al., 2006), development (Schier, 2007), transcription (Brannan et al., 2012), and translation (Hu et al., 2009).

The core of Dcp2 is comprised of two domains that are conserved from yeast to humans, and in yeast has an additional C-terminal extension (Piccirillo et al., 2003; She et al., 2006; She et al., 2008). This extension is disordered and not required for general decapping, although the first section is involved in binding to decapping coactivator Edc3 (Fromm et al., 2012; Gaudon et al., 1999; Harigaya et al., 2010). In addition, it has been observed that Dcp2 can shuttle into the nucleus and this C-terminal extension can affect

transcription (Gaudon et al., 1999; Grousl et al., 2009; Haimovich et al., 2013).

The conserved N-terminal domain of Dcp2 is regulatory in function and binds to the decapping activator Dcp1 to stimulate catalysis 1,000 fold (Deshmukh et al., 2008; She et al., 2008). Dcp1 contains an EVH1 fold, a known protein-protein interaction platform, and can serve as a scaffold for further coactivators of decapping to modulate the catalytic activity of Dcp2 (Ball et al., 2002; Borja et al., 2011; Braun et al., 2012; Lai et al., 2012a). Additionally, deletion of the regulatory domain of Dcp2 gives rise to aberrant decapping products, suggesting this domain is also involved in proper substrate positioning (Piccirillo et al., 2003).

The conserved C-terminal domain of Dcp2 is the catalytic subunit of the decapping holoenzyme. It is sufficient for minimal decapping activity *in vitro*, and is a member of the Nudix hydrolase family of enzymes, which catalyze hydrolysis of a nucleoside diphosphate from another chemical group (Deshmukh et al., 2008; Mildvan et al., 2005; She et al., 2006; She et al., 2008). This family of enzymes contains the catalytic Nudix motif $GX_5EX_7REUXEEXGU$ (where X is any residue and U is a bulky hydrophobic residue) and this motif folds into a characteristic loop-helix-loop structure that forms the active site (Mildvan et al., 2005). Not surprisingly, mutations in this region of Dcp2 have disastrous effects on decapping activity both *in vitro* and *in vivo* (Deshmukh et al., 2008; Dunckley and Parker, 1999; She et al., 2006).

Structural and biophysical studies of Dcp2 have shown that the two conserved domains of Dcp2 exist as a bilobed structure that is highly dynamic in solution and forms a composite active site (Floor et al., 2012; Floor et al., 2010; She et al., 2006; She et al., 2008). Indeed, the co-crystal structure of Dcp1/Dcp2 has two different conformations of the decapping holoenzyme in the asymmetric unit: an open conformation where the two Dcp2 domains are far apart, and a compacted, closed structure containing an ATP crystallization additive (She et al., 2006). Given the observations that Dcp2 forms a composite active site (Floor et al., 2010), that proline mutations in the linker between the N- and C- terminal domains of Dcp2 inhibit decapping activity (She et al., 2008), and the characterization of a gatekeeper tryptophan that affects the coupling of the 2 domains of Dcp2 as well as activity (Floor et al., 2012), it is clear that conformational changes and closure of Dcp2 are crucial to its enzymatic activity.

The mechanism by which such conformational changes are coupled to chemistry in the active site of Dcp2 are not immediately obvious, however, and we therefore set out to understand the chemistry of decapping. Using x-ray crystallography, we solved the structure of wild-type and two mutant variants of the *S. cerevisiae* Nudix domain of Dcp2, which we used to pinpoint key active site glutamates involved in both general base activity of the enzyme, and binding of a catalytically essential metal ion. In addition, we used pH-dependent enzyme kinetics in an *in vitro* decapping assay to identify active site residues involved in substrate positioning and the acid/base

chemistry of decapping. A series of methyl NMR spectroscopy pH titrations further confirmed these observations, and identified dynamics of an active site loop containing a catalytically essential glutamate residue. Finally, molecular dynamics simulations suggest this active site loop is coupled to the chemical cycle of Dcp2. These studies provide a framework to explain stimulation of decapping by the regulatory domain of Dcp2 and associated coactivators, and are discussed in Chapter 2.

In addition to understanding how Dcp2 is regulated by intramolecular conformational changes in a general way, we were also interested in how Dcp2 activity could be modulated in a more specific manner by potential binding partners that associate with the decapping machinery. In particular, the nonsense-mediated mRNA decay (NMD) pathway targets mRNAs with premature termination codons (PTC's) for degradation. Substrates for this pathway often arise from errors in transcription or processing (He et al., 1993), but more recent evidence suggests a possible regulatory role for NMD as well (Rehwinkel et al., 2006). Once an mRNA has been identified through this pathway, it is degraded by multiple pathways, including 5'-3' exonucleolytic decay (Hagan et al., 1995; Muhlrad and Parker, 1994, 1999) and exosome-mediated 3'-5' decay (Cao and Parker, 2003; Mitchell and Tollervey, 2003). Several key NMD factors, Upf1, Upf2, and Upf3 have been shown to interact with the decapping machinery (Lejeune et al., 2003; Lykke-Andersen, 2002) at least indirectly, and in humans Upf1 forms a complex with Dcp1 and proline-rich nuclear

receptor co-regulatory protein 2 (PNRC2) (Cho et al., 2009; Lai et al., 2012b). We therefore sought to investigate any direct interaction between the yeast decapping machinery and Upf1. However, Upf1 proved to be a challenging protein for biochemical studies. Some initial experiments showed an interaction between one domain of Upf1 and Dcp2 in pulldown assays, but no appreciable effect was observed in a Dcp2 functional assay and further characterization was inhibited by low expression yields and instability of Upf1. These experiments are presented in Chapter 3.

Because NMD proved to be a limited avenue to explore coactivator regulation of Dcp2, we turned to another system: the Pat1/Lsm1-7 complex, which is required for normal mRNA decapping rates *in vivo* (Bouveret et al., 2000; Tharun et al., 2000). Because Pat1 interacts with the decapping complex (Braun et al., 2010; Nissan et al., 2010; Ozgur et al., 2010; Pilkington and Parker, 2008) as well as the 5'-3' exonuclease Xrn1 that degrades mRNAs after the decapping step (Bouveret et al., 2000; Nissan et al., 2010), and Xrn1 can bind to Dcp1 (Braun et al., 2012), it is very possible that the Pat1/Lsm1-7 complex and/or Xrn1 can modulate the decapping complex's activity. Our preliminary studies of this complex presented in Chapter 4 demonstrated successful annealing of Xrn1 and Pat1/Lsm1-7 to RNA using a gel shift assay. However, we failed to observe any increase of Dcp2 activity using an *in vitro* decapping assay. Reconstitution of any large protein complex is an arduous task, however, and it is entirely

possible that further work in this area could yield further insight into the regulation of Dcp2 by coactivators.

REFERENCES

Anderson, J.S.J., and Parker, R. (1998). The 3 ' to 5 ' degradation of yeast mRNAs is a general mechanism for mRNA turnover that requires the SKI2 DEVH box protein and 3 ' to 5 ' exonucleases of the exosome complex. Embo Journal *17*, 1497-1506.

Ball, L.J., Jarchau, T., Oschkinat, H., and Walter, U. (2002). EVH 1 domains: structure, function and interactions. Febs Letters *513*, 45-52.

Beelman, C.A., Stevens, A., Caponigro, G., LaGrandeur, T.E., Hatfield, L., Fortner, D.M., and Parker, R. (1996). An essential component of the decapping enzyme required for normal rates of mRNA turnover. Nature *382*, 642-646.

Borja, M.S., Piotukh, K., Freund, C., and Gross, J.D. (2011). Dcp1 links coactivators of mRNA decapping to Dcp2 by proline recognition. RNA *17*, 278-290.

Bouveret, E., Rigaut, G., Shevchenko, A., Wilm, M., and Seraphin, B. (2000). A Sm-like protein complex that participates in mRNA degradation. Embo Journal *19*, 1661-1671.

Brannan, K., Kim, H., Erickson, B., Glover-Cutter, K., Kim, S., Fong, N., Kiemele, L., Hansen, K., Davis, R., Lykke-Andersen, J., *et al.* (2012). mRNA decapping factors and the exonuclease Xrn2 function in widespread premature termination of RNA polymerase II transcription. Mol Cell *46*, 311-324.

Braun, J.E., Tritschler, F., Haas, G., Igreja, C., Truffault, V., Weichenrieder, O., and Izaurralde, E. (2010). The C-terminal alpha-alpha superhelix of Pat is required for mRNA decapping in metazoa. Embo Journal *29*, 2368-2380.

Braun, J.E., Truffault, V., Boland, A., Huntzinger, E., Chang, C.T., Haas, G., Weichenrieder, O., Coles, M., and Izaurralde, E. (2012). A direct interaction between DCP1 and XRN1 couples mRNA decapping to 5' exonucleolytic degradation. Nat Struct Mol Biol *19*, 1324-1331.

Cao, D., and Parker, R. (2003). Computational modeling and experimental analysis of nonsense-mediated decay in yeast. Cell *113*, 533-545.

Chen, C.Y.A., and Shyu, A.B. (2011). Mechanisms of deadenylation-dependent decay. Wiley Interdisciplinary Reviews-Rna *2*, 167-183.

Cho, H., Kim, K.M., and Kim, Y.K. (2009). Human Proline-Rich Nuclear Receptor Coregulatory Protein 2 Mediates an Interaction between mRNA Surveillance Machinery and Decapping Complex. Molecular Cell *33*, 75-86.

Deshmukh, M.V., Jones, B.N., Quang-Dang, D.U., Flinders, J., Floor, S.N., Kim, C., Jemielity, J., Kalek, M., Darzynkiewicz, E., and Gross, J.D. (2008). mRNA decapping is promoted by an RNA-binding channel in Dcp2. Mol Cell *29*, 324-336.

Dunckley, T., and Parker, R. (1999). The DCP2 protein is required for mRNA decapping in Saccharomyces cerevisiae and contains a functional MutT motif. EMBO J *18*, 5411-5422.

Floor, S.N., Borja, M.S., and Gross, J.D. (2012). Interdomain dynamics and coactivation of the mRNA decapping enzyme Dcp2 are mediated by a gatekeeper tryptophan. Proc Natl Acad Sci U S A *109*, 2872-2877.

Floor, S.N., Jones, B.N., Hernandez, G.A., and Gross, J.D. (2010). A split active site couples cap recognition by Dcp2 to activation. Nat Struct Mol Biol *17*, 1096-1101.

Fromm, S.A., Truffault, V., Kamenz, J., Braun, J.E., Hoffmann, N.A., Izaurralde, E., and Sprangers, R. (2012). The structural basis of Edc3- and Scd6-mediated activation of the Dcp1:Dcp2 mRNA decapping complex. EMBO J *31*, 279-290.

Gaudon, C., Chambon, P., and Losson, R. (1999). Role of the essential yeast protein PSU1 in transcriptional enhancement by the ligand-dependent activation function AF-2 of nuclear receptors. Embo Journal *18*, 2229-2240.

Gross, J.D., Moerke, N.J., von der Haar, T., Lugovskoy, A.A., Sachs, A.B., McCarthy, J.E.G., and Wagner, G. (2003). Ribosome loading onto the mRNA cap is driven by conformational coupling between eIF4G and eIF4E. Cell *115*, 739-750.

Grousl, T., Ivanov, P., Frydlova, I., Vasicova, P., Janda, F., Vojtova, J., Malinska, K., Malcova, I., Novakova, L., Janoskova, D., *et al.* (2009). Robust heat shock induces eIF2 alpha-phosphorylation-independent assembly of stress granules containing eIF3 and 40S ribosomal

subunits in budding yeast, Saccharomyces cerevisiae. Journal of Cell Science *122*, 2078-2088.

Hagan, K.W., Ruizechevarria, M.J., Quan, Y., and Peltz, S.W. (1995). Characterization of Cis-Acting Sequences and Decay Intermediates Involved in Nonsense-Mediated Messenger-Rna Turnover. Molecular and Cellular Biology *15*, 809-823.

Haimovich, G., Medina, D.A., Causse, S.Z., Garber, M., Millan-Zambrano, G., Barkai, O., Chavez, S., Perez-Ortin, J.E., Darzacq, X., and Choder, M. (2013). Gene Expression Is Circular: Factors for mRNA Degradation Also Foster mRNA Synthesis. Cell *153*, 1000-1011.

Harigaya, Y., Jones, B.N., Muhlrad, D., Gross, J.D., and Parker, R. (2010). Identification and analysis of the interaction between Edc3 and Dcp2 in Saccharomyces cerevisiae. Mol Cell Biol *30*, 1446-1456.

He, F., Peltz, S.W., Donahue, J.L., Rosbash, M., and Jacobson, A. (1993). Stabilization and Ribosome Association of Unspliced Premessenger Rnas in a Yeast Upfl- Mutant. Proceedings of the National Academy of Sciences of the United States of America *90*, 7034-7038.

Hilgers, V., Teixeira, D., and Parker, R. (2006). Translation-independent inhibition of mRNA deadenylation during stress in Saccharomyces cerevisiae. RNA *12*, 1835-1845.

Hodel, A.E., Gershon, P.D., Shi, X.N., Wang, S.M., and Quiocho, F.A. (1997). Specific protein recognition of an mRNA cap through its alkylated base. Nature Structural Biology *4*, 350-354.

Houseley, J., LaCava, J., and Tollervey, D. (2006). RNA-quality control by the exosome. Nature Reviews Molecular Cell Biology *7*, 529-539.

Hu, W., Sweet, T.J., Chamnongpol, S., Baker, K.E., and Coller, J. (2009). Co-translational mRNA decay in Saccharomyces cerevisiae. Nature *461*, 225-229.

Krogan, N.J., Cagney, G., Yu, H.Y., Zhong, G.Q., Guo, X.H., Ignatchenko, A., Li, J., Pu, S.Y., Datta, N., Tikuisis, A.P*., et al.* (2006). Global landscape of protein complexes in the yeast Saccharomyces cerevisiae. Nature *440*, 637-643.

Lai, T., Cho, H., Liu, Z., Bowler, M.W., Piao, S., Parker, R., Kim, Y.K., and Song, H. (2012a). Structural basis of the PNRC2-mediated link between mrna surveillance and decapping. Structure *20*, 2025-2037.

Lai, T.F., Cho, H., Liu, Z., Bowler, M.W., Piao, S.F., Parker, R., Kim, Y.K., and Song, H.W. (2012b). Structural Basis of the PNRC2-Mediated Link between mRNA Surveillance and Decapping. Structure *20*, 2025-2037.

Lejeune, F., Li, X.J., and Maquat, L.E. (2003). Nonsense-mediated mRNA decay in mammalian cells involves decapping, deadenylating, and exonucleolytic activities. Molecular Cell *12*, 675-687.

Li, Y., Dai, J., Song, M., Fitzgerald-Bocarsly, P., and Kiledjian, M. (2012). Dcp2 decapping protein modulates mRNA stability of the critical interferon regulatory factor (IRF) IRF-7. Mol Cell Biol *32*, 1164-1172.

Li, Y., and Kiledjian, M. (2010). Regulation of mRNA decapping. Wiley Interdisciplinary Reviews-Rna *1*, 253-265.

Lykke-Andersen, J. (2002). Identification of a human decapping complex associated with hUpf proteins in nonsense-mediated decay. Mol Cell Biol *22*, 8114-8121.

Mildvan, A.S., Xia, Z., Azurmendi, H.F., Saraswat, V., Legler, P.M., Massiah, M.A., Gabelli, S.B., Bianchet, M.A., Kang, L.W., and Amzel, L.M. (2005). Structures and mechanisms of Nudix hydrolases. Arch Biochem Biophys *433*, 129-143.

Mitchell, P., Petfalski, E., Shevchenko, A., Mann, M., and Tollervey, D. (1997). The exosome: A conserved eukaryotic RNA processing complex containing multiple 3'->5' exoribonucleases. Cell *91*, 457-466.

Mitchell, P., and Tollervey, D. (2003). An NMD pathway in yeast involving accelerated deadenylation and exosome-mediated 3 '-> 5 ' degradation. Molecular Cell *11*, 1405-1413.

Muhlrad, D., and Parker, R. (1994). Premature Translational Termination Triggers Messenger-Rna Decapping. Nature *370*, 578-581.

Muhlrad, D., and Parker, R. (1999). Aberrant mRNAs with extended 3 ' UTRs are substrates for rapid degradation by mRNA surveillance. Rna-a Publication of the Rna Society *5*, 1299-1307.

Nissan, T., Rajyaguru, P., She, M.P., Song, H.W., and Parker, R. (2010). Decapping Activators in Saccharomyces cerevisiae Act by Multiple Mechanisms. Molecular Cell *39*, 773-783.

Ozgur, S., Chekulaeva, M., and Stoecklin, G. (2010). Human Pat1b Connects Deadenylation with mRNA Decapping and Controls the Assembly of Processing Bodies. Molecular and Cellular Biology *30*, 4308-4323.

Piccirillo, C., Khanna, R., and Kiledjian, M. (2003). Functional characterization of the mammalian mRNA decapping enzyme hDcp2. RNA *9*, 1138-1147.

Pilkington, G.R., and Parker, R. (2008). Pat1 contains distinct functional domains that promote P-body assembly and activation of decapping. Molecular and Cellular Biology *28*, 1298-1312.

Rehwinkel, J., Raes, J., and Izaurralde, E. (2006). Nonsense-mediated mRNA decay: target genes and functional diversification of effectors. Trends in Biochemical Sciences *31*, 639-646.

Schier, A.F. (2007). The maternal-zygotic transition: death and birth of RNAs. Science *316*, 406-407.

She, M., Decker, C.J., Chen, N., Tumati, S., Parker, R., and Song, H. (2006). Crystal structure and functional analysis of Dcp2p from Schizosaccharomyces pombe. Nat Struct Mol Biol *13*, 63-70.

She, M., Decker, C.J., Svergun, D.I., Round, A., Chen, N., Muhlrad, D., Parker, R., and Song, H. (2008). Structural basis of dcp2 recognition and activation by dcp1. Mol Cell *29*, 337-349.

Stevens, A., and Maupin, M.K. (1987). A 5'----3' exoribonuclease of Saccharomyces cerevisiae: size and novel substrate specificity. Arch Biochem Biophys *252*, 339-347.

Sweet, T., Kovalak, C., and Coller, J. (2012). The DEAD-box protein Dhh1 promotes decapping by slowing ribosome movement. PLoS Biol *10*, e1001342.

Tharun, S., He, W.H., Mayes, A.E., Lennertz, P., Beggs, J.D., and Parker, R. (2000). Yeast Sm-like proteins function in mRNA decapping and decay. Nature *404*, 515-518.

CHAPTER 2

Active site conformational dynamics are coupled to catalysis in the mRNA decapping enzyme Dcp2

Robin Aglietti, Stephen Floor, Chris McClendon, Matthew Jacobson and John Gross

*This work was previously published in *Structure*, 21 (9), 1571-80, 2013, and is reprinted here with permission.

ABSTRACT

Removal of the 5’ cap structure by Dcp2 is a major step in several 5’-3’ mRNA decay pathways. The activity of Dcp2 is enhanced by Dcp1 and bound coactivators, yet the details of how these interactions are linked to chemistry are poorly understood. Here we report three crystal structures of the catalytic Nudix hydrolase domain of Dcp2 that demonstrate binding of a catalytically essential metal ion, and enzyme kinetics are used to identify several key active site residues involved in acid/base chemistry of decapping. Using NMR and molecular dynamics, we find that a conserved metal binding loop on the catalytic domain undergoes conformational changes during the catalytic cycle. These findings describe key events during the chemical step of decapping, suggest local active site conformational changes are important for activity, and provide a framework to explain stimulation of catalysis by the regulatory domain of Dcp2 and associated coactivators.

INTRODUCTION

Eukaryotic mRNAs contain a 7-methylguanosine cap at the 5' end that promotes different steps in the mRNA lifecycle, including splicing, export, translation and decay (Moore, 2005). Removal of this 5'-cap is the committed step in 5'-to-3' mRNA decay, resulting in exposure of the 5' terminal phosphate on an RNA that is recognized and degraded by a conserved 5'-3' exonuclease (Stevens and Maupin, 1987). Decapping is carried out by several enzymes (Chang et al., 2012; Ghosh et al., 2004; Jiao et al., 2010; Liu et al., 2002; Song et al., 2010; Wang and Kiledjian, 2001), including the Nudix hydrolase Dcp2 and its obligate *in vivo* activator Dcp1. Dcp2 activity is involved in bulk mRNA decay (Beelman et al., 1996; Dunckley and Parker, 1999; Wang et al., 2002) as well as multiple specific pathways including nonsense mediated decay (Amrani et al., 2004; Isken and Maquat, 2007), miRNA-induced decay (Behm-Ansmant et al., 2006; Chen et al., 2009; Eulalio et al., 2007), AU-rich element-mediated decay (Chen et al., 1995; Fenger-Gron et al., 2005), and 3'-uridylation (Heo et al., 2009; Rissland and Norbury, 2009; Shen and Goodman, 2004; Song and Kiledjian, 2007). Dcp2 is at the core of a large network of protein-protein interactions involving multiple decapping factors that can act in either a generic or pathway specific manner (e.g. Edc 1-3, Upf1, Lsm 1-7, Pat1, Dhh1) (Arribas-Layton et al., 2012). These decapping complexes have been implicated in many cellular processes including stress response (Hilgers et al., 2006), development (Schier, 2007), transcription

(Brannan et al., 2012), translation (Hu et al., 2009), immune response (Li et al., 2012), differentiation (Sweet et al., 2012), and transcript quality control (Lykke-Andersen, 2002).

Dcp2 has two conserved domains that exist as a bilobed structure which is thought to undergo an open to closed transition to form a composite active site upon activation of the enzyme (Floor et al., 2012; Floor et al., 2010; She et al., 2006; She et al., 2008). The decapping activity of Dcp2 is located in its catalytic Nudix domain, which is functionally active *in vitro*, although addition of the N-terminal regulatory domain of Dcp2 enhances decapping activity dramatically, in part by binding the essential activator Dcp1 (Deshmukh et al., 2008; She et al., 2006; She et al., 2008). Coactivators of decapping Edc1 and Edc2 can enhance Dcp2 activity *in vitro* by binding to Dcp1, possibly promoting the closed active form of Dcp2 within the decapping holoenzyme (Borja et al., 2011; Floor et al., 2012). Other Dcp1 interaction partners such as Xrn1 (Braun et al., 2012) and PNRC2 (Lai et al., 2012) may activate decapping in a similar manner. In addition, Dcp2 binding partners can also enhance decapping (Fromm et al., 2012; Harigaya et al., 2010). However, the mechanistic details about how coactivators can accelerate decapping by coupling conformational changes to the chemical step remains unclear.

Some clues about the chemical mechanism of Dcp2 can be taken from studies of related Nudix enzymes (Mildvan et al., 2005). Nudix enzymes catalyze hydrolysis of a nucleoside diphosphate from another chemical group and contain the catalytic Nudix motif

$GX_5EX_7REUXEEXGU$, where X is any residue and U is a bulky hydrophobic residue (Mildvan et al., 2005). This motif folds into a characteristic loop-helix-loop structure that forms the active site. Hydrolysis typically occurs by nucleophilic substitution at the substrate phosphorus and requires a variable number of divalent cations. Several conserved glutamates within the Nudix motif coordinate metal, and one usually serves as a general base in the catalytic cycle, though the identity and location of the general base varies between family members. A general acid near the active site often enhances catalysis by stabilizing departure of the leaving group. Additional insertions or domains outside the canonical Nudix hydrolase fold can make specific contacts with the substrate and position it for catalysis (Gabelli et al., 2002). However, due to the large variation in substrates for this family of enzymes, these features are tailored to each family member to provide specificity in substrate recognition, and the potential for regulation by protein interactions in the case of Dcp2.

Cap hydrolysis by Dcp2 results in formation of an m7GDP product and 5' monophosphate RNA body. Four conserved glutamates are crucial for decapping activity both *in vivo* and *in vitro* (Deshmukh et al., 2008; Dunckley and Parker, 1999; She et al., 2006). Three of these glutamates are located on the Nudix helix (*S. cerevisiae* E149, E152, and E153*)*, while a fourth (E198) is located on a loop near the active site that changes conformation in the open, unliganded and closed, liganded Dcp1/Dcp2 co-crystal structure containing an ATP

crystallization additive (She et al., 2006). The latter finding echoes observations made for other Nudix enzymes that conformational rearrangements of metal binding loops or the general base can be coupled to substrate binding (Gabelli et al., 2002). However, it is unknown how these residues contribute to cap hydrolysis by Dcp2.

Here, we provide insight into the catalytic cycle of Dcp2 by integrating data from X-ray crystallography, pH-dependent enzyme kinetics, nuclear magnetic resonance (NMR) spectroscopy, and molecular dynamics simulations. The crystal structure of the catalytic domain of *S. cerevisiae* Dcp2 with bound Mg^{2+}, along with structures of two mutants, implicate distinct glutamate residues in metal binding and general base activity, including a glutamate located on a loop near the active site. Kinetic studies are employed to determine which glutamate is the general base and further identify a cationic general acid important for substrate positioning and leaving-group stabilization. Methyl-NMR spectroscopy and molecular dynamics simulations suggest that a loop containing the fourth essential glutamate changes conformation depending on protonation of the general base. These findings provide roles for conserved catalytic residues of the Nudix domain of Dcp2, document how a local conformational change in a metal binding loop is coupled to protonation of the general base, and suggest a mechanism of how protein interactions with Dcp2 could be linked to efficient decapping chemistry.

RESULTS

Essential metal binding site of Dcp2 revealed by X-ray crystallography

To determine which residues in the active site of Dcp2 are involved in metal binding and acid/base chemistry, we determined crystal structures of the wild-type, and E198Q and E153Q catalytic glutamate mutants of the Dcp2 Nudix domain (*S. cerevisiae* 100-245). These structures were solved to 2.1, 1.8 and 1.7 Å, respectively (Table 1 and Figure 1). For the wild-type Nudix domain, there is one molecule of Dcp2 in the asymmetric unit, which has an overall conformation very similar to the previously reported structure (She et al., 2006; She et al., 2008). Density for an octahedrally coordinated metal ion was clearly visible in the wild-type structure (Figure 1B). Since the crystallization buffer contained magnesium formate as the sole source of divalent metal and Dcp2 is known to be a Mg-dependent enzyme (Steiger et al., 2003), we conclude the metal ion bound to Dcp2 is magnesium. Three conserved glutamates coordinate the magnesium ion through a water mediated contact (E152, E153, and E198), while a fourth (E149) directly contacts the metal, implying E149 plays a crucial role in metal binding (Figures 1A,B).

In contrast to the structure of wild-type Nudix domain, the E198Q mutant lacked clear density for a metal ion in the active site and failed to crystallize in the presence of any divalent cation (Figure

1C). The final structure has two molecules of Dcp2 in the asymmetric unit that differ in the position of loops near the catalytic Nudix helix, including a loop harboring E198Q (Figures S1A, C; henceforth known as the 190's loop). The overall structures of both E198Q chains superimpose to an average all-atom 0.374 Å root-mean-square deviation (RMSD) as compared to the wild-type structure. The E198Q 190's loops in isolation have an elevated average all-atom root-mean-square deviation of 0.519 Å as compared to the wild-type 190's loop, and importantly, this change in conformation is not mediated by crystal contacts. These observations suggest that E198 is important for metal binding and that the conformation of the 190's loop is altered in the absence of metal.

In contrast, the crystal structure of the E153Q mutant of Dcp2 has 3 molecules in the asymmetric unit, which superimpose to an average all-atom 0.253 Å RMSD as compared to the wild-type structure (Figure S1B, D). Interestingly, there is clear electron density for an octahedrally coordinated Mg^{2+} in the E153Q structure, similar to wild-type (Figure 1D), suggesting E153 is not necessary for metal binding and may instead serve as the general base in the decapping reaction.

Discovery of the catalytic general base and general acid of Dcp2

To determine the function of residues known to be essential to catalysis by Dcp2, we performed kinetic studies for wild-type and mutant Dcp1/Dcp2 complexes as a function of pH. This approach has been used to identify and determine the pKa of both the general acid

and general base in the related Nudix enzyme MutT (Harris et al., 2000; Waley, 1975). Single-turnover experiments were performed under k_{max} conditions ([E] >> K_M) to monitor the effect of pH on all steps that occur after substrate binding but before product release. Because product release is fast, k_{max} corresponds to k_{cat} measured under multiple-turnover conditions (Deshmukh et al., 2008). As expected, decapping activity is dramatically affected by pH (Figure 2A). Between pH 5.5 and 7.5, log(k_{max}) increases linearly by approximately two log-units (Figure 2B), with a maximum occurring between pH 7.5 and 8.0. This is typical behavior for an enzyme utilizing a general base, which should have a near-neutral pKa in order to efficiently abstract a proton from water during catalysis. The decrease in decapping rates between pH 8.0 - 9.5 indicates the presence of a general acid: a positively charged residue that is deprotonated at high pH and unable to stabilize the negatively charged leaving group, resulting in decreased decapping activity. Fitting the log(k_{max})-versus-pH dependence of wild type Dcp2 yields a general base pKa of 7.7 ± 0.5 and a general acid pKa of 8.1 ± 0.7, in good agreement with other Nudix enzymes (Harris et al., 2000).

Our wild-type and mutant Dcp2 crystal structures led us to hypothesize that E153 serves as a general base in the decapping reaction, and so we first examined the pH dependence of k_{max} for the E153Q mutant (Figure 2B). Not surprisingly, E153Q was severely catalytically compromised, with a reduction in k_{max} of approximately three log-units at pH 7.5 compared to wild-type. Notably, E153Q

exhibited multiple products (Figures 3A-C). Incubation of E153Q decapping reaction products with Nucleoside Diphosphate Kinase (NDPK) identified the major product as m7GTP (as compared to the wild-type product m7GDP) and the two other products as m7GDP and m7GMP (Figure S2). Such loss of specificity of the cleavage site is consistent with a severe positioning defect of either the substrate or the attacking nucleophile. Because each product formed at the same rate and the endpoint ratios did not vary with pH or enzyme concentration, data were analyzed for total product formed over time (Table S1, S2; see Methods and Discussion). The E153Q mutant displayed a linear dependence on pH over the range studied (pH 7 - 9.5). Decapping data for E153Q at pH values lower than pH 7.0 were not consistent, most likely due to enzyme instability over the longer time courses needed for the slower reaction. However, the linear behavior observed from pH 7 to 9.5 for E153Q is consistent with E153 functioning as the general base. A similar analysis was performed for the E198Q mutant, which also gave rise to multiple products, consistent with its altered metal binding properties (Figure S2). However, decapping rates were extremely variable, likely due to protein instability under the assay conditions used.

Additionally, we sought to use this same approach to identify the general acid of the Dcp2 chemical step. K135 of *S. cerevisiae* Dcp2 is conserved, and is important for decapping in yeast and *in vitro*, but its role in catalysis is unclear (Deshmukh et al., 2008; She et al., 2008). Therefore, we suspected it might function as a catalytic general acid.

To definitively identity the general acid, we reasoned that mutating this residue should abolish the descending limb of the k_{max} vs pH plot at the higher pHs. To this end, we examined the pH dependence of k_{max} for the K135A mutant, which was previously shown to reduce catalysis by 300-fold *in vitro* (Figure 2B) (Deshmukh et al., 2008). The K135A mutant also displayed multiple products, and was analyzed as total product formed (Figures 3C-E; Tables S1, S2) (Deshmukh et al., 2008). The K135A mutation abolished the descending limb of the log(k_{max}) versus pH profile, indicating it plays the role of general acid, likely by stabilizing the departure of the 5' monophosphate RNA leaving group as suggested previously (Deshmukh et al., 2008). The formation of multiple products by the K135A variant suggests K135 may also play a role in positioning substrate relative to the attacking water and general base within the active site of Dcp2.

Measurement of catalytic glutamate pKa values by NMR spectroscopy

To directly monitor the electrostatic environment in the active site of Dcp2 during a pH titration, we turned to NMR spectroscopy. NMR allows pKa measurements to be determined with site-specific resolution (Markley, 1975; Oda et al., 1994; Zhang and Vogel, 1993). Typically, side chain chemical shifts of acidic or basic amino acids are monitored as a function of pH but indirect methods such as monitoring the effect of backbone amide chemical shifts are also employed. We used methyl group ^{13}C NMR spectroscopy to indirectly

detect titration of protonatable groups in Dcp2, since these probes allow for sensitive and robust detection of NMR signals in proteins at low concentration, and relevant regions of Dcp2 are unresolved by backbone nitrogen HSQC experiments (data not shown; Floor et al 2010). We reasoned that during a pH titration, methyl groups near the general base should exhibit a change in chemical shift due to changes in the protonation state of the general base. In Dcp2, Ile, Leu and Val (ILV) residues are well distributed near the active site, enabling indirect monitoring of the chemical environment using ^{13}C methyl NMR spectroscopy (Figure 4A). We focused on the catalytic Nudix domain of Dcp2 to observe chemical shift changes due to protonation events only and eliminate confounding effects of large scale domain reorientation in solution (Floor et al., 2012). At neutral pH, the Dcp2 Nudix domain ^{13}C-ILV HSQC spectrum is well-resolved with homogenous peak intensity (Figure S3A) with the exception of I199, which is addressed below. Multiple peaks show chemical shift changes as a function of pH, including those corresponding to residues V121, I136, V195, and I199 (Figure 4B). That only a small set of residues are perturbed over five pH units indicates the fold of the enzyme is relatively insensitive to pH. To determine the apparent pKa (pKa_{app}) of the environment surrounding I199 and V121 as representative residues near the active site, the total chemical shift change was plotted as a function of pH and fitted to a sigmoidal function, yielding pKa_{app} values of 7.3 ± 0.02 and 7.2 ± 0.02 respectively (Figure 4C). Given the only histidine on this domain is approximately 30 Å from these residues in our wild-type

crystal structure and the titration was qualitatively similar in the presence of excess magnesium (data not shown), these data suggest that the titratable group belongs to the catalytic general base.

To determine which residues are responsible for the observed chemical shift changes, we systematically mutated the Nudix motif glutamates 149, 152, 153 and 198 of Dcp2 to glutamine and repeated the pH titration. Mutation of E149Q had little effect on pH-sensitive chemical shift changes, with the exception of abrogating the perturbation at I136 (data not shown). Interestingly, despite its proximity to I199 and conservation across species (Figure S3B), mutation at E198 had little effect besides marginal reduction of the magnitude of chemical shift change (Figure 4D, ~3ppm to ~2ppm in ^{13}C). Mutation of either glutamate 152 or 153 to glutamine strongly attenuated all observed pH-dependent chemical shift changes (Figure 4E; data not shown for E152). Since either E149 or E198 mutation have little effect, and E152 is not required for decapping by Dcp2 *in vivo* (Dunckley and Parker, 1999), we conclude that E153 is the general base, as predicted by our kinetic data.

General base protonation remodels a conserved metal binding loop

The pH dependent chemical shift changes in the ^{13}C HSQC depend on the general base (E153) and are consistent with rapid exchange between protonated and deprotonated forms of this residue (Figure 4). One residue (I199) has a large normalized chemical shift change of around 1.5 ppm (~3ppm in ^{13}C; Figure 4B), which is

consistent with a conformational change in the 190's loop. Another significantly perturbed residue (V121) is in the beta core of the protein and close to E153. Linewidth changes result from fluctuations in the magnetic environment that occur on the chemical shift timescale (ms-μsec). The only residue with significant pH dependent linewidth changes is I199 (Figure 5). Collinear chemical shift changes of I199 suggest protonation of E153 by lowering the pH or by removing a titratable group by conservative mutation to glutamine could bias the conformation of the 190s loop into one state (Figure S4). This suggests the dynamics of the 190s loop is coupled to protonation of E153, although we cannot exclude the possibility that the linewidth effects are due to structural dynamics of nearby residues that are not detected in our ILV labeling scheme. Accordingly, the pH dependent spectral changes could be due to change in electrostatic environment from protonation of E153, a coupled conformational transition or a combination of both effects.

To explore the structural consequences of protonation of E153 we performed a series of molecular dynamics simulations of the catalytic domain of Dcp2 from both *S. cerevisiae* and *S. pombe*. We simulated wild-type Dcp2 with E153 (*S. pombe* E147) deprotonated to emulate high pH, E153 with one of the terminal oxygens protonated to emulate low pH, and E153 mutated to glutamine (for *S. pombe* only). The starting structure for the *S. cerevisiae* simulations was the NMR structure of Dcp2 100-245 (PDB 2JVB), which partially unfolded during the simulations; we focused instead on the results from *S. pombe*

(started from the crystal structure PDB 2A6T), which were qualitatively similar (Figures S5A, B). Residue numbers for the remainder of this section therefore refer to *S. pombe*. When E147 (*S. cerevisiae* E153) was protonated or mutated to glutamine we observed increased association of the 190's loop with a beta strand adjacent to the catalytic Nudix helix (Figure 6). Specifically, snapshots from the simulations show that I193 and V114 (*S. cerevisiae* I198 and V121) pack close together when E147 is protonated or mutated (Figure 6A). Meanwhile, I193 had a higher chance of being exposed when E147 was charged (Figure 6B). The simulations suggest that uncharged E147 hydrogen bonds with the backbone amide of K127, while charged E147 can alternatively interact with cationic residues in the 190's loop, leading to a conformational change in the 190's loop.

To quantitatively assess the effect of protonation of E147 on the conformation of the 190's loop, the distance between the terminal methyl groups of V114 and I193 was measured for each of three states: E147 protonated (Figure 6C), E147Q (Figure 6D), and E147 charged (Figure 6E). These two residues were selected as they exhibit large chemical shift changes across NMR pH titrations (Figure 4A; V121 and I199). For both E147 protonated and E147Q, the distance histogram shows a single peak corresponding to close packing of V114 and I193 for most of the simulation, with a few snapshots exhibiting longer distances (Figures 6 C, D). In contrast, when E147 is negatively charged, a second peak emerges in the distance histogram corresponding to a second conformation of the 190's loop with greater

separation of V114 and I193 (Figure 6E). The observed conformational changes are not sensitive to the choice of reference residue used to calculate distance histograms (Figures S5 C, D). We conclude that the conformation of the 190's loop is coupled to the protonation state of the general base E147 (E153 in *S. cerevisiae*).

DISCUSSION

Using a suite of complementary techniques we have defined the role of multiple conserved glutamate residues in the mRNA decapping enzyme Dcp2, and identified loop motions that are coupled to protonation of the general base, a key step that occurs during the catalytic cycle. NMR spectroscopy and pH-dependent kinetics show that E153 is the catalytic general base, while a trio of crystal structures demonstrate that metal is coordinated by E149, E152 and E198. Additionally, using molecular dynamics simulations and NMR, we show that protonation of the general base influences the catalytic 190's loop, which was previously shown to be involved in collective, interdomain motions in Dcp2 (Floor et al., 2012). This work describes the role of catalytic residues in Dcp2 for the first time, uncovers dynamics associated with the catalytic cycle, and suggests an alternative mechanism by which closure of Dcp2 could stimulate enzyme activity.

Several observations suggest E153 plays the role of general base in Dcp2. First, wild-type Dcp2 and the E153Q mutant bind metal in the

same manner, yet decapping complexes harboring substitutions at E153 are still somehow severely catalytically compromised both *in vitro* and *in vivo* (Dunckley and Parker, 1999; She et al., 2006). Second, the E153Q mutation abolishes the ascending limb of the log(k_{max}) versus pH profile. Third, NMR pH titrations detect a residue with a near neutral pKa that is abolished by the E153Q mutation. Furthermore, the change in major product from m7GDP to m7GTP of the E153Q variant is consistent with a general base mutation, leaving the enzyme dependent on ambient hydroxide ions in the active site to serve as a nucleophile. Taken together, these data identify E153 as the general base in decapping, and explain why E153 has been shown to be critical for decapping both *in vitro* and *in vivo* (Dunckley and Parker, 1999; She et al., 2006).

The identification of K135 as a cationic residue responsible for stabilizing the leaving group is reminiscent of other Nudix enzymes that utilize a general acid to promote catalysis (Harris et al., 2000; Legler et al., 2002; Maksel et al., 2001; Mildvan et al., 2005). This offers an explanation for its previously reported effect on k_{max} (Deshmukh et al., 2008) and the measured pKa of 8.1 is similar to catalytic acids for other Nudix enzymes (Harris et al., 2000). In the *S. pombe* Dcp1/Dcp2 closed crystal structure, K129 (K135 in *S. cerevisiae)* is poised near the phosphates of the crystallization additive ATP, suggesting it may play a role in contacting one of the phosphates of cap (She et al., 2008), consistent with the multiple products formed in the K135A decapping reaction (Deshmukh et al., 2008).

The 190's loop of Dcp2, and E198 in particular, exhibits a spectrum of conformations: in the crystal structure of *S. pombe* Dcp2, E192 (the *S. cerevisiae* E198 equivalent) is pointed towards solvent, whereas in the crystal structure of the ATP-bound *S. pombe* Dcp1:Dcp2 complex, this side chain is pointed towards the catalytic center (She et al., 2006; She et al., 2008). Additionally, in the open form of the *S. pombe* Dcp1:Dcp2 complex crystal structure, the 190's loop is unresolved (She et al., 2008). Our results are consistent with the observed flexibility of the 190's loop and specifically E198. Apparently, ILV methyl labeling can be used to detect protonation states of titratable residues in proteins in addition to reflecting slower exchange processes. This approach may be of broad utility for investigating pH dependent processes in enzymes, molecular machines and ion channels because methyl-TROSY NMR can be applied on assemblies as large as 0.5 MDa (Sprangers and Kay, 2007).

What is the functional role of flexibility in the 190's loop? Loop conformational changes involving a catalytic residue are reminiscent of the mechanism of Nudix hydrolase ADP-ribose pyrophosphatase (ADPRP), which contains a loop that undergoes an open-to-closed transition of a full 10 Å over the course of the catalytic cycle, bringing the general base into position (Gabelli et al., 2002). Though our experiments show Dcp2 differs from ADPRP in the location of the general base, changing conformations of the 190's loop in Dcp2 could aid in product release following catalysis. Alternatively, motions of E198 and the 190's loop could contribute to metal coordination

changes over the catalytic cycle, analogous to the metal hand-off role E98 plays in *E. coli* MutT (Harris et al., 2000).

It was proposed that the closed form of Dcp2 is the more active form of the enzyme because the regulatory domain and catalytic domain both bind cap using a composite active site, and that coactivators can affect this domain closure to stimulate decapping (Floor et al., 2010; She et al., 2008). The results reported here are consistent with this notion, but also suggest two possible mechanisms for how Dcp2 activity might be fine-tuned by coactivators affecting conformational dynamics. If inter-domain closure stimulates catalysis by Dcp2 via substrate positioning, then mutations in both the regulatory and catalytic domains should result in aberrant cleavage events; indeed, we observe multiple products upon mutation of catalytic residues, and deletion of the regulatory domain gives rise to multiple products (Piccirillo et al., 2003). There is also a second possible route for catalytic rate enhancement: coupled inter-domain and catalytic loop motions of Dcp2. Regions adjacent to the catalytic helix are involved in collective motions in apo Dcp2 (Floor et al., 2012), and here we find that the conformation of the 190's loop is influenced by the catalytically essential glutamates E153 and E198. While it is possible that that global conformational changes may be coupled to both changes in substrate positioning and local rearrangements of the 190's loop, definitive proof requires future structural work with substrate RNA.

ACESSION NUMBERS

The coordinates and structure-factor amplitudes of the wild-type, E198Q and E153Q crystal structures of Dcp2 have been deposited in the Protein Data Bank under accession codes under 4K6E (wild-type), 4KG4 (E198Q), and 4KG3 (E153Q).

ACKNOWLEDGEMENTS

We thank Mark Kelly for NMR support; Pascal Wassam for computer support; Jamie Fraser for help with x-ray data collection and refinement, and D. Flemming Hansen for the FuDA software. The Advanced Light Source is supported by the U.S. Department of Energy under Contract No. DE-AC02-05CH11231. This work was supported by US National Institutes of Health grant R01GM078360 to J.D.G., fellowships from the Sandler Family Foundation for Basic Sciences and the Achievement Awards for College Scientists Foundation to S.N.F, supercomputer time provided by the National Science Foundation Teragrid program at the Texas Advanced Supercomputing Center (Project TG-MCB090109 to M.P.J.), and funding from the UCSF integrated Program in Quantitative Biology fellowship and the UCSF Cancer Research Coordinating Committee for C.L.M. M.P.J. is a consultant to Schrödinger, L.L.C.

FIGURES

Figure 1: Mg^{2+} coordination in the Dcp2 catalytic domain. **(A)** Ribbon diagram of Mg^{2+} coordination in the wild-type *S. cerevisiae* Dcp2 catalytic Nudix domain at the catalytic helix. Four conserved glutamates (E149, E152, E153, E198) and K135 are shown as sticks in green. Water molecules are shown as blue spheres, and the Mg^{2+} is shown as a black sphere. Colored in grey is the backbone carbonyl of N243 in a symmetry related molecule. **(B)** Fo-Fc difference electron density map of wild-type Dcp2 depicted as black mesh at an I/σ cutoff of 2.5. **(C)** Fo-Fc difference electron density map for the E198Q mutant at an I/σ cutoff of 2.0. **(D)** Fo-Fc difference electron density map of E153Q mutant at an I/sigma cutoff of 3.0.

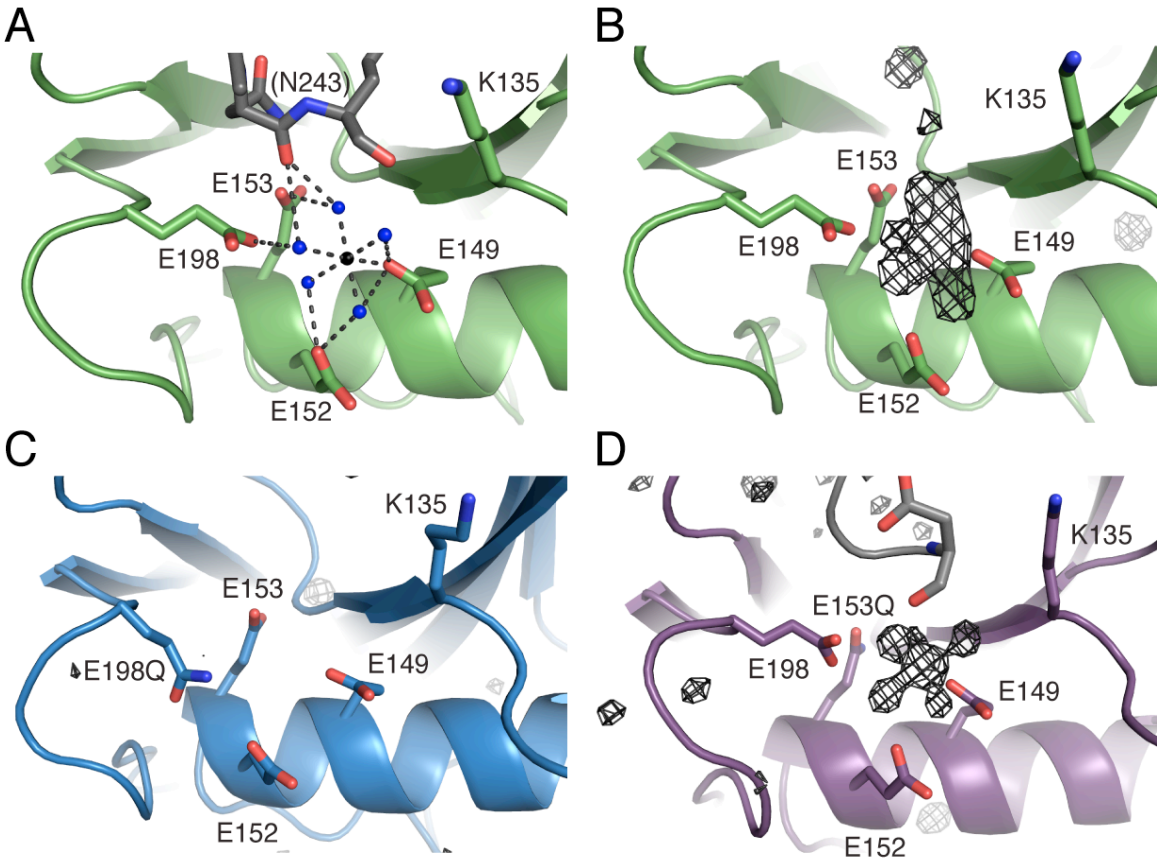
A
(N243)
K135
E153
E198
E149
E152
B
K135
E153
E198
E149
E152
C
K135
E153
E198Q
E149
E152
D
K135
E153Q
E198
E149
E152

Figure 2: Decapping rates for wild-type and mutant Dcp1/Dcp2 are affected by pH. **(A)** Representative time courses of the fraction m7GDP released and the corresponding first-order exponential fits to obtain k_{obs} over a range of pH values for wild-type Dcp1/Dcp2 decapping complex. **(B)** Plot of log (k_{max}) versus pH for wild-type decapping complex (green), K135A (yellow) and E153Q (purple). Symbols are the mean of at least 3 independent experiments and error bars shown are standard deviation. Wild-type and K135A are fit using the 4-parameter equation used to model the dependence of k_{max} on pH (Harris et al., 2000). E153Q is fit to a line due to the linear dependence of k_{max} on pH.

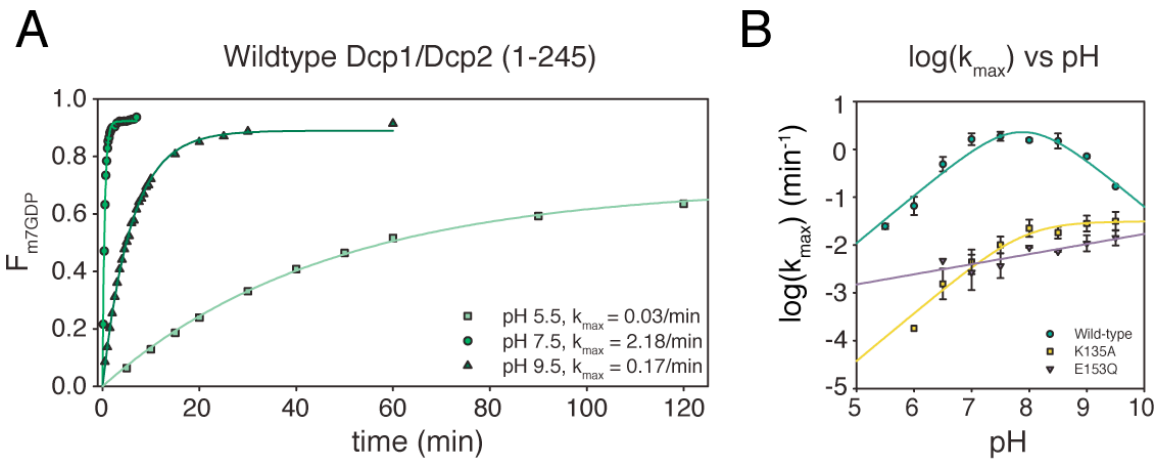

Figure 3: Active site mutations in Dcp1/2 complex result in multiple decapping reaction products. **(A)** Representative TLC plate decapping assay data for Dcp1/2 E153Q decapping complex at pH 8.0. Arrows point out the location of RNA substrate (black), m7GTP (green), m7GDP (blue) and m7GMP (red) as identified by incubation with NDPK (Figure S2E). **(B)** Representative time course of the fraction of each E153Q product formed as a function of time. m7GTP, m7GDP, and m7GMP are shown in green, blue, and red respectively. Total product formed is shown in black. Single exponential fits were used to obtain the individual k_{obs} for each product (see methods and Tables S1, S2). **(C)** Distribution of each product formed in the decapping reactions of wild-type, E153Q, and K135A variants, calculated by an average ratio of endpoints for each product across all pH values fit using a single exponential (Table S1). **(D)** Representative TLC plate for K135A showing multiple products. Arrows point out the location of RNA substrate (black), m7GTP (green), m7GDP (blue) and m7GMP (red) as identified by incubation with NDPK (Figure S2E). **(E)** Representative time course for the fraction of each K135A product formed as a function of time. Coloring is the same as in (B). Single exponential fits were used to obtain the individual k_{obs} for each product (see methods and Tables S1, S2).

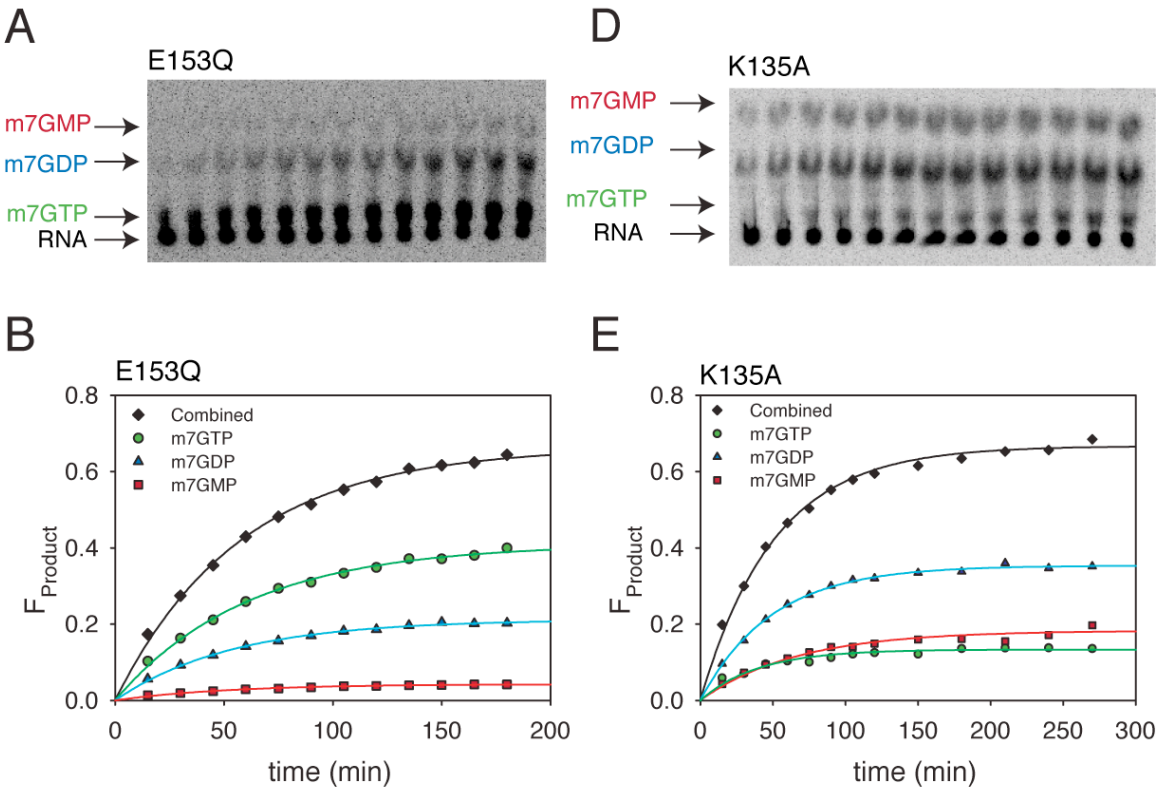
A
E153Q
m7GMP
m7GDP
m7GTP
RNA
D
K135A
m7GMP
m7GDP
m7GTP
RNA
B
E153Q
Combined
m7GTP
m7GDP
m7GMP
F Product
time (min)
E
K135A
Combined
m7GTP
m7GDP
m7GMP
F Product
time (min)
C
F Product
m7GTP
m7GDP
m7GMP
WT
E153Q
K135A

Figure 4: Methyl NMR pH titrations confirm E153 is the general base. **(A)** Select Ile, Leu, and Val residues on the catalytic domain of *S. cerevisiae* Dcp2 are highlighted in blue with catalytic glutamates E149, E152, E153, and E198 highlighted in green and the Nudix helix in red. Residues are visualized on PDB 2JVB. **(B)** A superposition of ILV-methyl ^{13}C-^{1}H HSQC spectra of wild-type scDcp2 (100-245) at pH 4.5 (red), 5.5 (orange), 6.5 (lime), 7.1 (green), 7.6 (cyan), 8.0 (magenta) and 9.0 (purple). **(C)** Quantification of the normalized chemical shift change (Δδ) for L120, V121 and I199 across the pH titration. Note that the sidechain of L120 points in the opposite direction from V121. Solid lines are sigmoidal fits, with pKa_{app} values of 7.3 ± 0.02 and 7.2 ± 0.02 for I199 and V121, respectively. **(D)** ^{13}C-^{1}H HSQC spectra of the E198Q mutant Dcp2 catalytic domain collected at pH values of 5 (red), 5.6 (orange), 6.0 (lime), 6.6 (green), 7.2 (cyan), 8.1 (magenta) and 8.9 (purple). Weak peaks in (D) are likely from residual contamination by the GB1 solubility tag. **(E)** ^{13}C-^{1}H HSQC spectra of the E153Q mutant Dcp2 catalytic domain collected at pH values of 5.5 (orange), 6.6 (lime), 7.0 (green), 7.6 (cyan) and 8.5 (purple).

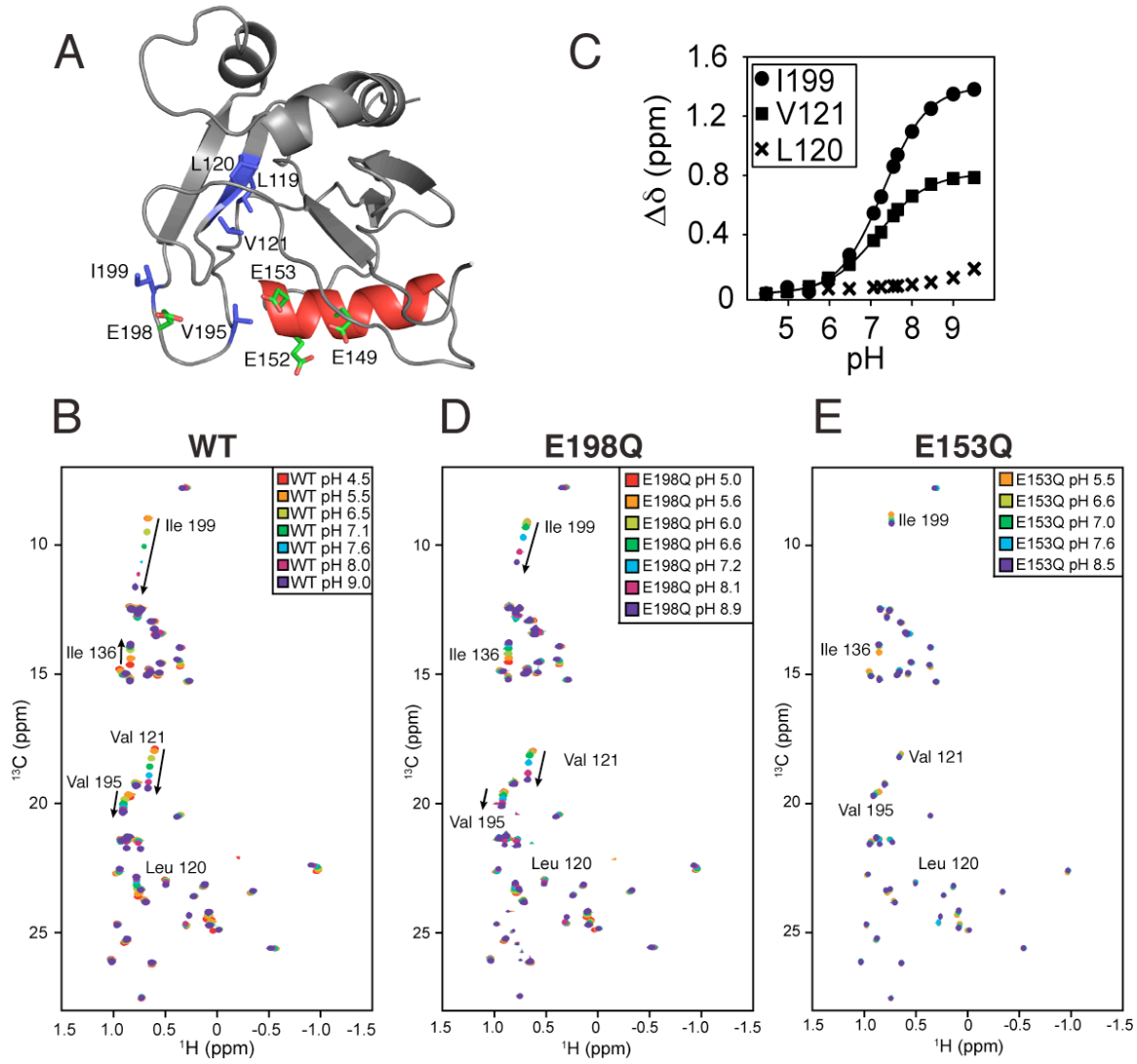
A
L120
L119
V121
I199
E153
E198
V195
E152
E149
C
I199
V121
L120
Δδ (ppm)
pH
B
WT
WT pH 4.5
WT pH 5.5
WT pH 6.5
WT pH 7.1
WT pH 7.6
WT pH 8.0
WT pH 9.0
Ile 199
Ile 136
Val 121
Val 195
Leu 120
^{13}C (ppm)
^{1}H (ppm)
D
E198Q
E198Q pH 5.0
E198Q pH 5.6
E198Q pH 6.0
E198Q pH 6.6
E198Q pH 7.2
E198Q pH 8.1
E198Q pH 8.9
E
E153Q
E153Q pH 5.5
E153Q pH 6.6
E153Q pH 7.0
E153Q pH 7.6
E153Q pH 8.5

Figure 5: Change in pH Induces Changes in Dynamics. **(A)** The ^{13}C linewidth (FWHM) for residues I199, V121 and L115 across the pH titration. **(B-E)** Example fitted ^{13}C linewidths of I199 at pH values indicated. The experimental data is in points with the mixed Gaussian-Lorentzian fit as a line. Intensity is in units of signal-to-noise (S:N) with noise measured in NMRPipe.

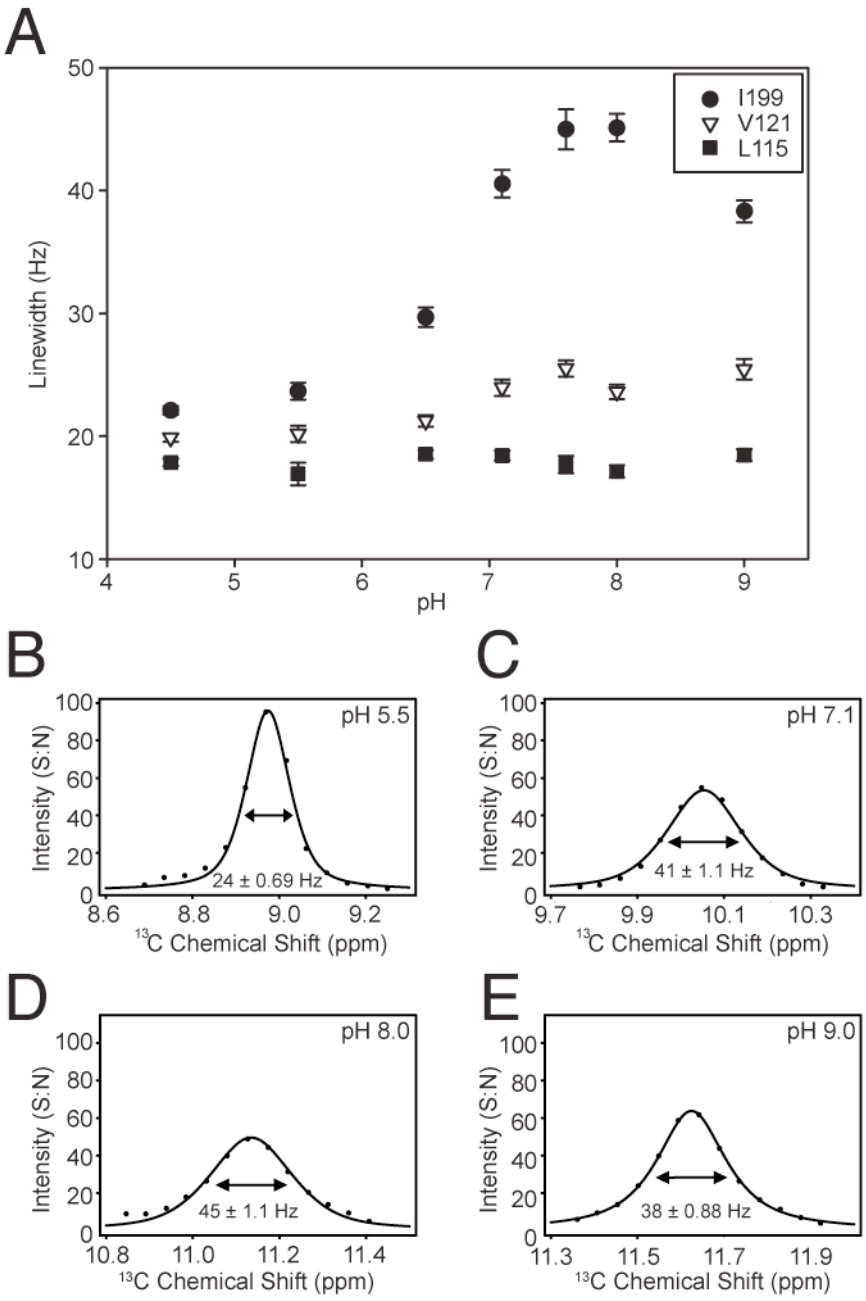

Figure 6: Molecular dynamics simulations show qualitative and quantitative conformational changes between *S. pombe* Dcp2 with charged or protonated E147. **(A)** Simulations with protonated E147 to mimic the low pH state show relatively little flexibility in the 190's loop. I193 (I199 in *S. cerevisiae*) is shown in blue sticks, V114 in red sticks, and the Nudix helix is colored green. **(B)** Simulations with charged E147 to mimic the high pH state show increased flexibility with I193 solvent exposed in the final state of two out of six simulations. Colors are the same as in (A). Histograms of the distance between the terminal methyl groups of V114 and I193 when E147 is protonated to mimic the low pH state **(C)**, when E147 is mutated to glutamine **(D)**, or when E147 is charged to mimic the high pH state **(E)**. The ordinate of all three histograms is probability density per bin; $n \approx 600{,}000$ per histogram. Residues I193, V114 and E147 in *S. pombe* are *S. cerevisiae* I199, V121 and E153, respectively.

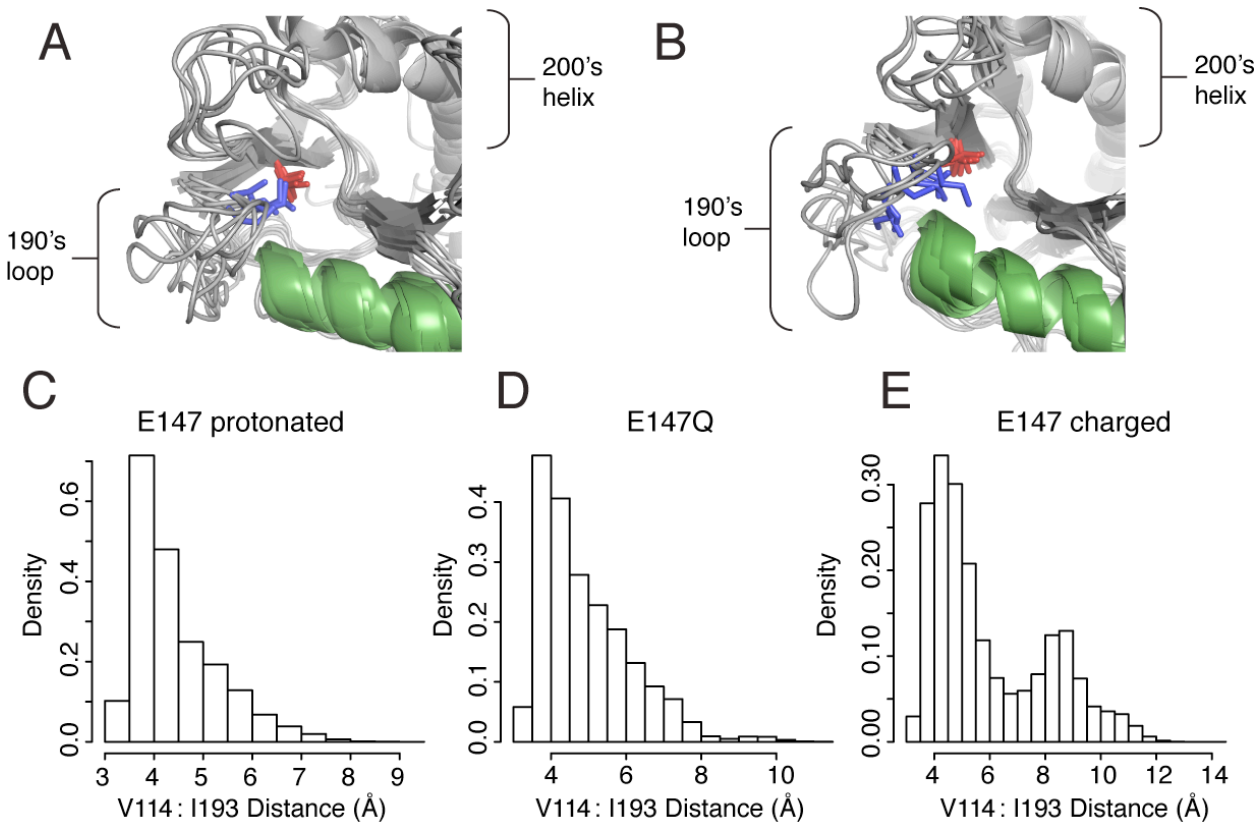
A
200's helix
190's loop
B
200's helix
190's loop
C
E147 protonated
Density
0.0
0.2
0.4
0.6
3
4
5
6
7
8
9
V114 : I193 Distance (Å)
D
E147Q
Density
0.0
0.1
0.2
0.3
0.4
4
6
8
10
V114 : I193 Distance (Å)
E
E147 charged
Density
0.00
0.10
0.20
0.30
4
6
8
10
12
14
V114 : I193 Distance (Å)

TABLES

Table 1: Crystallographic Data and Refinement Statistics. Statistics for highest-resolution shell are shown in parentheses.

	Wild-type	E198Q	E153Q
Wavelength (Å)	0.95372	1.11587	1.11587
Resolution range (Å)	50– 2.1 (2.14 – 2.1)	50– 1.8 (1.83 – 1.8)	50- 1.7 (1.75– 1.7)
Space group	P 62	P 1 21 1	C 121
Unit cell (Å)	85.054 85.054 48.749 90 90 120	57.352 47.804 60.957 90 97.29 90	140.789 49.27 84.022 90 91.37 90
Molecules/ASU	1	2	3
Total Reflections	86873	53880	81472
Unique reflections	11889	29454	54478
Multiplicity	7.3 (7.3)	1.8 (1.8)	10.4 (11.0)
Completeness (%)	99.97 (99.92)	96.48 (94.68)	85.69 (60.92)
I/σ	26.8 (3.5)	28.6(2.7)	20.5 (1.4)
Wilson B-factor	28.33	27.42	20.84
R-merge	0.081 (0.557)	0.04 (0.383)	0.099 (0.447)
R-work	0.1530 (0.1903)	0.1871 (0.2359)	0.1770 (0.3545)
R-free	0.1910 (0.2442)	0.2140 (0.2836)	0.2127 (0.4151)
RMS (bonds)	0.007	0.007	0.007
RMS (angles)	1.09	1.16	1.11
Ramachandran favored (%)	97	95	97
Ramachandran outliers (%)	0.7	1.1	0.24
Clashscore	3.33	3.89	3.23
Average B-factor	43.30	41.80	40.5

EXPERIMENTAL PROCEDURES

Protein Expression and Purification: Wild type and mutant *S. cerevisiae* Nudix domain constructs were expressed with an N-terminal GB1 tag (Card and Gardner, 2005) followed by a hexahistidine affinity tag, a TEV protease site and the coding region of *S. cerevisiae* Dcp2 residues 100-245 in *Escherichia coli* BL21-Star cells (Invitrogen). Proteins for crystallography were purified from cells grown in LB media with an induction lasting 18 hours at 20˚C. Cells were harvested at 5000g, sonicated, clarified at 25,000g, purified using Ni-NTA affinity chromatography, and cleaved overnight at room temperature with TEV protease. Purification proceeded by Ni-NTA backpass to remove the His-GB1 tag followed by gel filtration chromatography into NMR buffer: 21.1 mM NaH_2PO_4 and 28.8 mM Na_2HPO_4 (pH 7.0), 200 mM NaCl, 100 mM Na_2SO_4, and 5 mM DTT in H_2O. Samples were used promptly following purification and were > 95% pure as judged by coomassie staining. Protein samples for NMR were obtained from cells expressed in H_2O M9 minimal media supplemented with 10 mg biotin per liter, and forty minutes prior to induction by 1mM IPTG, 50 mg L^{-1} of ^{13}C-methyl alpha-ketobutyric acid and 100 mg L^{-1} of ^{13}C-dimethyl alpha-ketoisovaleric acid (Cambridge Isotopes) were added directly to the media. Purification proceeded as above. For kinetic assays, the wild-type and mutant S. cerevisiae Dcp1/Dcp2 decapping complex constructs GB1-t-Dcp1/Dcp2 (1-245) were expressed in BL21 (DE3)-Rosetta cells, purified by nickel affinity

chromatography and treated with 10 mM EDTA for 1 hour, followed by gel filtration into Dcp2 storage buffer (50 mM HEPES, 100 mM NaCl, 20 % glycerol, 5 mM DTT pH 7.5), flash frozen and stored at –80 ˚C.

X-ray Crystallography: After purification *S. cerevisiae* Dcp2 (100-245) was buffer exchanged into 10 mM HEPES pH 7.0, 1 mM DTT, 50 mM NaCl, 100 mM Na_2SO_4 and then mixed with an equal volume of crystallization conditions and grown at room temperature by the hanging drop vapor diffusion method. Wild-type protein was mixed with 0.1 M Mg Formate, 0.1 M sodium acetate pH 4.4, 20% PEG 3350; E198Q protein was mixed with 0.25 M Na Acetate, 0.1 M Na cacodylate pH 6.5, 20% PEG 3350; and E153Q was mixed with 0.1 Mg Formate, 0.1 M HEPES pH 7.4, 20% PEG 3350. The wild-type data was collected at room temperature at a wavelength of 0.95372 Å. The E198Q and E153Q crystals were transferred to the well solution containing 20% glycerol and then flash frozen before data collection at a wavelength of 1.11587 Å and 100 K. All data was collected at ALS (Advanced Light Source) 8.3.1, and indexed, integrated and scaled using HKL2000 (Otwinowski and Minor, 1997). Phasing was done via molecular replacement using the previously solved *S. pombe* structure with loops 189-202 and 213-219 removed (PDB 2A6T) (She et al., 2006) using Phaser in PHENIX, model building was performed in Coot (Adams et al., 2010; Emsley and Cowtan, 2004; McCoy et al., 2007) and the structures were refined in PHENIX (Adams et al., 2010) with the use of TLS.

Kinetic Assays: Decapping reactions were carried out at 4 ˚C on wild-type or mutant budding yeast Dcp1/2 complexes as previously described (Jones et al., 2008) under saturating single-turnover conditions for all constructs tested. Saturation was verified by doubling the enzyme concentration at pH values 5.5, 7.5, and 9.5. The final buffer concentration used was 50 mM NH_4Cl, 0.01% NP-40, 1 mM DTT, 5 mM $MgCl_2$ and either 50 mM Bis-Tris methane (pH 5.5 – 6.5), 50 mM Tris-HCl (pH 7.0 – 8.0), or 50 mM Bis-Tris propane (pH 8.5 – 9.5). Stored protein (see protein purification) was diluted to 3X final concentration in 1X decapping reaction buffer, incubated at 4 ˚C for 15 minutes to allow for complete temperature and pH equilibration, and then the reaction was initiated by addition of RNA substrate in 1X reaction buffer. Kinetic data were processed and fit as previously described (Jones et al., 2008). The data for the K135A mutation were analyzed as fraction total product formed (see text, Figures 3C-E). For pH values 7.5- 9.5, K135A data were fit to a single exponential curve yielding k_{obs} (Figure S2A). For pH values lower than 7.5, the reaction rates were too slow to reliably obtain data that could be fit exponentially and instead initial rates were measured (Figure S2B). The initial linear rate of the reaction (no more than 30% complete) was divided by an endpoint of 0.75, which was an average of all endpoints for K135A timecourses fit with a single exponential to obtain k_{obs}. E153Q was also analyzed as fraction total product formed (see text, Figures 3 A-E), by single exponential fit for pH values 8.0 - 9.5 (**Figure**

S2C), and by initial rates for pH values lower than 8.0 (Figure S2D). For wild-type and K135A decapping complexes, the k_{max} dependence on pH was fit using previously established methods (Harris et al., 2000) to obtain the general acid and general base pKa's. Fitting the E153Q data in this manner was not successful, while a linear model of E153Q k_{max} pH dependence had better agreement with the experimental results.

NMR Spectroscopy: NMR experiments were performed using the gradient-enhanced ^{13}C-^{1}H HSQC (Kay et al., 1992) on either a Varian Inova 600 MHz or Bruker Avance 800 MHz spectrometer, both outfitted with cryogenic four-channel probes. Assignments are BMRB entry 7325 (Deshmukh et al., 2008). Changes in pH were performed by direct addition of NaOH or HCl to the sample while monitoring pH with a micro-electrode. Titrations were performed with protein concentrations between 100 μM and 200 μM at 298K. A mild amount of precipitation was observed at pH extrema. Experiments over pH 9 or less than pH 5.5 that showed global chemical shift changes, indicative of unfolding, were discarded. Structure figures were generated with PyMOL (http://pymol.org) and NMR spectra figures were generated with Sparky (T.D. Goddard and D.G. Kneller, UCSF). Changes in chemical shift were calculated according to the total chemical shift change: $\Delta\delta_C = \sqrt{(\Delta\delta(^{13}C)/2)^2 + (\Delta\delta(^{1}H))^2}$ NMR data were processed using NMRPipe (Delaglio et al., 1995) with apodization, linear prediction and low-frequency deconvolution to remove residual H_2O. Peak shapes

were fit using FuDA (D.F. Hansen; http://www.biochem.ucl.ac.uk/hansen/fuda) by a mixed Lorentzian and Gaussian curve.

Molecular Dynamics: 100 ns simulations of *S. cerevisiae* Dcp2 wild-type and with protonated E153 from PDB 2JVB, along with *S. pombe* Dcp2 wild-type, E153 protonated, and E153Q from PDB 2A6T were performed with the OPLS forcefield (Kaminski et al., 2001) and SPC water (H.J.C. Berendsen, 1981) as previously described, except with 0.5 M NaCl (Rapp et al., 2013). Additional details can be found in the supplemental info.

REFERENCES

Adams, P.D., Afonine, P.V., Bunkoczi, G., Chen, V.B., Davis, I.W., Echols, N., Headd, J.J., Hung, L.W., Kapral, G.J., Grosse-Kunstleve, R.W., *et al.* (2010). PHENIX: a comprehensive Python-based system for macromolecular structure solution. Acta Crystallogr D Biol Crystallogr *66*, 213-221.

Amrani, N., Ganesan, R., Kervestin, S., Mangus, D.A., Ghosh, S., and Jacobson, A. (2004). A faux 3'-UTR promotes aberrant termination and triggers nonsense-mediated mRNA decay. Nature *432*, 112-118.

Arribas-Layton, M., Wu, D., Lykke-Andersen, J., and Song, H. (2012). Structural and functional control of the eukaryotic mRNA decapping machinery. Biochim Biophys Acta *1829*, 580-589.

Beelman, C.A., Stevens, A., Caponigro, G., LaGrandeur, T.E., Hatfield, L., Fortner, D.M., and Parker, R. (1996). An essential component of the decapping enzyme required for normal rates of mRNA turnover. Nature *382*, 642-646.

Behm-Ansmant, I., Rehwinkel, J., Doerks, T., Stark, A., Bork, P., and Izaurralde, E. (2006). mRNA degradation by miRNAs and GW182

requires both CCR4:NOT deadenylase and DCP1:DCP2 decapping complexes. Genes Dev *20*, 1885-1898.

Brannan, K., Kim, H., Erickson, B., Glover-Cutter, K., Kim, S., Fong, N., Kiemele, L., Hansen, K., Davis, R., Lykke-Andersen, J., *et al.* (2012). mRNA decapping factors and the exonuclease Xrn2 function in widespread premature termination of RNA polymerase II transcription. Mol Cell *46*, 311-324.

Braun, J.E., Truffault, V., Boland, A., Huntzinger, E., Chang, C.T., Haas, G., Weichenrieder, O., Coles, M., and Izaurralde, E. (2012). A direct interaction between DCP1 and XRN1 couples mRNA decapping to 5' exonucleolytic degradation. Nat Struct Mol Biol *19*, 1324-1331.

Card, P.B., and Gardner, K.H. (2005). Identification and optimization of protein domains for NMR studies. Methods Enzymol *394*, 3-16.

Chang, J.H., Jiao, X., Chiba, K., Oh, C., Martin, C.E., Kiledjian, M., and Tong, L. (2012). Dxo1 is a new type of eukaryotic enzyme with both decapping and 5'-3' exoribonuclease activity. Nat Struct Mol Biol *19*, 1011-1017.

Chen, C.Y., Xu, N., and Shyu, A.B. (1995). mRNA decay mediated by two distinct AU-rich elements from c-fos and granulocyte-macrophage colony-stimulating factor transcripts: different deadenylation kinetics and uncoupling from translation. Mol Cell Biol *15*, 5777-5788.

Chen, C.Y., Zheng, D., Xia, Z., and Shyu, A.B. (2009). Ago-TNRC6 triggers microRNA-mediated decay by promoting two deadenylation steps. Nat Struct Mol Biol *16*, 1160-1166.

Delaglio, F., Grzesiek, S., Vuister, G.W., Zhu, G., Pfeifer, J., and Bax, A. (1995). NMRPipe: a multidimensional spectral processing system based on UNIX pipes. J Biomol NMR *6*, 277-293.

Deshmukh, M.V., Jones, B.N., Quang-Dang, D.U., Flinders, J., Floor, S.N., Kim, C., Jemielity, J., Kalek, M., Darzynkiewicz, E., and Gross, J.D. (2008). mRNA decapping is promoted by an RNA-binding channel in Dcp2. Mol Cell *29*, 324-336.

Dunckley, T., and Parker, R. (1999). The DCP2 protein is required for mRNA decapping in Saccharomyces cerevisiae and contains a functional MutT motif. EMBO J *18*, 5411-5422.
Emsley, P., and Cowtan, K. (2004). Coot: model-building tools for molecular graphics. Acta Crystallogr D Biol Crystallogr *60*, 2126-2132.

Eulalio, A., Rehwinkel, J., Stricker, M., Huntzinger, E., Yang, S.F., Doerks, T., Dorner, S., Bork, P., Boutros, M., and Izaurralde, E. (2007).

Target-specific requirements for enhancers of decapping in miRNA-mediated gene silencing. Genes Dev *21*, 2558-2570.

Fenger-Gron, M., Fillman, C., Norrild, B., and Lykke-Andersen, J. (2005). Multiple processing body factors and the ARE binding protein TTP activate mRNA decapping. Mol Cell *20*, 905-915.

Floor, S.N., Borja, M.S., and Gross, J.D. (2012). Interdomain dynamics and coactivation of the mRNA decapping enzyme Dcp2 are mediated by a gatekeeper tryptophan. Proc Natl Acad Sci U S A *109*, 2872-2877.

Floor, S.N., Jones, B.N., Hernandez, G.A., and Gross, J.D. (2010). A split active site couples cap recognition by Dcp2 to activation. Nat Struct Mol Biol *17*, 1096-1101.

Fromm, S.A., Truffault, V., Kamenz, J., Braun, J.E., Hoffmann, N.A., Izaurralde, E., and Sprangers, R. (2012). The structural basis of Edc3- and Scd6-mediated activation of the Dcp1:Dcp2 mRNA decapping complex. EMBO J *31*, 279-290.

Gabelli, S.B., Bianchet, M.A., Ohnishi, Y., Ichikawa, Y., Bessman, M.J., and Amzel, L.M. (2002). Mechanism of the Escherichia coli ADP-ribose pyrophosphatase, a Nudix hydrolase. Biochemistry *41*, 9279-9285.

Ghosh, T., Peterson, B., Tomasevic, N., and Peculis, B.A. (2004). Xenopus U8 snoRNA binding protein is a conserved nuclear decapping enzyme. Mol Cell *13*, 817-828.

H.J.C. Berendsen, J.P., W. van Gunsteren, J. Hermans (1981). Intermolecular Forces (Reidel, Dordrecht).

Harigaya, Y., Jones, B.N., Muhlrad, D., Gross, J.D., and Parker, R. (2010). Identification and analysis of the interaction between Edc3 and Dcp2 in Saccharomyces cerevisiae. Mol Cell Biol *30*, 1446-1456.

Harris, T.K., Wu, G., Massiah, M.A., and Mildvan, A.S. (2000). Mutational, kinetic, and NMR studies of the roles of conserved glutamate residues and of lysine-39 in the mechanism of the MutT pyrophosphohydrolase. Biochemistry *39*, 1655-1674.

Heo, I., Joo, C., Kim, Y.K., Ha, M., Yoon, M.J., Cho, J., Yeom, K.H., Han, J., and Kim, V.N. (2009). TUT4 in concert with Lin28 suppresses microRNA biogenesis through pre-microRNA uridylation. Cell *138*, 696-708.

Hilgers, V., Teixeira, D., and Parker, R. (2006). Translation-independent inhibition of mRNA deadenylation during stress in Saccharomyces cerevisiae. RNA *12*, 1835-1845.

Hu, W., Sweet, T.J., Chamnongpol, S., Baker, K.E., and Coller, J. (2009). Co-translational mRNA decay in Saccharomyces cerevisiae. Nature *461*, 225-229.

Isken, O., and Maquat, L.E. (2007). Quality control of eukaryotic mRNA: safeguarding cells from abnormal mRNA function. Genes Dev *21*, 1833-1856.

Jiao, X., Xiang, S., Oh, C., Martin, C.E., Tong, L., and Kiledjian, M. (2010). Identification of a quality-control mechanism for mRNA 5'-end capping. Nature *467*, 608-611.

Jones, B.N., Quang-Dang, D.U., Oku, Y., and Gross, J.D. (2008). A kinetic assay to monitor RNA decapping under single- turnover conditions. Methods Enzymol *448*, 23-40.

Kaminski, G.A., Friesner, R.A., Tirado-Rives, J., and Jorgensen, W.L. (2001). Evaluation and reparametrization of the OPLS-AA force field for proteins via comparison with accurate quantum chemical calculations on peptides. Journal of Physical Chemistry B *105*, 6474-6487.

Kay, L.E., Keifer, P., and Saarinen, T. (1992). Pure Absorption Gradient Enhanced Heteronuclear Single Quantum Correlation Spectroscopy with Improved Sensitivity. Journal of the American Chemical Society *114*, 10663-10665.

Lai, T., Cho, H., Liu, Z., Bowler, M.W., Piao, S., Parker, R., Kim, Y.K., and Song, H. (2012). Structural basis of the PNRC2-mediated link between mrna surveillance and decapping. Structure *20*, 2025-2037.

Legler, P.M., Massiah, M.A., and Mildvan, A.S. (2002). Mutational, kinetic, and NMR studies of the mechanism of E. coli GDP-mannose mannosyl hydrolase, an unusual nudix enzyme. Biochemistry *41*, 10834-10848.

Li, Y., Dai, J., Song, M., Fitzgerald-Bocarsly, P., and Kiledjian, M. (2012). Dcp2 decapping protein modulates mRNA stability of the critical interferon regulatory factor (IRF) IRF-7. Mol Cell Biol *32*, 1164-1172.

Liu, H., Rodgers, N.D., Jiao, X., and Kiledjian, M. (2002). The scavenger mRNA decapping enzyme DcpS is a member of the HIT family of pyrophosphatases. EMBO J *21*, 4699-4708.

Lykke-Andersen, J. (2002). Identification of a human decapping complex associated with hUpf proteins in nonsense-mediated decay. Mol Cell Biol *22*, 8114-8121.

Maksel, D., Gooley, P.R., Swarbrick, J.D., Guranowski, A., Gange, C., Blackburn, G.M., and Gayler, K.R. (2001). Characterization of active-site residues in diadenosine tetraphosphate hydrolase from Lupinus angustifolius. Biochem J *357*, 399-405.

Markley, J.L. (1975). Observation of Histidine Residues in Proteins by Means of Nuclear Magnetic Resonance Spectroscopy. Accounts of Chemical Research *8*, 70-80.

McCoy, A.J., Grosse-Kunstleve, R.W., Adams, P.D., Winn, M.D., Storoni, L.C., and Read, R.J. (2007). Phaser crystallographic software. J Appl Crystallogr *40*, 658-674.

Mildvan, A.S., Xia, Z., Azurmendi, H.F., Saraswat, V., Legler, P.M., Massiah, M.A., Gabelli, S.B., Bianchet, M.A., Kang, L.W., and Amzel, L.M. (2005). Structures and mechanisms of Nudix hydrolases. Arch Biochem Biophys *433*, 129-143.

Oda, Y., Yamazaki, T., Nagayama, K., Kanaya, S., Kuroda, Y., and Nakamura, H. (1994). Individual ionization constants of all the carboxyl groups in ribonuclease HI from Escherichia coli determined by NMR. Biochemistry *33*, 5275-5284.

Otwinowski, Z., and Minor, W. (1997). Processing of X-ray diffraction data collected in oscillation mode. Macromolecular Crystallography, Pt A *276*, 307-326.

Piccirillo, C., Khanna, R., and Kiledjian, M. (2003). Functional characterization of the mammalian mRNA decapping enzyme hDcp2. RNA *9*, 1138-1147.

Rapp, C., Klerman, H., Levine, E., and McClendon, C.L. (2013). Hydrogen bond strengths in phosphorylated and sulfated amino acid residues. PLoS One *8*, e57804.

Rissland, O.S., and Norbury, C.J. (2009). Decapping is preceded by 3' uridylation in a novel pathway of bulk mRNA turnover. Nat Struct Mol Biol *16*, 616-623.

Schier, A.F. (2007). The maternal-zygotic transition: death and birth of RNAs. Science *316*, 406-407.

She, M., Decker, C.J., Chen, N., Tumati, S., Parker, R., and Song, H. (2006). Crystal structure and functional analysis of Dcp2p from Schizosaccharomyces pombe. Nat Struct Mol Biol *13*, 63-70.

She, M., Decker, C.J., Svergun, D.I., Round, A., Chen, N., Muhlrad, D., Parker, R., and Song, H. (2008). Structural basis of dcp2 recognition and activation by dcp1. Mol Cell *29*, 337-349.

Shen, B., and Goodman, H.M. (2004). Uridine addition after microRNA-directed cleavage. Science *306*, 997.

Song, M.G., and Kiledjian, M. (2007). 3' Terminal oligo U-tract-mediated stimulation of decapping. RNA *13*, 2356-2365.

Song, M.G., Li, Y., and Kiledjian, M. (2010). Multiple mRNA decapping enzymes in mammalian cells. Mol Cell *40*, 423-432.

Sprangers, R., and Kay, L.E. (2007). Quantitative dynamics and binding studies of the 20S proteasome by NMR. Nature *445*, 618-622.

Stevens, A., and Maupin, M.K. (1987). A 5'----3' exoribonuclease of Saccharomyces cerevisiae: size and novel substrate specificity. Arch Biochem Biophys *252*, 339-347.

Sweet, T., Kovalak, C., and Coller, J. (2012). The DEAD-box protein Dhh1 promotes decapping by slowing ribosome movement. PLoS Biol *10*, e1001342.

Waley, S.G. (1975). The pH-dependence and group modification of beta-lactamase I. Biochem J *149*, 547-551.

Wang, Z., Jiao, X., Carr-Schmid, A., and Kiledjian, M. (2002). The hDcp2 protein is a mammalian mRNA decapping enzyme. Proc Natl Acad Sci U S A *99*, 12663-12668.

Wang, Z., and Kiledjian, M. (2001). Functional link between the mammalian exosome and mRNA decapping. Cell *107*, 751-762.

Zhang, M., and Vogel, H.J. (1993). Determination of the side chain pKa values of the lysine residues in calmodulin. J Biol Chem *268*, 22420-22428.

SUPPLEMENTARY INFORMATION

Active site conformational dynamics are coupled to catalysis in the mRNA decapping enzyme Dcp2

Robin Aglietti, Stephen Floor, Chris McClendon, Matthew Jacobson and John Gross

*This work was previously published in *Structure*, 21 (9), 1571-80, 2013, and is reprinted here with permission.

Figure S1. Dcp2 mutant crystal structure comparisons to wild-type Dcp2 catalytic domain. Related to Figure 1. **(A)** Active site overlay of the two chains in the crystal structure of E198Q with the wild-type crystal structure. Chain A is shown in navy, chain B is shown in light blue, and wild-type is in green with the Mg2+ ion in black. The four active site glutamates E149, E152, E153, and E198 (or E198Q in the mutant structures) and K135 are shown as sticks. **(B)** Overlay of the wild-type Dcp2 structure with the three chains in the asymmetric unit of the E153Q structure. Wild-type Dcp2 is colored green, and chains A-C of the E153Q structure are colored in dark purple, amethyst and lavender respectively. Each magnesium ion is shown as a sphere in the corresponding color. Residues E149, E152, E153 (or E153Q), E198, and K135 are shown as sticks. **(C)** Comparison of the 2 chains in the E198Q structure to the wild-type structure. The c-alpha root-mean-square deviation (RMSD) for E198Q as compared to the wild-type structure is plotted by residue number, with chain A in navy and chain B in light blue. **(D)** Comparison of the 3 chains in the E153Q structure with the wild-type structure. The c-alpha root-mean-square deviation (RMSD) for each residue of E153Q as compared to wild-type is plotted by residue number. Chain A is shown in dark purple, chain B is shown in lavender, and chain C is shown in grey.

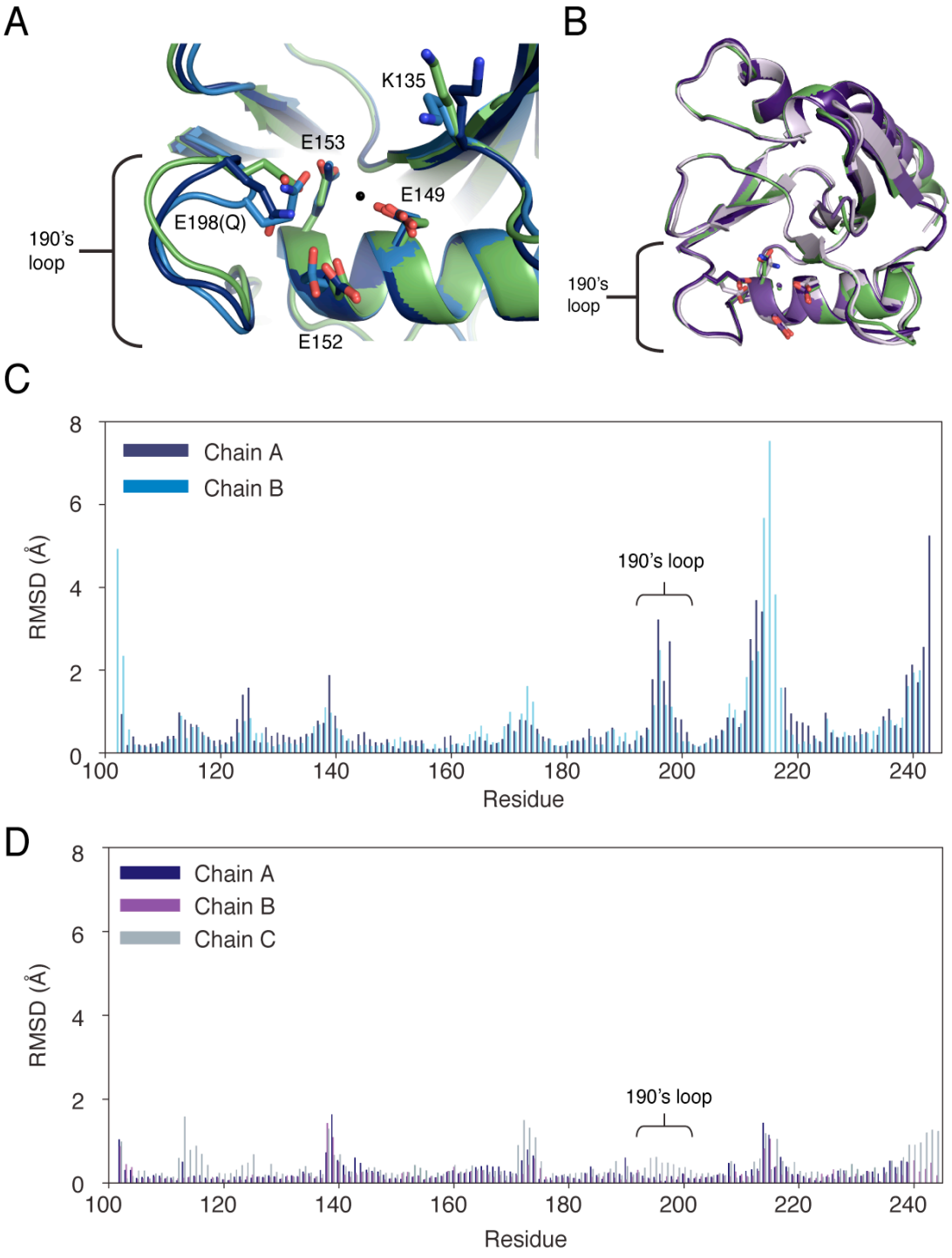
A
K135
E153
E149
E198(Q)
190's
loop
E152
B
190's
loop
C
Chain A
Chain B
190's loop
RMSD (Å)
Residue
D
Chain A
Chain B
Chain C
190's loop
RMSD (Å)
Residue

Figure S2. Representative decapping assay data for Dcp2 catalytic domain mutants. Related to Figure 3. **(A)** Representative timecourse for K135A data at pH 9.0, plotted as the fraction of total product released and the corresponding fit to obtain kobs. **(B)** Representative timecourse for K135A data at pH 6.5, plotted as the fraction of total product formed. Data was fit linearly and divided by an average endpoint for K135A at high pH to calculate k_{obs}. **(C)** Representative timecourse for E153Q data at pH 9.0, plotted as the fraction of total product formed and the corresponding fit to obtain k_{obs}. **(D)** Representative timecourse for E153Q at pH 7.0, plotted as the fraction of total product formed. Data was fit linearly and divided by an average endpoint for E153Q at high pH to calculate k_{obs}. **(E)** Incubation of decapping reaction products with nucleoside diphosphate kinase (NDPK), which catalyzes the conversion of nucleoside diphosphates to nucleoside triphosphates, identifies the middle spot as m7GDP and bottom spot as m7GTP. **(F)** Representative TLC plate for E198Q showing multiple products formed, indicated by 3 arrows. **(G)** Representative time course of the fraction of each E198Q product formed as a function of time. Bottom product is in green, middle product is in blue, top product is in black, and combined total product formed is in red. Fits shown are the single exponential fits used to obtain the individual k_{obs} for each product.

A

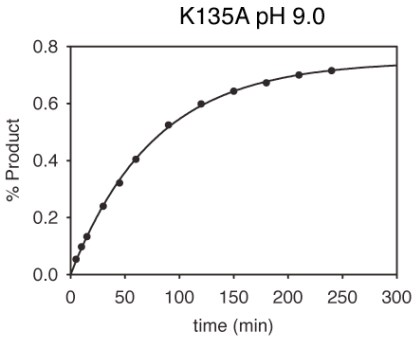
K135A pH 9.0
% Product
time (min)

B

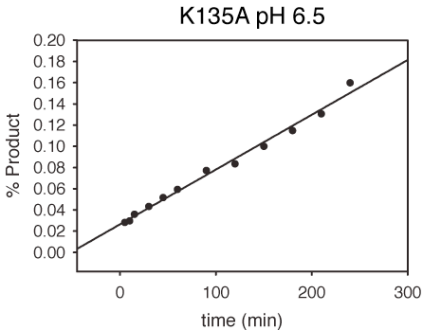
K135A pH 6.5
% Product
time (min)

C

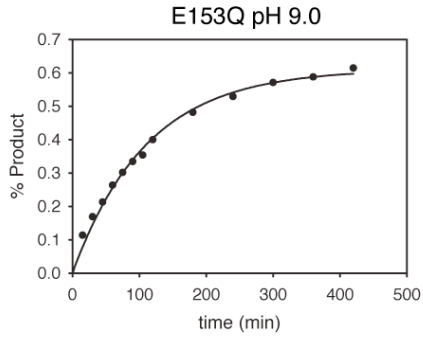
E153Q pH 9.0
% Product
time (min)

D

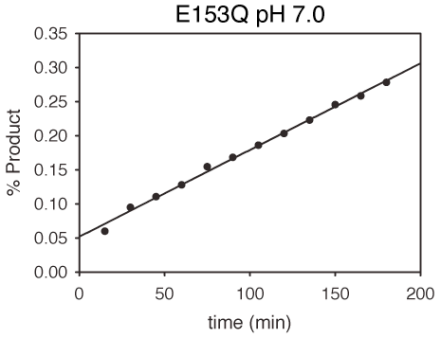
E153Q pH 7.0
% Product
time (min)

E

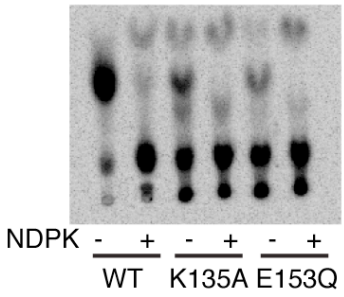
NDPK - + - + - +
WT K135A E153Q

F

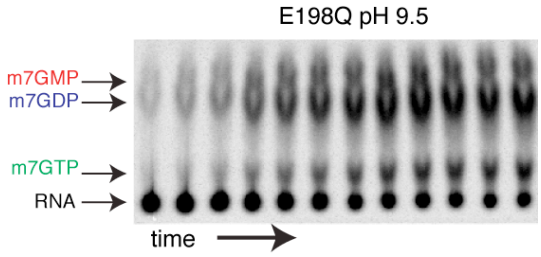
E198Q pH 9.5
m7GMP
m7GDP
m7GTP
RNA
time

G

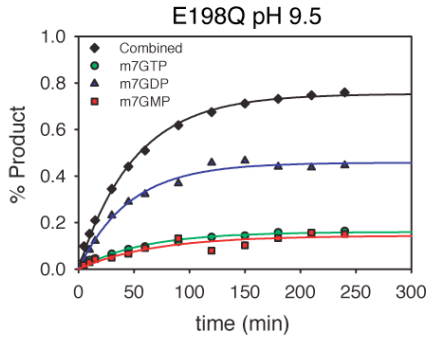
E198Q pH 9.5
Combined
m7GTP
m7GDP
m7GMP
% Product
time (min)

Figure S3. Conserved residue I199 is dynamically active. Related to Figure 4. **(A)** ^{13}C-^{1}H HSQC of the Dcp2 catalytic domain methyl labeled on Ile, Leu and Val residues at pH 7.0 is well resolved with homogenous peak intensity with the exception of I199. **(B)** A sequence alignment of the 190's loop (including I199 in *S. cerevisiae)* of Dcp2 from seven organisms and fellow Nudix family members NUDT16, ADPRP and MutT showing conserved residues unique to Dcp2.

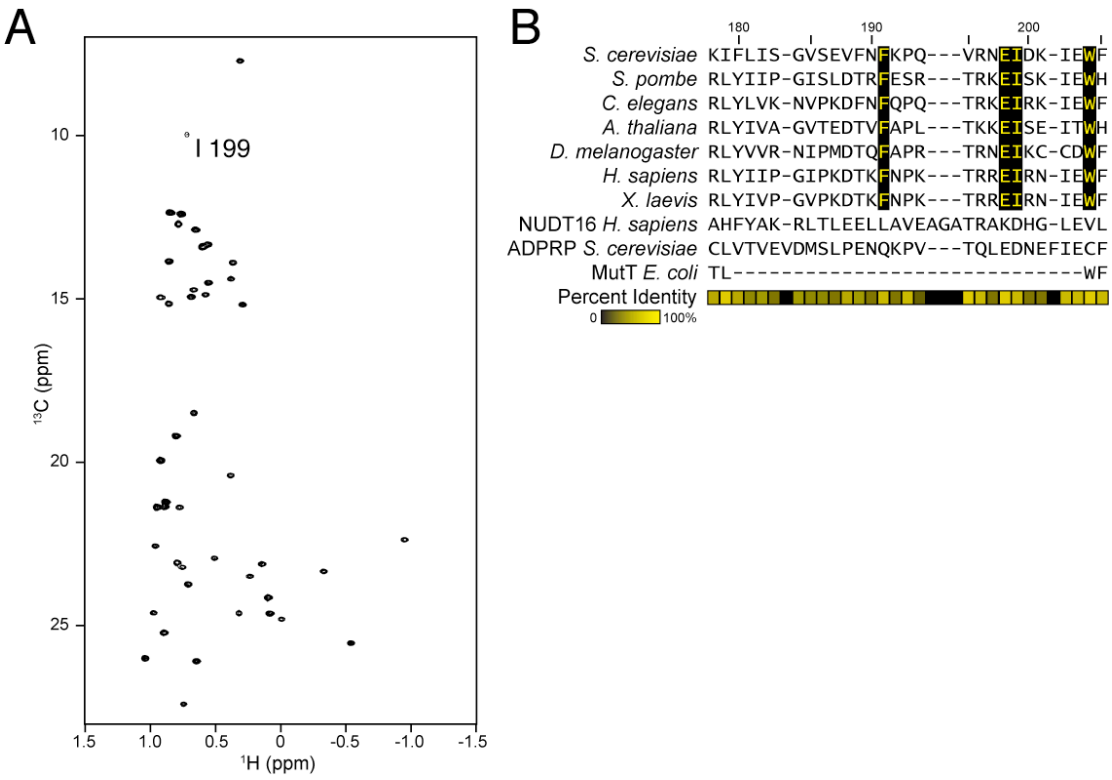

Figure S4. Catalytic glutamate mutants are intermediates between the neutral and low pH states. Related to Figure 5. **(A)** Overlay of four 13C-1H HSQC spectra: wild-type Dcp2 at pH 7.1 (grey), wild-type Dcp2 at pH 5.0 (green), E198Q Dcp2 at pH 7.0 (blue), and E153Q Dcp2 at pH 7.0 (purple). Small deviations form the collinearity observed between wild-type, E198Q, and E153Q may reflect chemical shift changes caused by the point mutation itself. **(B)** The difference in chemical shift between wild-type Dcp2 at pH 7.0 and wild-type Dcp2 at pH 5.0 (green), Dcp2 E153Q (purple), and Dcp2 E198Q (blue). Collinear peaks are indicated by arrows, while I110, I136, and L235 are only affected by pH but not mutation.

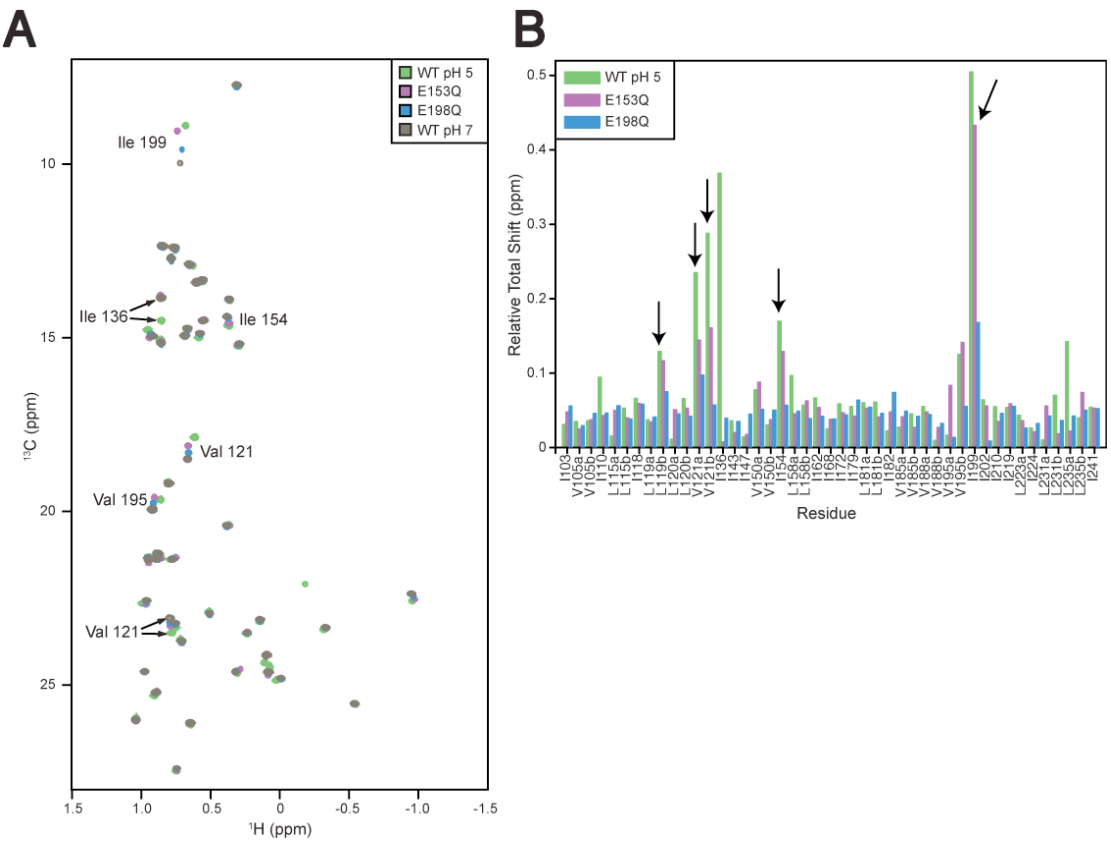

Figure S5. Molecular dynamics simulations show the 190's loop conformation is coupled to the protonation state of the general base. Related to Figure 6. **(A-B)** Shown are snapshots from the final state of each of six simulations of *S. cerevisiae* Dcp2 catalytic domain with protonated (A) or charged (B) E153. In each panel I199 is blue and V121 is red. Qualitatively, the 190's loop is more flexible in the simulation where E153 is charged, consistent with the *S. pombe* results in Figure 6. However, these simulations were less stable than the *S. pombe* simulations as evident from the poor alignment of the Nudix helix (green) and the 200's helix responsible for RNA binding in back, which led to issues in quantification. **(C-D)** Histograms of the distance between the alpha-carbons of either E147 and E192 (C) or E147 and I193 (D) when the general base 147 is protonated (low pH), mutated to glutamine (E147Q), or charged (high pH) for *S. pombe* Dcp2. The ordinate of all histograms is probability density per bin; $n \approx 600{,}000$ per histogram. Residues E147, E192, and I193 in *S. pombe* are *S. cerevisiae* E153, E198 and I199 respectively.

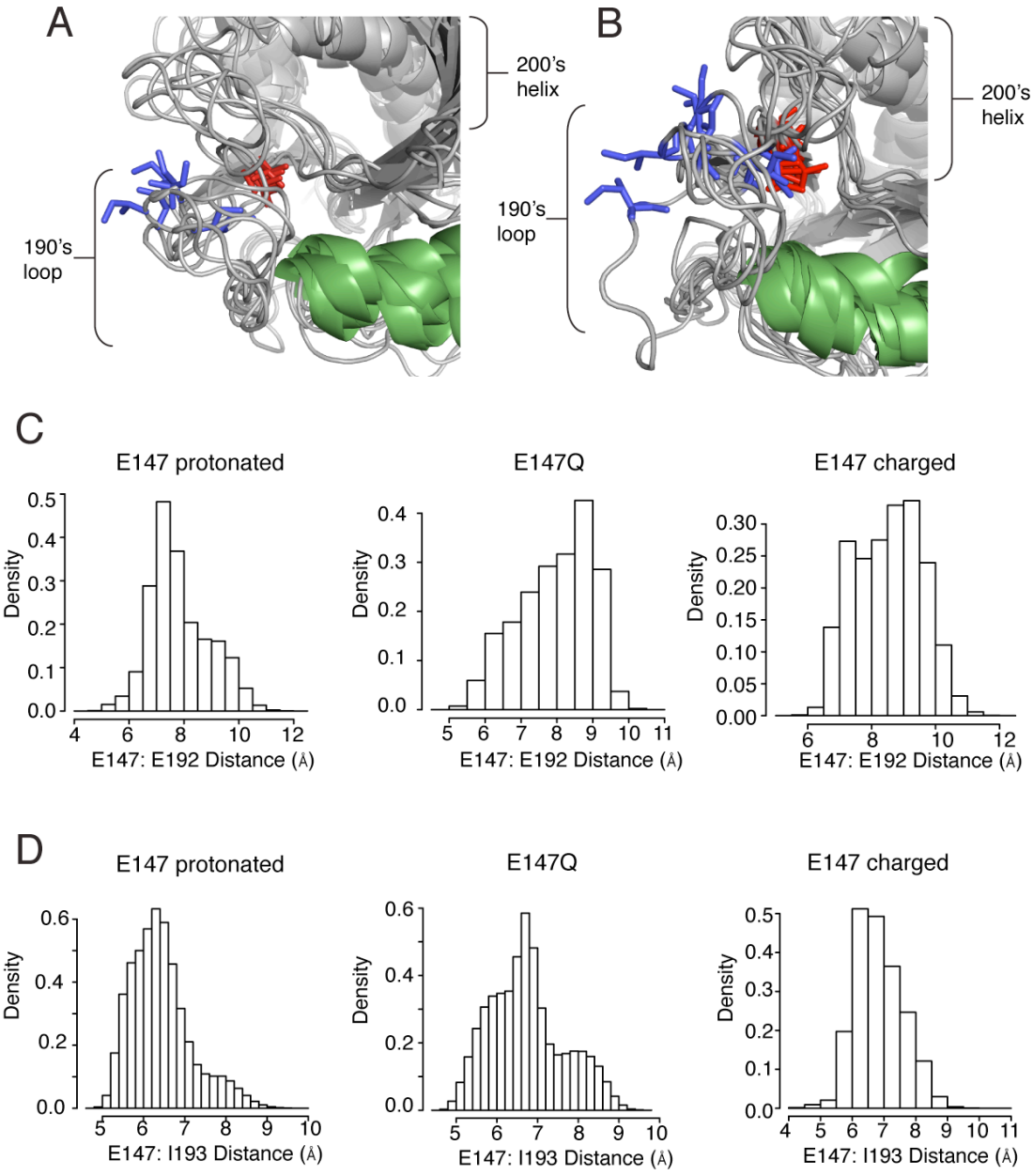
A
200's helix
190's loop
B
200's helix
190's loop
C
E147 protonated
E147Q
E147 charged
Density
E147: E192 Distance (Å)
D
E147 protonated
E147Q
E147 charged
Density
E147: I193 Distance (Å)

TABLES

Table S1: Product ratios of Dcp1/Dcp2 mutations. Relative percentages were calculated by averaging all endpoints for each mutation across all pH values fit using a single exponential to calculate k_{obs}. Standard deviation is shown in parenthesis. Related to Figure 3.

	% m7GTP	**% m7GDP**	**%m7GMP**
K135A	20.6 (0.9)	52.6 (1.5)	26.9 (0.6)
E153Q	61.6 (1.3)	32.5 (1.2)	6.0 (0.6)
E198Q	22.8 (2.3)	63.1 (3.3)	15.4 (5.1)

Table S2: Mutation of active site residues results in multiple products formed at the same rate. The mean individual rates of each product formed by K135A, E153Q and E198Q at pH 9.0. Standard deviation for at least 3 separate experiments is shown in parenthesis. Related to Figure 3.

	k_{obs} m7GTP (min^{-1})	**k_{obs} m7GDP (min^{-1})**	**k_{obs} m7GMP (min^{-1})**	**k_{obs} combined (min^{-1})**
K135A	0.035 (3.6e-3)	0.037 (1.4e-3)	0.034 (2.3e-3)	0.036 (1.6e-3)
E153Q	0.010(5.3e-3)	0.010(4.6e-3)	0.012(1.4e-2)	0.010(4.9e-3)
E198Q	0.012 (0.8e-3)	0.011 (2.2e-3)	0.005 (2.5e-3)	0.010 (0.8e-3)

SUPPLEMENTAL EXPERIMENTAL PROCEDURES

Multiple Sequence Alignments: Sequences for Dcp2 and other Nudix hydrolases were retrieved from the NCBI and aligned using MUSCLE (Edgar, 2004). Alignments were visualized using JALVIEW (Waterhouse et al., 2009). Alignments were performed with Dcp2 from *S. cerevisiae*, *S. pombe*, *Caenorhabditis elegans*, *Arabidopsis thaliana*, *Drosophila melanogaster*, *Homo sapiens*, *Xenopus laevis*, *Mus musculus* and *Danio rerio*, along with NUDT16 from *H. sapiens*, ADP-ribose pyrophosphatase from *S. cerevisiae* and MutT from *E. coli*.

Molecular Dynamics: Simulations were prepared using Maestro (Maestro-Desmond Interoperability Tools, version 2.4, Schrödinger, New York, NY, 2010). Preparation included addition of hydrogens and closure of missing loops using Schrodinger's PRIME software, which provided a front-end interface to the PLoP software package. Simulations were 100 ns in duration each and performed using Desmond (Bowers et al., 2006) on the Texas Advanced Computing Center's Ranger supercomputer. Molecular dynamics simulations in explicit solvent used the OPLS-AA/SPC forcefield (Berendsen et al., 1981; Kaminski et al., 2001). An orthorhombic simulation box was used with a buffer of 10 Å on each side. Na^+ and Cl^- ions were added to neutralize the system, then 0.5 M NaCl was added. After minimization and equilibration, six replicate production runs of 100 ns with different random seeds were performed on each system using the

Martyna-Tobias-Klein integrator (Martyna et al., 1994) at 300 K (Nose-Hoover thermostat (Hoover, 1985)) and 1 atm. Snapshots were output every 1.002 ps. All bonds involving hydrogens were constrained. A 2 fs time step for the bonded and short-range nonbonded interactions was used, and long-range nonbonded interactions were updated every 6 fs using the RESPA multiple time step approach (Tuckerman et al., 1992). Short-range coulombic and van der Waals nonbonded interactions were cut-off at 9.0 Å, and long-range electrostatics were computed using the smooth particle-mesh Ewald method. Pairlists were constructed using a distance of 10.5 Å and a migration interval of 12 ps. Results from the six replicate simulations were combined to generate the interatomic distance histograms using R.

SUPPLEMENTAL REFERENCES

Berendsen, H.J.C., Postma, J.P.M., van Gunsteren, W.F., and Hermans, J. (1981). Intermolecular Forces (Dordrecht, D. Reidel Publishing Company).

Bowers, K.J., Chow, E., Huafeng, X., Dror, R.O., Eastwood, M.P., Gregersen, B.A., Klepeis, J.L., Kolossvary, I., Moraes, M.A., Sacerdoti, F.D., *et al.* (2006). Scalable Algorithms for Molecular Dynamics Simulations on Commodity Clusters. Paper presented at: SC 2006 Conference, Proceedings of the ACM/IEEE.

Edgar, R.C. (2004). MUSCLE: multiple sequence alignment with high accuracy and high throughput. Nucleic Acids Res *32*, 1792-1797.

Hoover, W.G. (1985). Canonical dynamics: Equilibrium phase-space distributions. Physical Review A *31*, 1695–1697.

Kaminski, G.A., Friesner, R.A., Tirado-Rives, J., and Jorgensen, W.L. (2001). Evaluation and Reparametrization of the OPLS-AA Force Field for Proteins via Comparison with Accurate Quantum Chemical

Calculations on Peptidesâ€ The Journal of Physical Chemistry B *105*, 6474-6487.

Martyna, G.J., Tobias, D.J., and Klein, M.L. (1994). Constant pressure molecular dynamics algorithms. The Journal of Chemical Physics *101*, 4177-4189.

Tuckerman, M., Berne, B.J., and Martyna, G.J. (1992). Reversible Multiple Time Scale Molecular-Dynamics. J Chem Phys *97*, 1990-2001.

Waterhouse, A.M., Procter, J.B., Martin, D.M., Clamp, M., and Barton, G.J. (2009). Jalview Version 2--a multiple sequence alignment editor and analysis workbench. Bioinformatics *25*, 1189-1191.

CHAPTER 3

Exploring the link between mRNA decapping machinery and Upf1

Robin Aglietti, John Gross

INTRODUCTION

Nonsense mediated decay (NMD) is a major quality control pathway for eukaryotic cellular mRNAs, which targets mRNAs with a premature stop codon (PTC) for degradation. Substrates of NMD are often aberrant transcripts that have acquired nonsense mutations through errors in processing or transcription (He et al., 1993). Not only does this preserve cellular resources and avoid dominant negative effects of translating truncated versions of proteins, but there is some evidence of NMD being involved in more general cellular processes such as post-transcriptional regulation of gene expression and axon guidance (Colak et al., 2013; Lejeune and Maquat, 2005; Rehwinkel et al., 2006). NMD requires both general mRNA decapping machinery and the NMD specific factors Upf1, Upf2, and Upf3 (He et al., 1997; Serin et al., 2001), in addition to active mRNA translation (Amrani et al., 2006; Maquat, 2005). The Upf proteins directly interact to form the surveillance complex that is at the core of protein-protein interactions required for NMD (Figure 1).

In mammalian cells, NMD is thought to be triggered by a "pioneer round" of translation, dependent on recognition of the exon junction complex (EJC) by the Upf proteins (Ishigaki et al., 2001; Kurosaki and Maquat, 2013; Maquat, 2005). Consistent with this idea, Upf3 directly interacts with EJC components and is thought to bridge the surveillance complex to the EJC (Fribourg et al., 2003; Gehring et al., 2003; Kim et al., 2001; Lykke-Andersen et al., 2001; Singh et al.,

2007). However, the idea that the EJC and a pioneer round of translation play a crucial role in triggering NMD is not supported in *D. melanogaster*, *C. elegans*, or yeast (Gatfield et al., 2003; Longman et al., 2007).

Rather, at least for yeast, the distinction between normal and aberrant termination codons seems to be determined by the distance between the termination codon and the 3' mRNP, named the faux 3' UTR model (Amrani et al., 2004). This is supported by the report that mRNAs with extended 3' UTR's are substrates for NMD (Muhlrad and Parker, 1999). Furthermore, ribosomes encountering a PTC pause, fail to release, and reinitiate at upstream AUG sequences, suggesting that terminating ribosomes require a properly configured 3'-UTR to disengage and terminate translation (Amrani et al., 2004). Indeed, mRNAs with PTC's are stabilized if PAPB (Poly-A Binding Protein, normally found at the 3' end of mRNAs) is tethered downstream of the PTC, but this effect is lost in Upf1 knockout strains (Amrani et al., 2004). The faux-3' UTR model is not without faults, however: NMD has been observed to be independent of both an mRNA poly-A tail and the poly-A binding protein (Meaux et al., 2008).

Recently, a more universal hypothesis has been proposed with elements of both the EJC and faux 3'-UTR models, coined the "unified 3' UTR model" (Singh et al., 2008). In this model, recognition of a PTC is based on a balance between two opposing forces that affect the recruitment of the Upf surveillance complex to terminating ribosomes: factors that stimulate recruitment such as the EJC, and factors that

antagonize Upf protein recruitment like PABP. Such a balance between multiple, potentially redundant factors suggests a much more unified NMD mechanism across evolution and merges many of the conflicting observations between species.

Upf1, arguably the core NMD factor, consists of two main domains: an N terminal zinc finger domain (cysteine-histidine-rich CH domain), and a C terminal domain that is both a group 1 RNA helicase and an ATPase (Figure 2) (Czaplinski et al., 1995). Additionally, Upf1 associates with ribosomes through interaction with release factors to promote translational repression (Czaplinski et al., 1998; Ivanov et al., 2008; Kashima et al., 2006). The activity of Upf1 seems to be modulated by NMD factor Upf2, which binds to the Upf1 ring domain in a bipartite binding regime, suggesting a two-step binding mode consisting of both a high-affinity and low-affinity interaction (Clerici et al., 2009). The lower-affinity interaction is mutually exclusive with Upf1 intramolecular interactions between the ring domain and helicase domain observed in a recent Upf1/RNA co-crystal structure (Chakrabarti et al., 2011). When coupled with the observation that the Upf1 ring domain has a cis-inhibitory effect on the helicase domain activity, this suggests that Upf2 functions at least in part to stimulate the activity of the Upf1 helicase domain by alleviating inhibition via the ring domain (Chakrabarti et al., 2011; Chamieh et al., 2008; Kadlec et al., 2006). The specific role of Upf1's helicase/ATPase activity is not entirely clear, but it is required for functional NMD (Weng et al., 1996).

Once the Upf proteins target an mRNA for NMD, it is degraded by multiple pathways, including exosome-mediated 3'-5' decay (Cao and Parker, 2003; Mitchell and Tollervey, 2003) and 5'-3' exonucleolytic decay (Hagan et al., 1995; Muhlrad and Parker, 1994, 1999). Along these lines, several observations suggest a link between decapping and NMD factors. First, it has been reported that Upf1, Upf2, and Upf3 coimmunoprecipitate with several 5'-3' decay factors including the decapping enzyme Dcp2, decapping activator Dcp1, and 5'-3' exonuclease Xrn1 (Lejeune et al., 2003; Lykke-Andersen, 2002). Secondly, down regulation of Dcp2 in mammalian cells abrogates NMD (Lejeune et al., 2003). Furthermore, human proline-rich nuclear receptor co-regulatory protein 2 (PNRC2) has been shown to interact with both hUpf1 and Dcp1, linking NMD and decapping in mammals (Cho et al., 2009; Lai et al., 2012). However, such a link remains elusive in yeast.

Here, a direct interaction between the yeast decapping machinery and Upf1 is investigated. Multiple constructs of both *S. cerevisiae* and *S. pombe* Upf1 were generated and tested for expression. Soluble constructs were used to observe a preliminary direct interaction in GST pull-downs between the decapping machinery and the Upf1 ring domain, although attempts to map this interaction were not informative and did not seem to appreciably affect *in vitro* decapping rates. A 2-domain construct of *S. cerevisiae* Upf1 failed to corroborate the initial interaction in a specific, reproducible manner and was limited by low purification yields of Upf1. While it is possible

that a direct interaction between the decapping machinery and Upf1 exists in yeast, further biochemical studies with well-behaved, well-expressing constructs are needed.

RESULTS AND DISCUSSION

Design, Expression, and Purification of Upf1 CH Ring Domain Constructs

To undertake any biochemical interaction study requires one to have well-behaving stable constructs of the proteins in question. Thus, a series of constructs of both the *S. cerevisiae* and *S. pombe* Upf1 ring domain were cloned (Table 1). Three tagging strategies (6x-Histadine, Glutathione-s-transferase, and Thioredoxin) and multiple boundaries were chosen and tested for expression (Table 1). All constructs tested were observed at relatively low levels regardless of the solubility of the expressed protein, and most were insoluble and observed only in the pellet fractions of the expression tests. Additionally, some of the *S. pombe* constructs were tested for coexpression with Dcp2 (*S. pombe* constructs were chosen as *S. cerevisiae* Dcp2 cannot be expressed on it own), but none of the combinations tested yielded soluble protein (Table 2). The two most promising constructs, *S. cerevisiae* GST- (9-219) and GST- (9-223), were scaled up to a full purification (Figures 3, 4). The GST- (9-223) construct was slightly cleaner upon purification (as judged by coomassie staining) and was chosen to proceed with.

Functional Studies of *S. cerevisiae* CH Ring Domain

To test the idea that Upf1 might affect decapping rates by binding to Dcp2, we first turned to *in vitro* pull-downs to directly observe any potential interaction between the two proteins. Since Upf1 was conveniently GST tagged, it was used as bait in a series of GST pull-downs. First we tested the *S. cerevisiae* decapping complex Dcp1/Dcp2 (1-315), which was eluted upon addition of reduced glutathione only in the presence of the Upf1 ring domain (Figure 5). Since the C-terminal helix of Dcp2 has been shown to be important for coactivator binding (Harigaya et al., 2010), we also tested the decapping complex Dcp1/Dcp2 (1-245) and found it behaved similarly to the longer construct (Figure 6). Interestingly, no interaction was observed with either the Nudix domain (100-245) or regulatory domain of Dcp2 (1-102), or with Dcp1 alone (Figures 7-9).

To ask what affect this interaction might have on Dcp2 activity, we compared Dcp1/Dcp2 activity with and without Upf1 using an *in vitro* decapping assay. However, very little effect was observed upon addition of the Upf1 ring domain (Figure 10). Since Dcp1 binding to Dcp2 seemed to be mutually exclusive with Upf1 binding (Figures 5,6), we hypothesized that any affect of Upf1 would be inhibited by increasing amounts of Dcp1 to yield a dosable response. We therefore repeated the decapping assay with Dcp2 and Upf1 with increasing amounts of Dcp1, but no effect was observed (data not shown). Given that these preliminary experiments were done using a single domain

of Upf1, we hypothesized that perhaps we needed both domains of Upf1 to affect decapping. We therefore turned our attention to more complete constructs of Upf1.

Design, Expression, and Purification of Upf1 CH-Helicase Constructs

Upf1 has a large helicase domain in addition to the CH ring domain, and it is possible that intra-molecular interactions or allostery between the two domains may affect any interactions with Dcp2. To account for this possibility, we took advantage of a generous gift from Dr. Elena Conti's lab at the Max Planck Institute of two constructs of *S. cerevisiae* Upf1, one containing both the CH domain and helicase domain (54-851) fused with a GST solubility tag, and a second construct consisting of just the helicase domain (221-851) and GST tag. These constructs were expressed and purified in a similar manner to previous publications (see experimental procedures; Chakrabarti et al., 2011). The purification was consistent but inefficient, and typically yielded a substantial fraction of improperly folded Upf1 that was separated via heparin resin (Figures 11-16).

Functional Studies of *S. cerevisiae* 2-Domain Upf1 Constructs

To directly assay the binding of the two-domain construct of Upf1 to Dcp2, we performed GST pull-downs with Upf1 (GST-Upf1 54-851) as bait and the decapping complex Dcp1/Dcp2 (1-315) as prey (Figure 17). However, unlike the pull-downs with the Upf1 ring domain in isolation (Figures 5, 6), no interaction was observed. Since it is

possible the helicase domain might have multiple conformations with varying affinities for Dcp2, we repeated the experiment in the presence of 2 mM ATP, but again no interaction was observed (Figure 18).

Because a negative pulldown result could mask an interaction with only a small portion of Upf1/Dcp2 caused by a low affinity, we turned to a functional assay to look for any affect of Upf1 binding on Dcp2 activity. We monitored decapping activity on an RNA with a ^{32}P labeled 5'-cap in the presence of increasing amounts of either the Upf1 2-domain construct (GST-Upf1 54-851) or the helicase domain (GST-Upf1 221-851) as a negative control for Upf1 ring-domain binding to Dcp2 (Figure 19). Although a dose-dependent effect was observed on the endpoint of these reactions, it was not specific to the presence of the ring domain, and is most likely a non-specific RNA-binding effect. These experiments were repeated in the presence of ATP, but the decapping reaction was inhibited even in a control without Upf1, and was not conclusive (data not shown).

Since the N-terminal boundary of the 2-domain construct (GST-Upf1 54-851) was significantly shorter than the ring domain construct used for the initial interaction studies, we cloned, expressed, and purified a longer 2-domain construct of Upf1 that included the N-terminal residues (GST-Upf1 9-851). This construct was expressed and purified using the same protocol as the GST-Upf1 (54-851) construct, but was not stable without the GST-solubility tag (data not shown), so the tag was left on for subsequent purifications. Even with the solubility tag, it was consistently much dirtier and more prone to

degradation than either the 2-domain construct (GST-Upf1 54-851) or the helicase domain (GST-Ufp1 221-851) (Figures 20, 21), consistent with the Upf1 ring domain's instability and poor behavior in isolation. We repeated the GST pull-downs with Dcp1/2 (1-315) and this longer Upf1 construct, and observed a faint band for Dcp2 via coomassie staining (Figure 22). Western blotting revealed a band of Dcp2 in the elution fraction, but was also observed in a control pulldown using the Upf1 helicase domain construct as well as at longer exposures of the Dcp1/2 negative control (Figure 23).

The observation that Dcp2 appears in the elutions of these controls suggests that the positive pulldown result is likely non-specific. Since Dcp2 and both constructs of Upf1 all bind RNA, it is quite possible that the observed interaction is RNA mediated. Repeating the pulldown experiments here with RNase would answer this question. And even if the interaction is RNA dependent, there is likely a link between NMD factors and the decapping complex in yeast, whether mediated through a PNRC2-like protein or another as-of-yet undiscovered mechanism.

FIGURES

Figure 1: Schematic representation of the Upf proteins in the NMD surveillance complex. Upf1 is comprised of two domains: a ring domain that binds to Upf2 and an ATPase/helicase domain. Upf2 has three MIF4G domains and binds to both Upf1 and Upf3, while Upf3 has an RNA binding domain (RBD) and binds to Upf2.

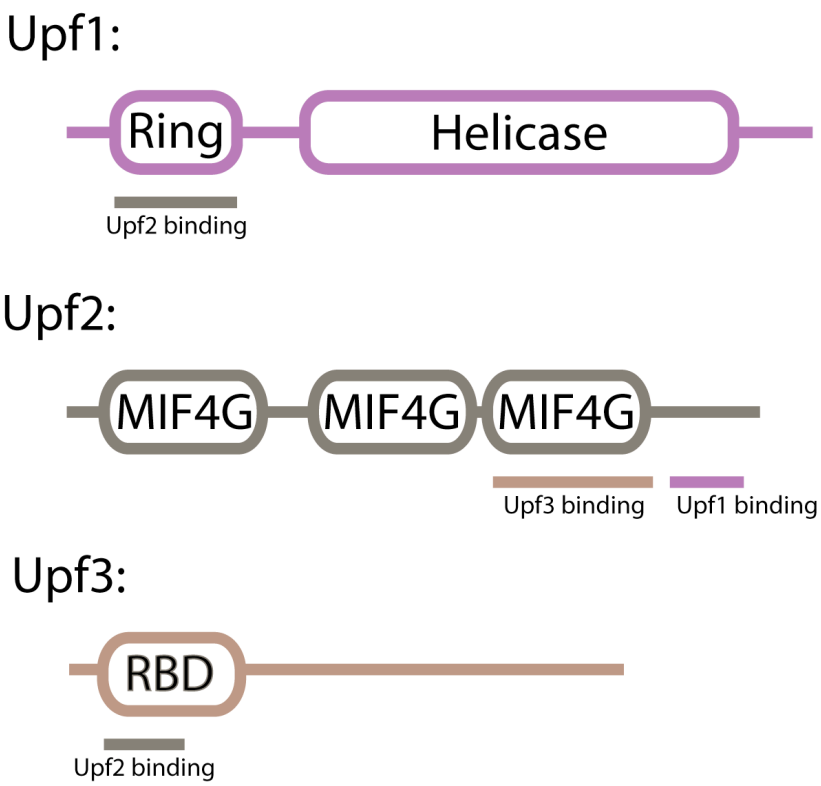

Figure 2: Crystal structure of Upf1 and Upf2 complex illustrating Upf1 domain architecture. The two domains of Upf1 are shown in purple with the 3 ring domain zinc ions as black spheres. Fragments of Upf2 are shown in grey bound to the ring domain of Upf1. Adapted from pdb entry 2WJV (Clerici et al., 2009).

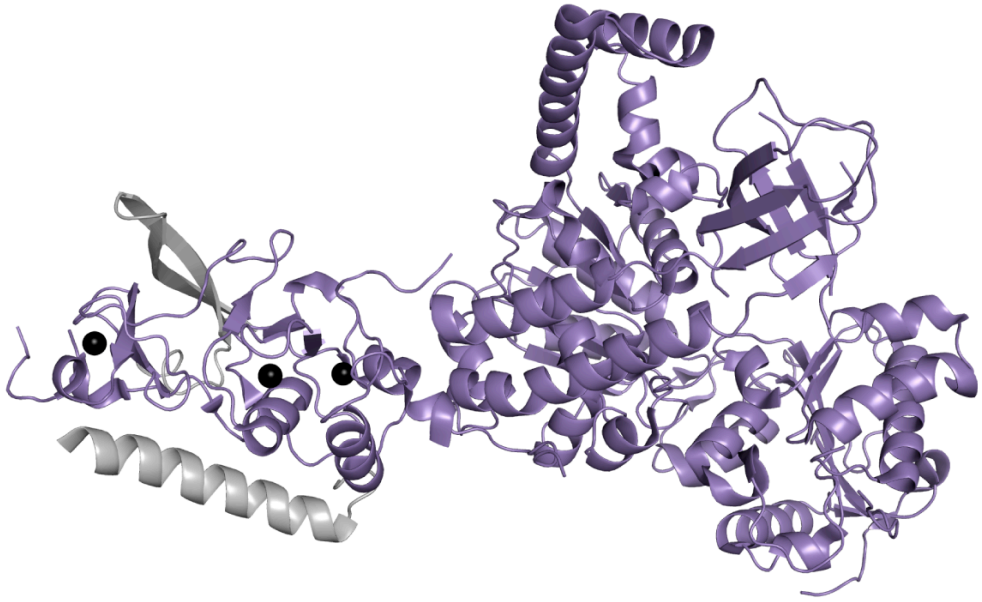

Figure 3: Coomassie stained expression test SDS page gel of GST-Upf1 (9-219) and GST-Upf1 (9-223) with molecular weights of 50 and 51 kDa respectively. Shown are the supernate and pellet fractions of uninduced cells, 15 ˚C induction, and 37 ˚C induction of both constructs.

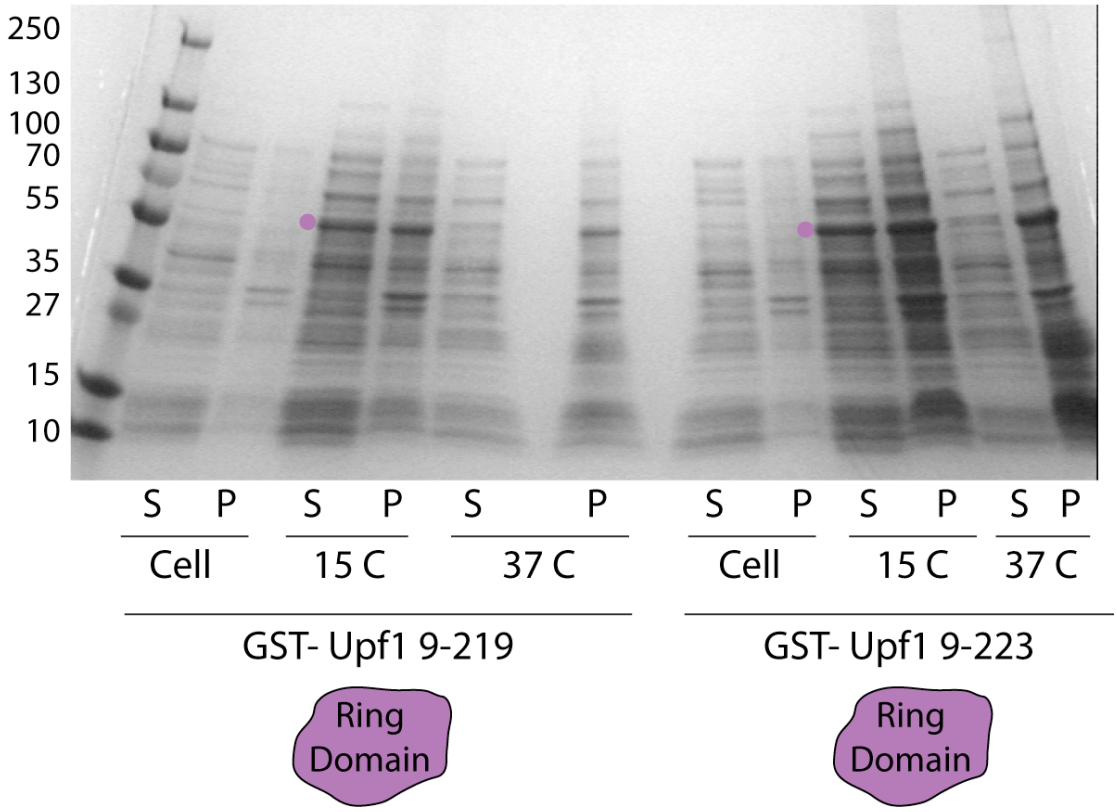

Figure 4: Coomassie stained SDS page gel of nickel purification fractions of GST-Upf1 (9-219) and GST-Upf1 (9-223) (50 and 51 kDa respectively) from a 1 L prep. FT = flow through, W = wash, and E = elution fractions.

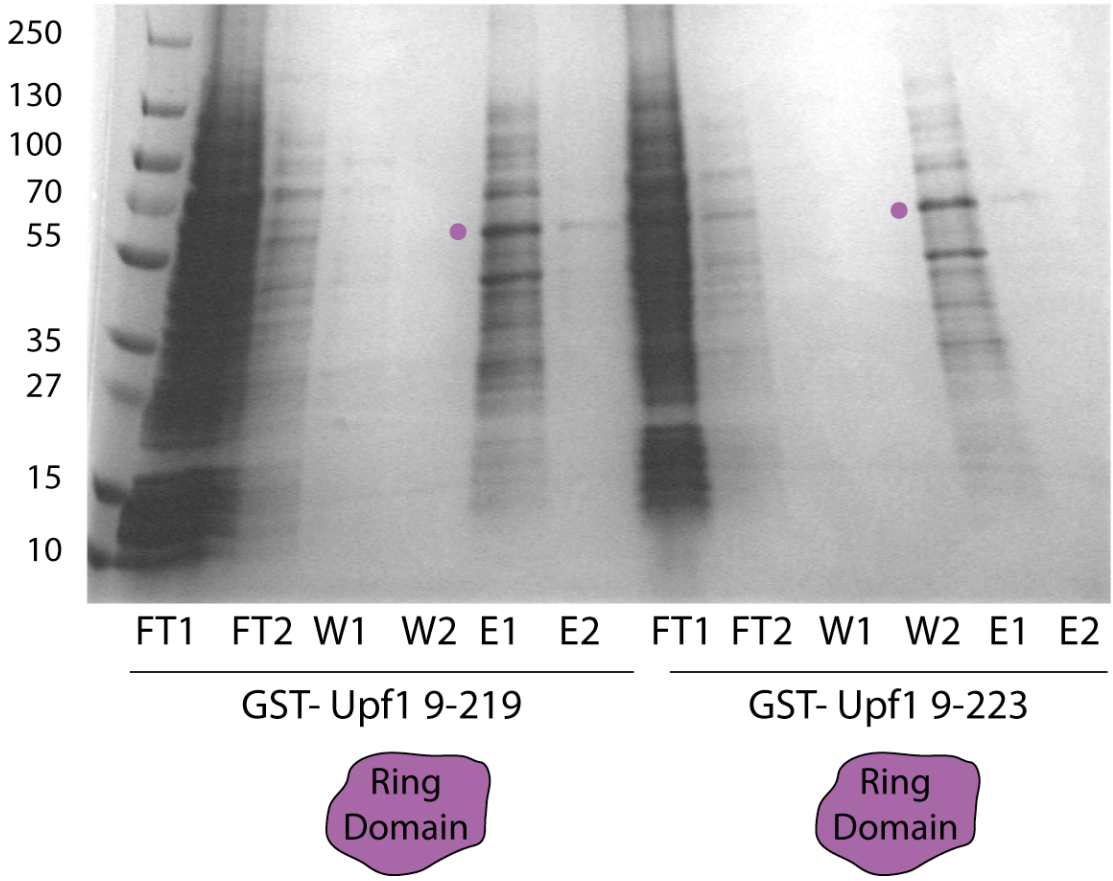

Figure 5: GST pulldown with Upf1 ring domain and decapping complex. **(A)** Coomassie stained SDS-page gel of a pulldown with 3 uM GST-Upf1 (9-223) and 60 uM Dcp1/2 (1-315) shows a Dcp2 band upon elution. **(B)** Negative control with 60 uM Dcp1/2 (1-315) only.

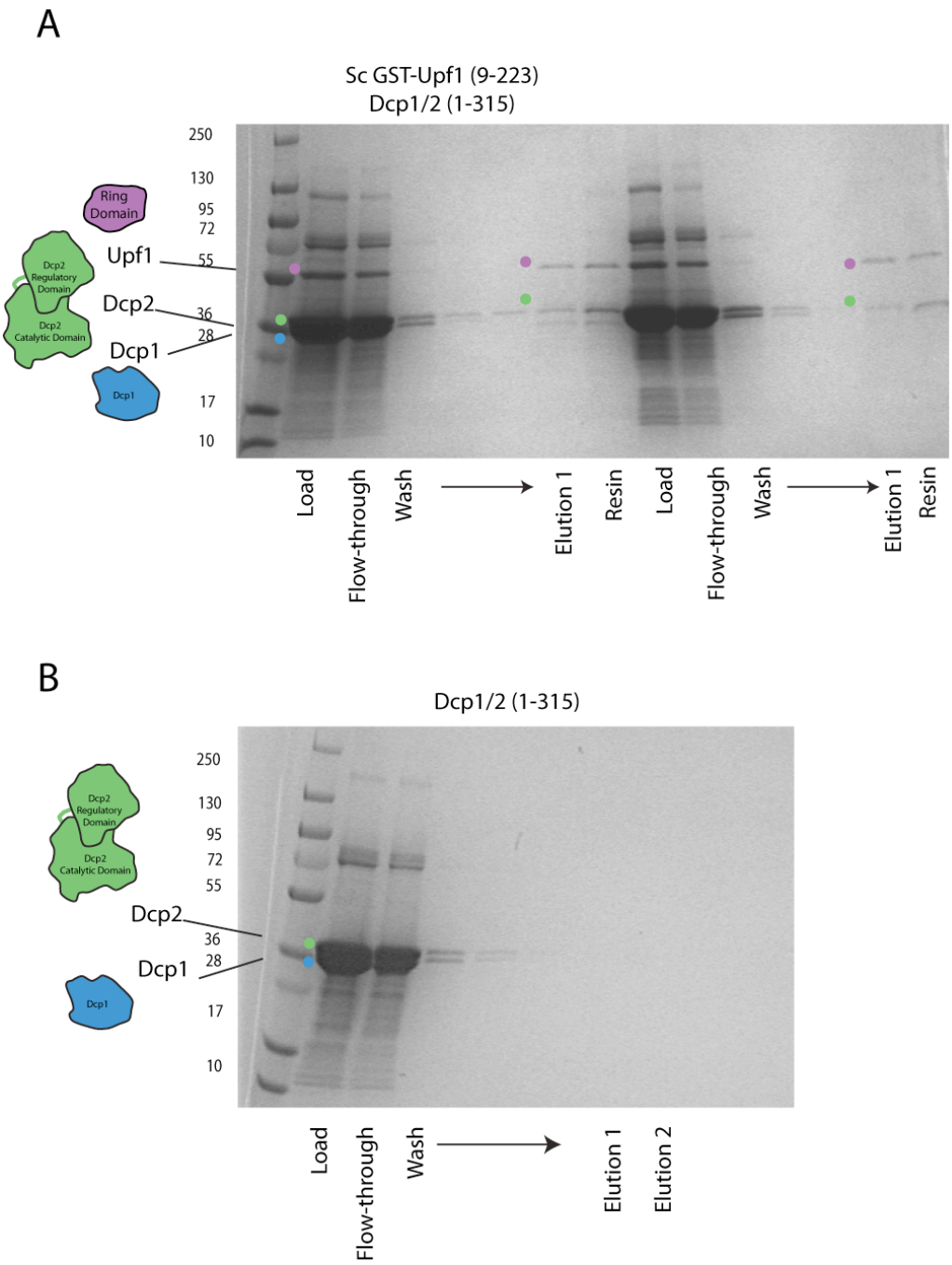

Figure 6: GST pulldown with Upf1 ring domain and decapping complex. **(A)** Coomassie stained SDS page gel of 3 uM GST-Upf1 (9-223) and 60 uM Dcp1/2 (1-245) pulldown shows elution of Dcp2 with Upf1 ring domain. **(B)** Negative control with 60 uM Dcp1/2 (1-245) only.

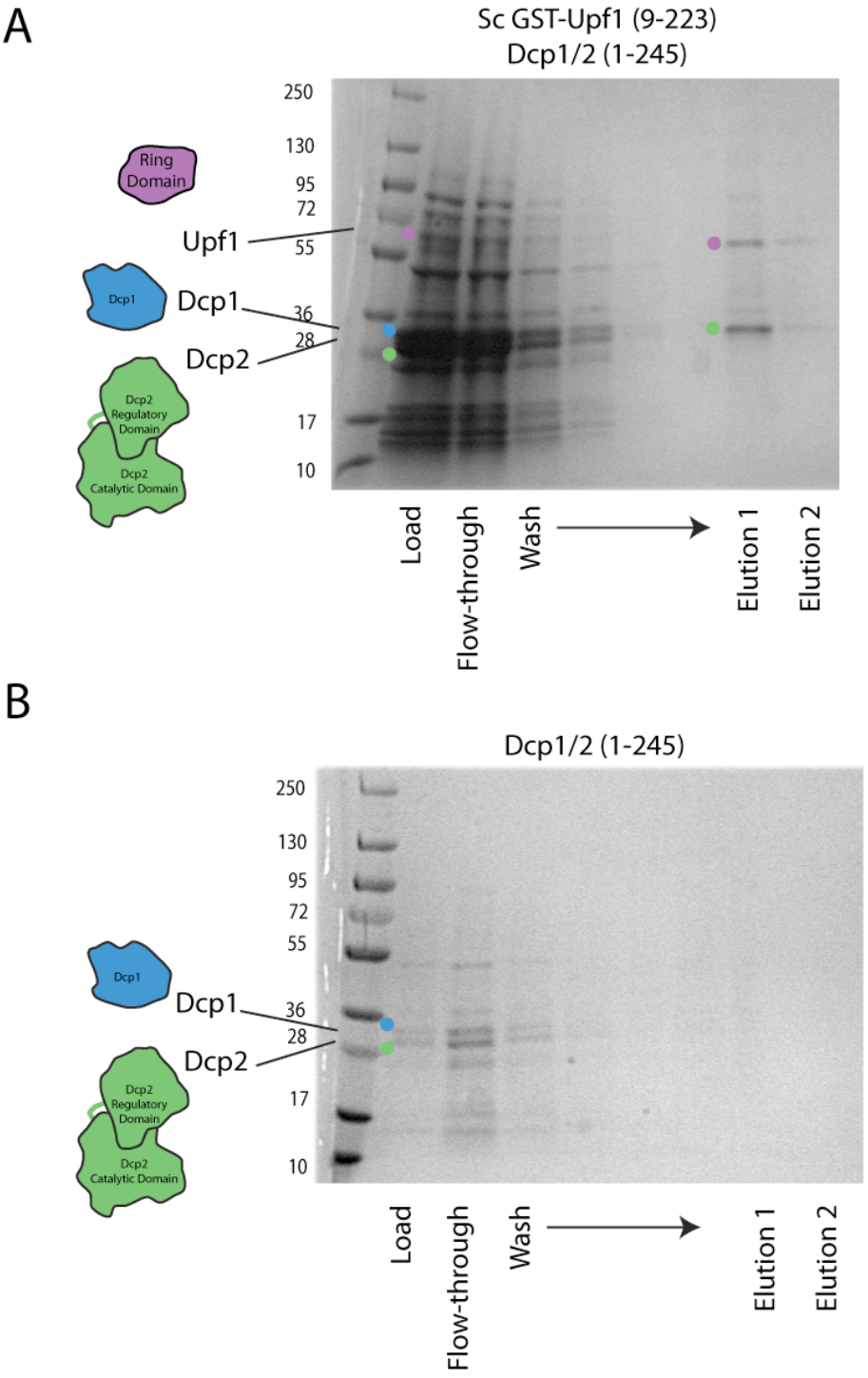

Figure 7: GST pulldown with Upf1 ring domain and Dcp2 catalytic Nudix domain shows no interaction. **(A)** Coomassie stained SDS page gel of pulldown with 3 uM GST-Upf1 (9-223) and 60 uM Dcp2 (100-245). **(B)** Negative control with 60 uM Dcp2 (100-245) only.

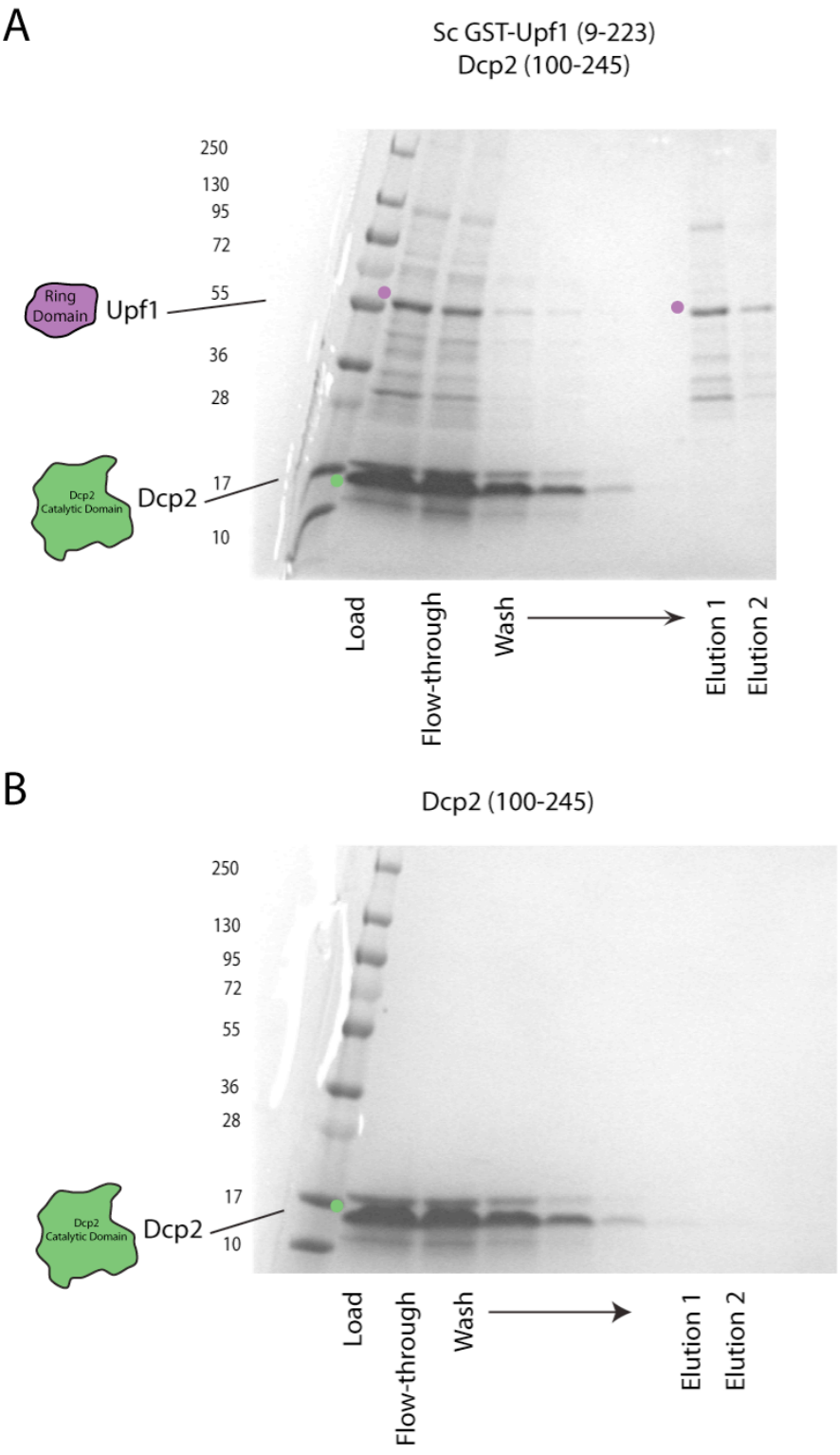

Figure 8: GST pulldown with Upf1 ring domain and Dcp2 regulatory domain shows no interaction. Pictured is a coomassie stained SDS page gel of a GST pulldown with 3 uM GST-Upf1 (9-223) and 60 uM Dcp1/Dcp2 (1-102).

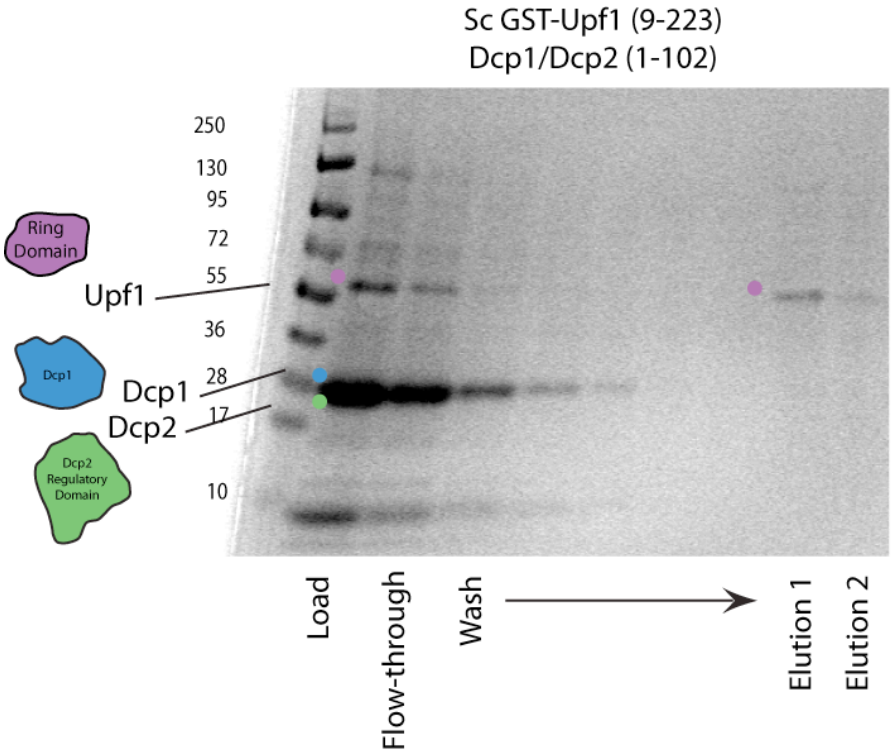

Figure 9: GST pulldown with Upf1 ring domain and Dcp1. **(A)** Coomassie stained SDS page gel of 3 uM GST-Upf1 (9-223) and 60 uM Dcp1 pulldown shows no interaction. **(B)** Negative control with 60 uM Dcp1 only.

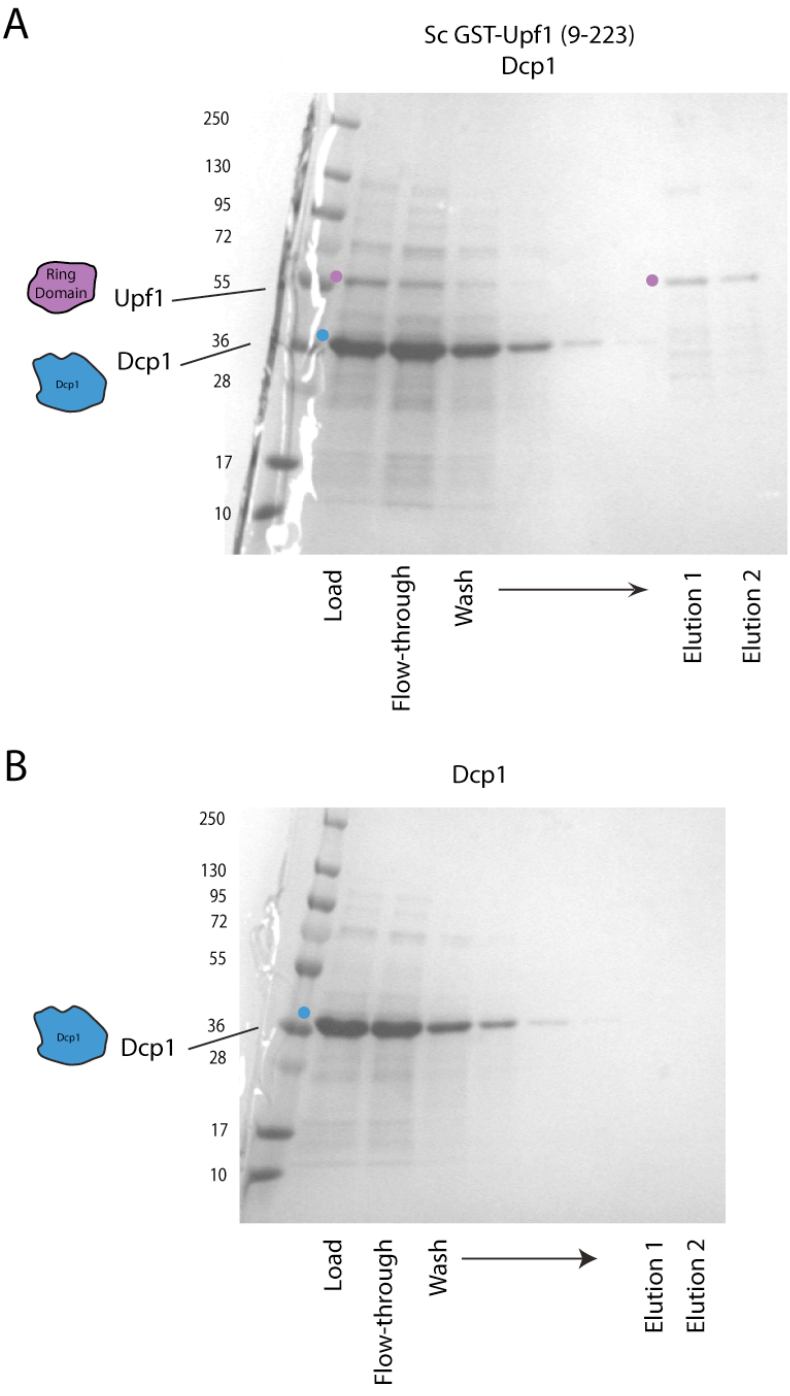

Figure 10: Upf1 ring domain shows no affect on Dcp2 activity. *In vitro* decapping assay with 50 nM Dcp1/Dcp2 (1-315) and 1 uM Upf1 (9-219) as visualized on a TLC plate.

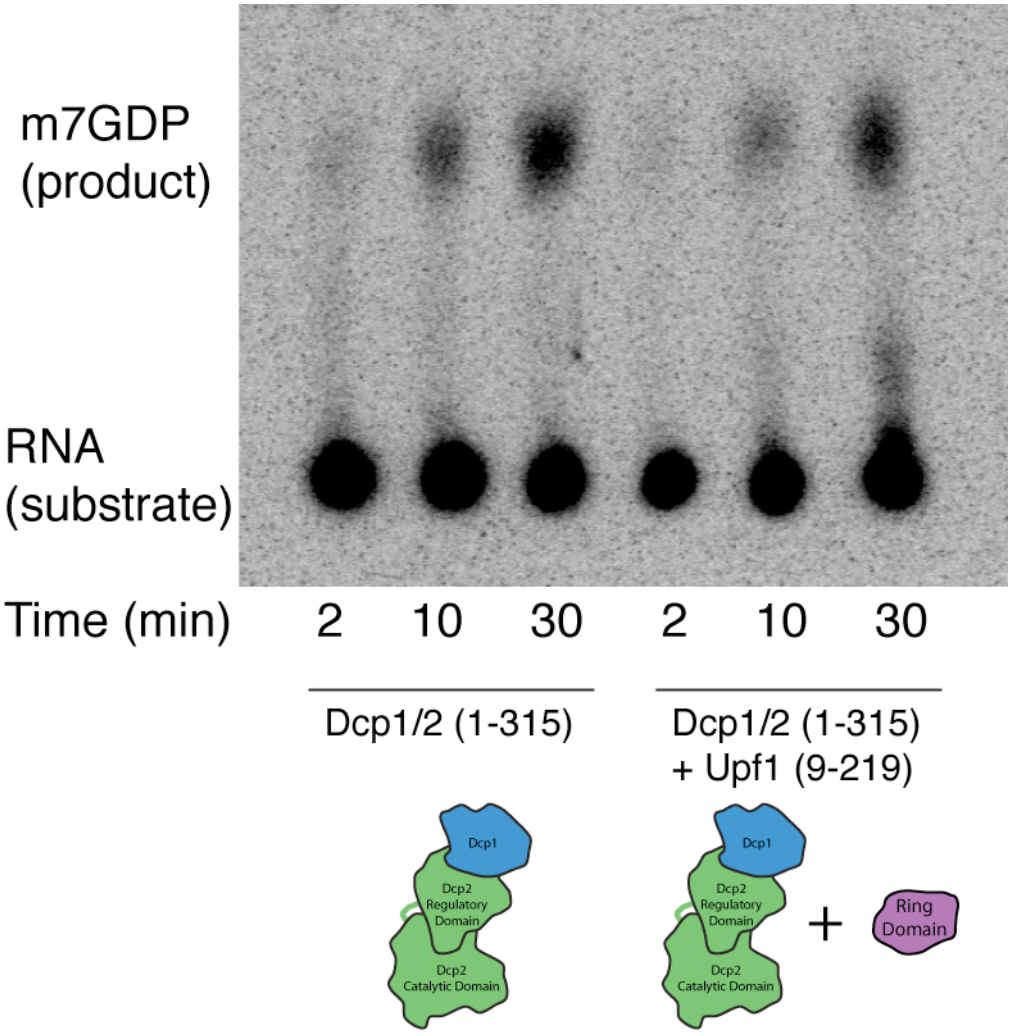

Figure 11: Coomassie stained SDS page gel of purification and cleavage of GST-Upf1 (54-851). Briefly, GST-Upf1 was purified by GST-affinity resin, separated from the GST solubility tag by TEV protease, and further purified over a heparin column (see Figure 12, Experimental Procedures).

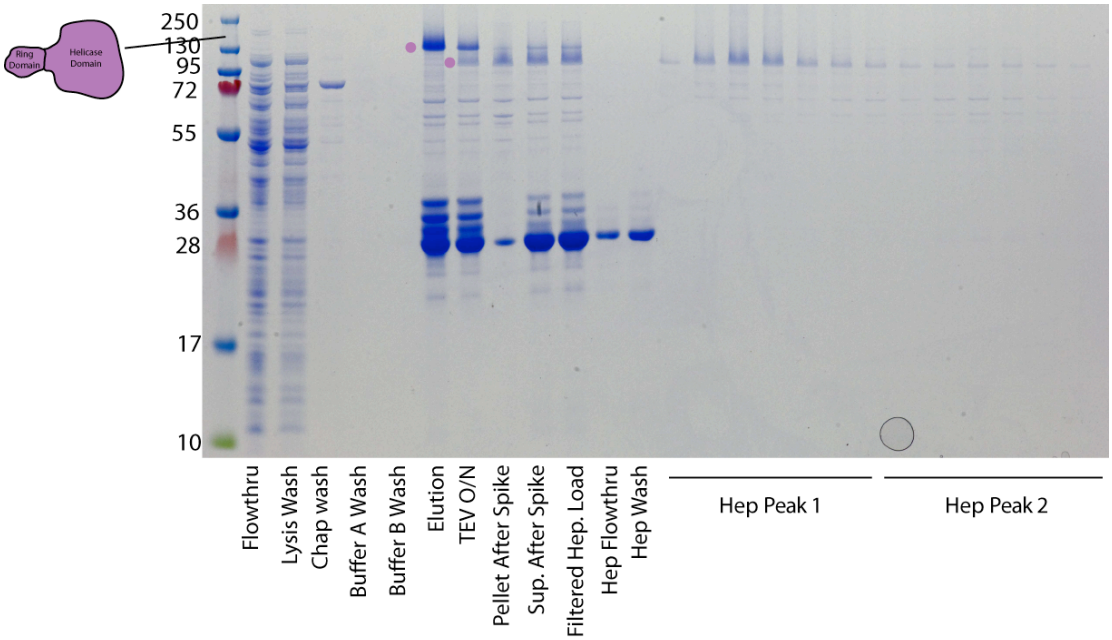

Figure 12: Heparin FPLC trace of cleaved GST-Upf1 (54 – 851). The first peak contains properly folded Upf1, while the second peak contains a Upf1 population that is prone to aggregation upon concentration for size exclusion (see Figure 13).

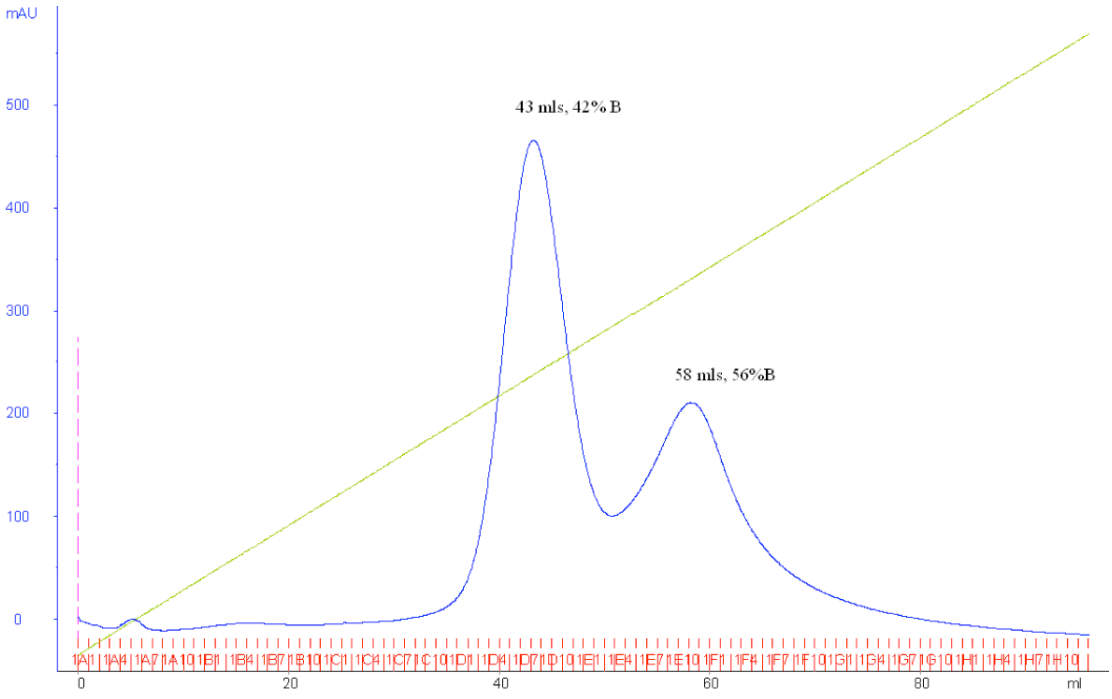

Figure 13: Size exclusion of the two peaks observed during heparin purification of cleaved GST-Upf1 (54 – 851). **(A)** Size exclusion chromatography trace of the first heparin peak. **(B)** Coomassie stained SDS page gel of fractions from (A). **(C)** Size exclusion chromatography trace of the second heparin peak. See Figure 12.

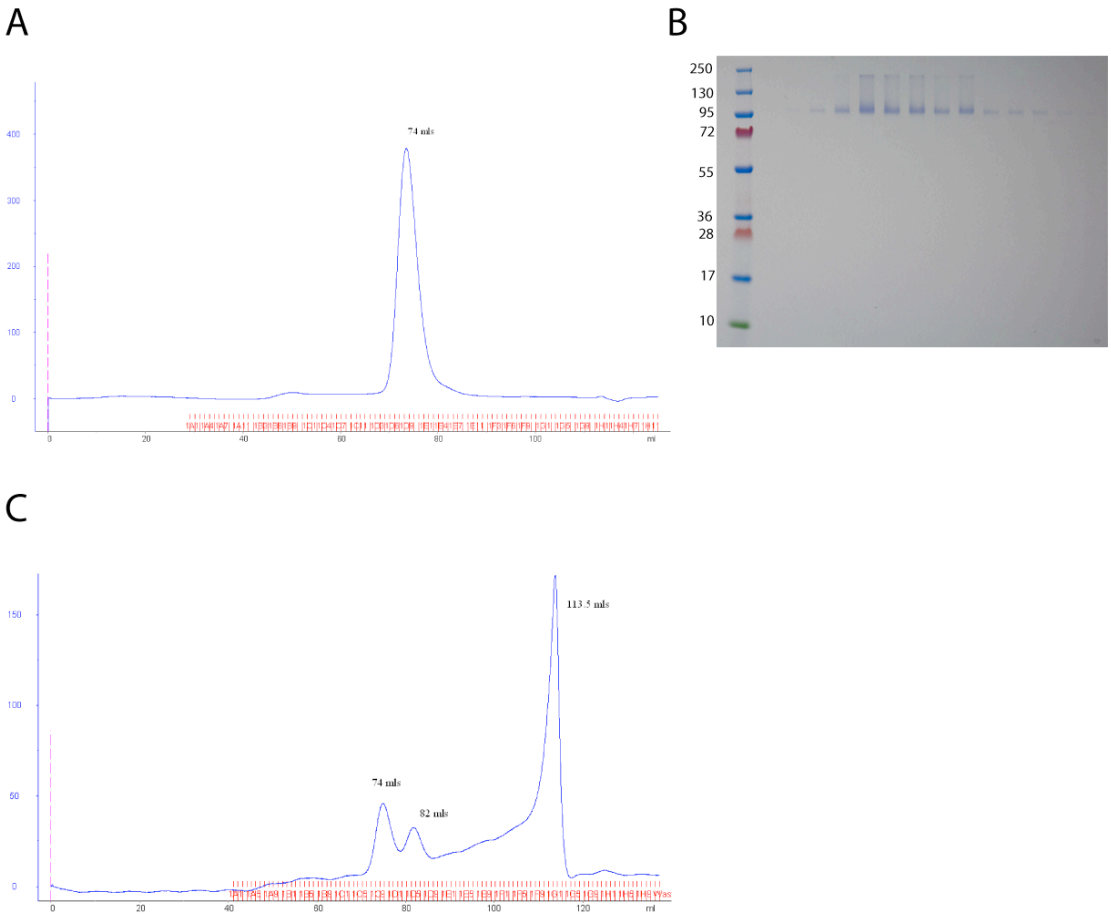

Figure 14: Coomassie stained SDS page gel of the purification and cleavage of the Upf1 helicase domain. Briefly, GST-Upf1 (221-851) was purified by GST-affinity resin, separated from the GST solubility tag by TEV protease, and further purified over a heparin column (see Figure 15, Experimental Procedures).

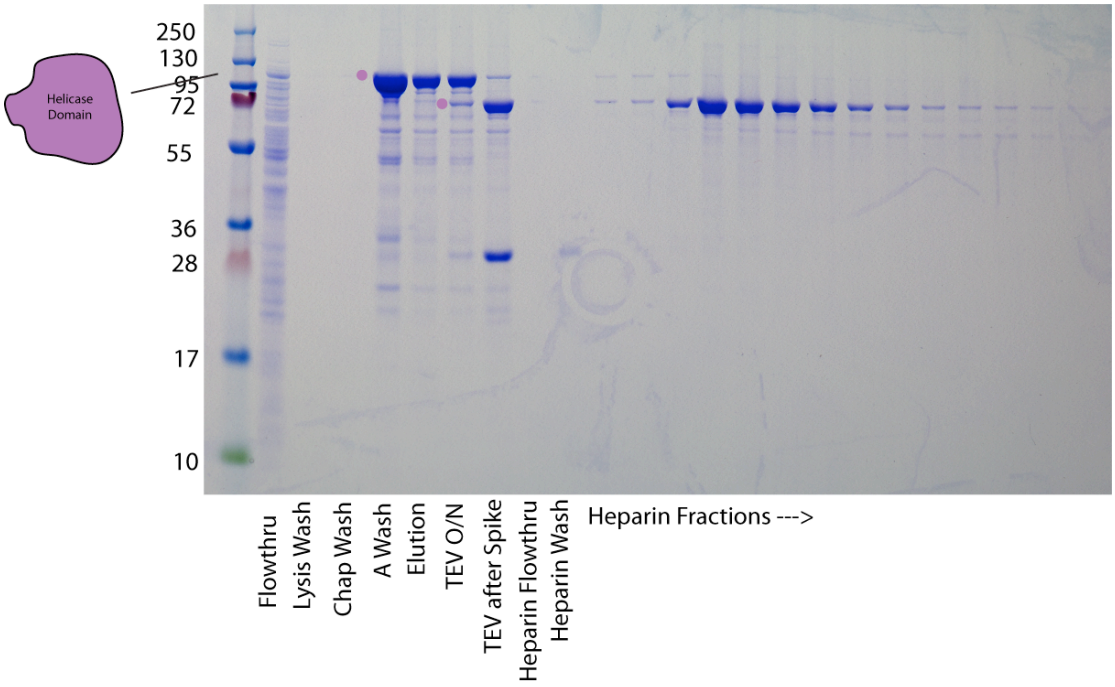

Figure 15: Heparin purification of GST-Upf1 (221- 851) helicase domain (see Figure 14 and Experimental Procedures).

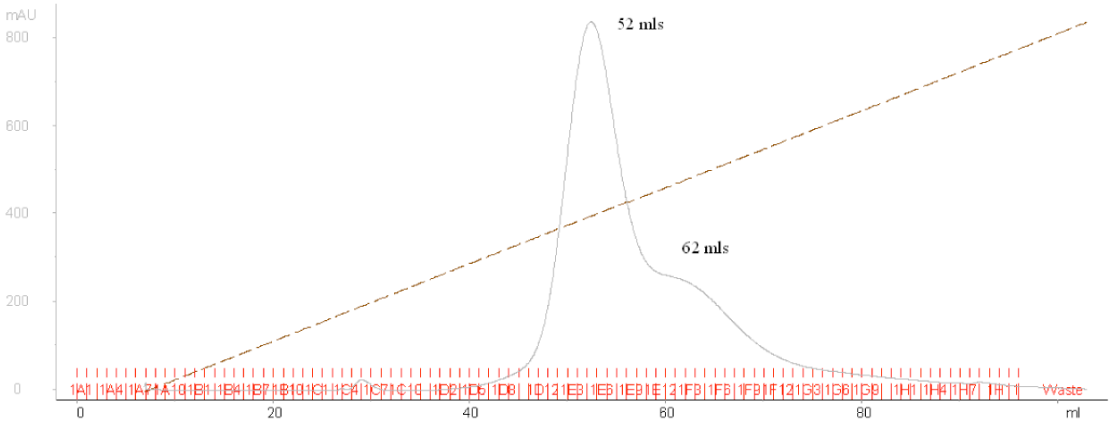

Figure 16: Size exclusion of cleaved GST-Upf1 (221 – 851). **(A)** G200 preparatory size exclusion run of heparin fractions B7-C10 yields a monodispersed peak at 68 mls. **(B)** Coomassie stained SDS page gel of fractions in (A). **(C)** G200 preparatory size exclusion run of heparin fractions C12- E7. See Figures 14, 15 and Experimental Procedures.

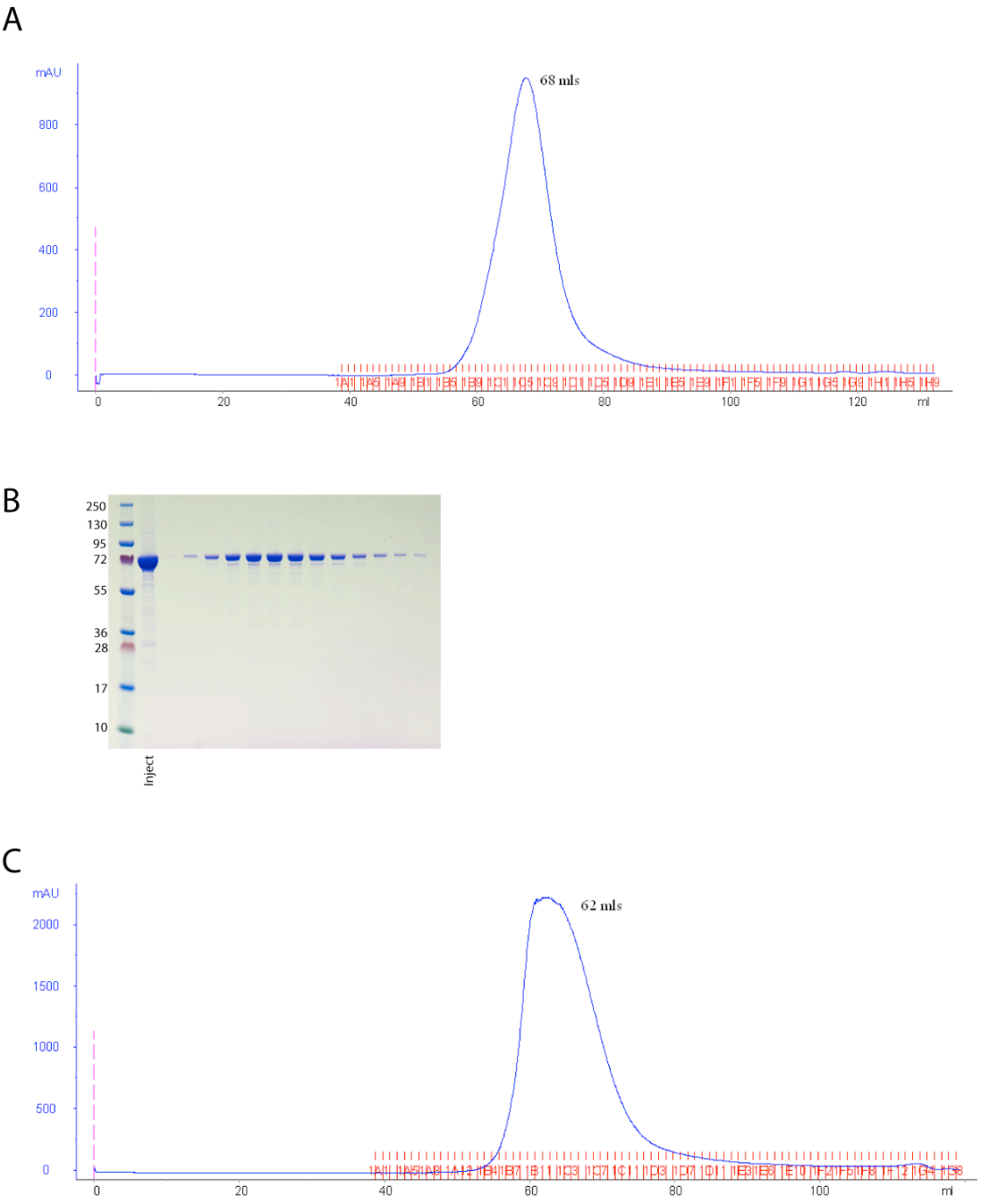

Figure 17: GST pulldown with Upf1 2-domain construct and decapping complex. **(A)** Coomassie stained SDS page gel of 3 uM GST-Upf1 (54-851) with 60 uM Dcp1/2 (1-315). **(B)** Coomassie stained SDS page gel of 60 uM Dcp1/2 (1-315) control. **(C)** Coomassie stained SDS page gel of 3 uM GST-Upf1 (54-851) control.

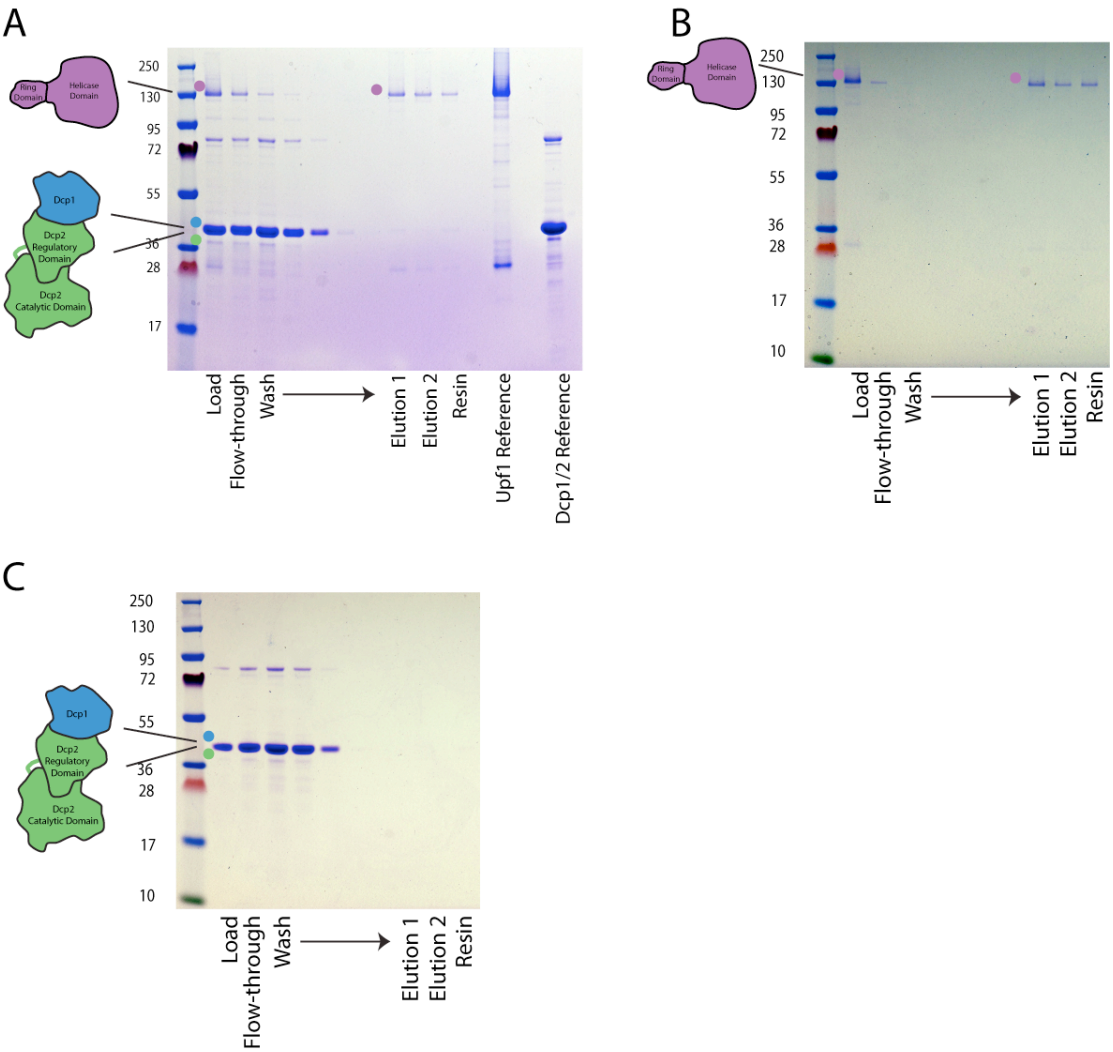

Figure 18: Upf1 decapping complex pulldown in the presence of 2 mM ATP. **(A)** Coomassie stained SDS page gel of 3 uM GST-Upf1 (54-851) and 60 uM Dcp1/2 (1-315) pulldown in the presence of 2mM ATP. **(B)** Coomassie stained SDS page gel of 60 uM Dcp1/2 (1-315) and 2 mM ATP control. **(C)** Coomassie stained SDS page gel of 3 uM GST-Upf1 (54-851) and 2 mM ATP control.

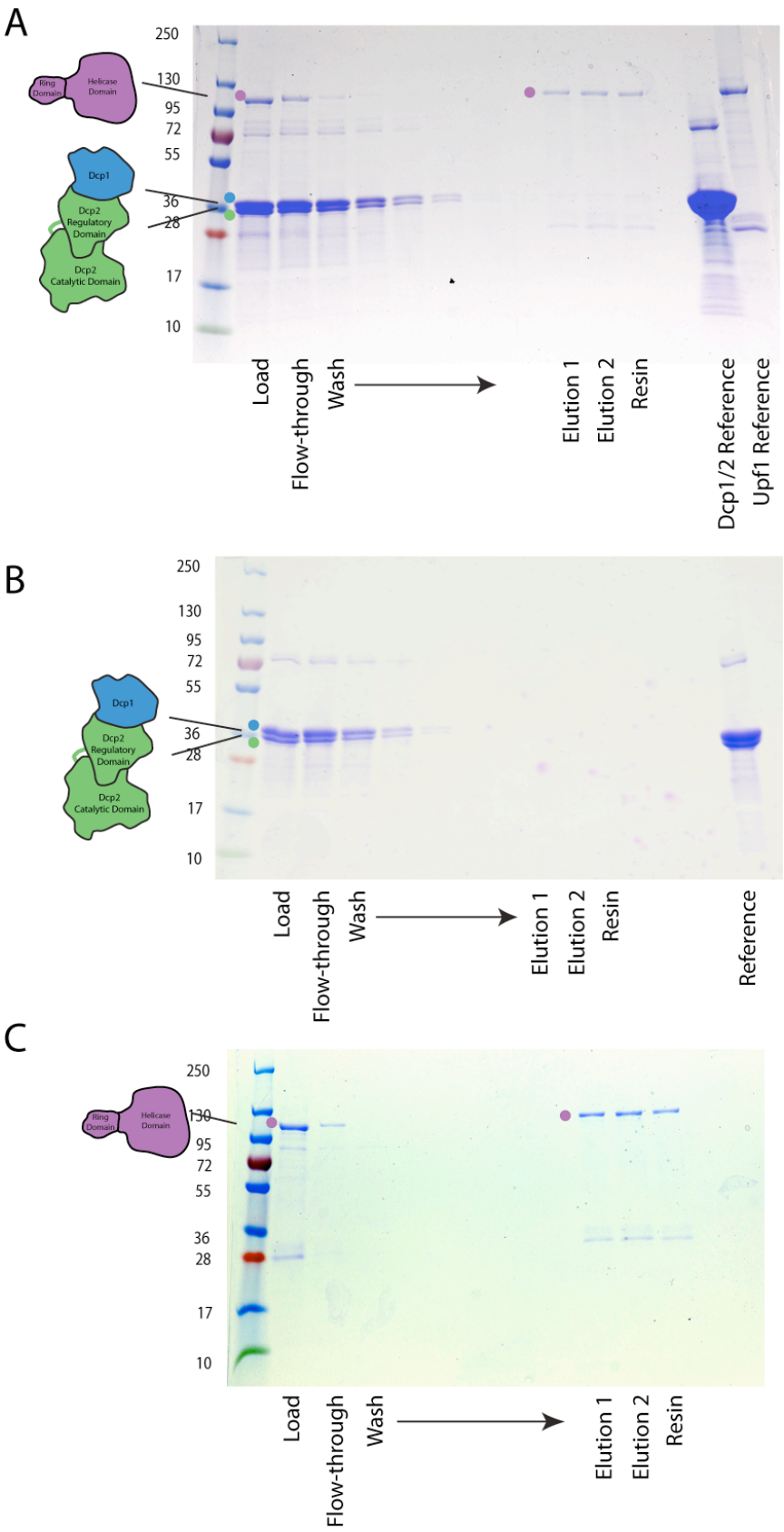
A
250
130
95
72
55
36
28
17
10
Ring Domain
Helicase Domain
Dcp1
Dcp2 Regulatory Domain
Dcp2 Catalytic Domain
Load
Flow-through
Wash
Elution 1
Elution 2
Resin
Dcp1/2 Reference
Upf1 Reference
B
250
130
95
72
55
36
28
17
10
Dcp1
Dcp2 Regulatory Domain
Dcp2 Catalytic Domain
Load
Flow-through
Wash
Elution 1
Elution 2
Resin
Reference
C
250
130
95
72
55
36
28
17
10
Ring Domain
Helicase Domain
Load
Flow-through
Wash
Elution 1
Elution 2
Resin

Figure 19: Upf1 effects on decapping assay. **(A)** Comparison time-courses of percentage m7GDP released in the presence of 50 nM Dcp1/2 (1-315) and either 0 nM Upf1 (54-851) or 0 nM Upf1 (221-851). Lines shown are single exponential fits used to calculate k_{obs}. **(B)** Same as A, but with 500 nM Upf1 (54-851) or 500 nM Upf1 (221-851). **(C)** Same as A, but with 5000 nM Upf1 (54-851) or 5000 nM Upf1 (221-851). **(D)** Fitted rates for experimental data in A-C. **(E)** Fitted endpoints for experimental data in A-C show a reduction in decapping reaction endpoint correlated with Upf1 concentration, regardless of the construct tested.

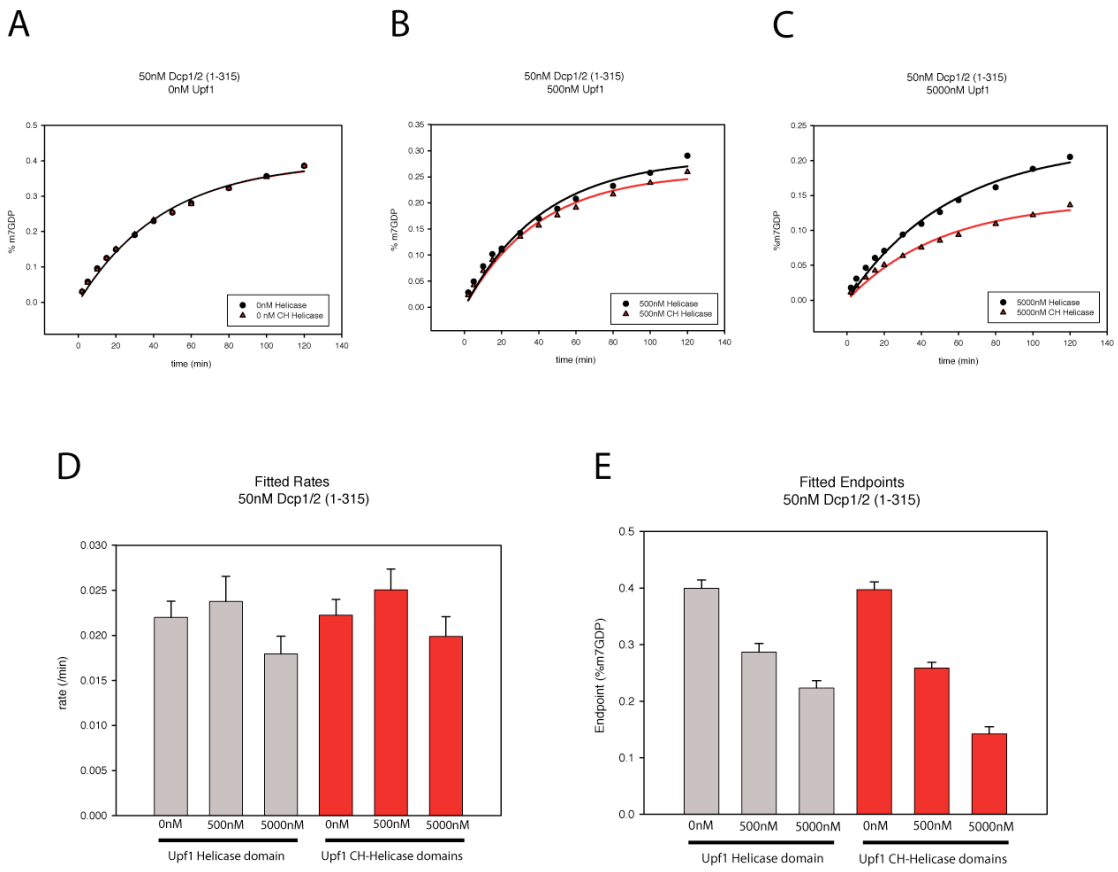

Figure 20: GST and heparin purification of GST-Upf1 (9-851) without cleavage. **(A)** Coomassie stained SDS-page gel of the GST-affinity and heparin purification of GST-Upf1 (9-851). **(B)** Heparin FPLC trace of GST-Upf1 (9-851) after GST affinity purification.

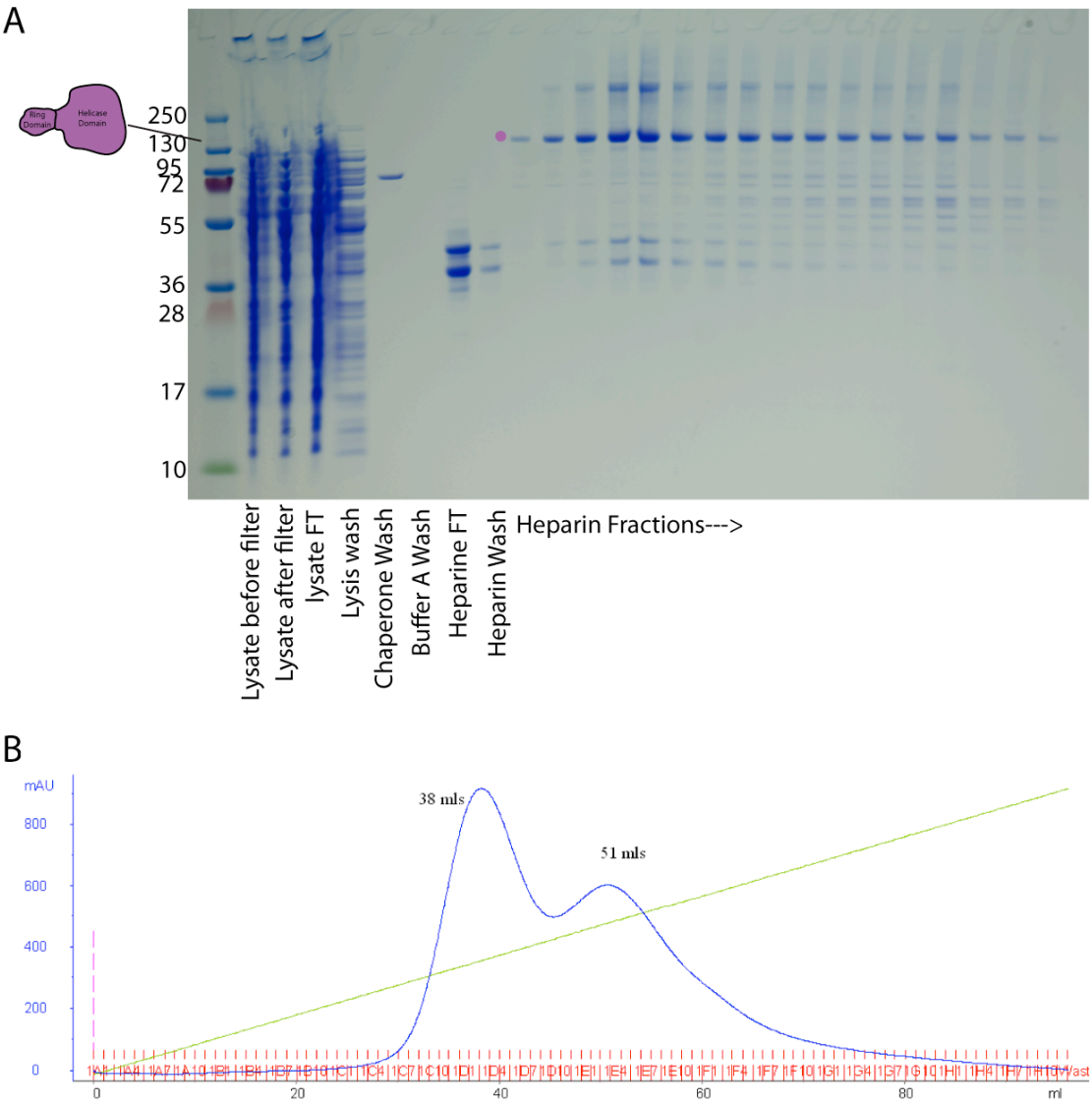

Figure 21: Size exclusion of uncleaved GST-Upf1 (9 – 851). **(A)** G200 preparatory size exclusion run of the first peak from the heparin purification (see Figure 20) yields a monodispersed peak. **(B)** Size exclusion run of the second peak from heparin purification is mainly eluted in the void. **(C)** SDS-page gel of peak fractions in A. **(D)** SDS-page gel of peak fractions in B.

A

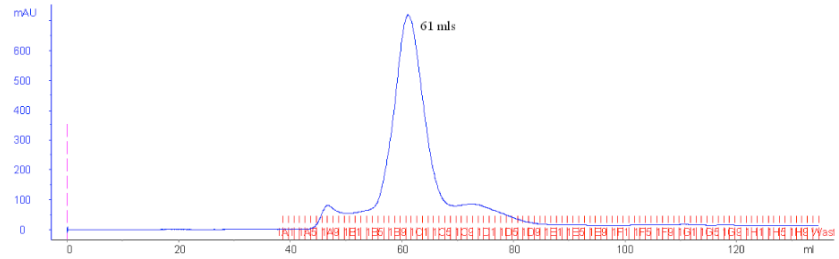

B

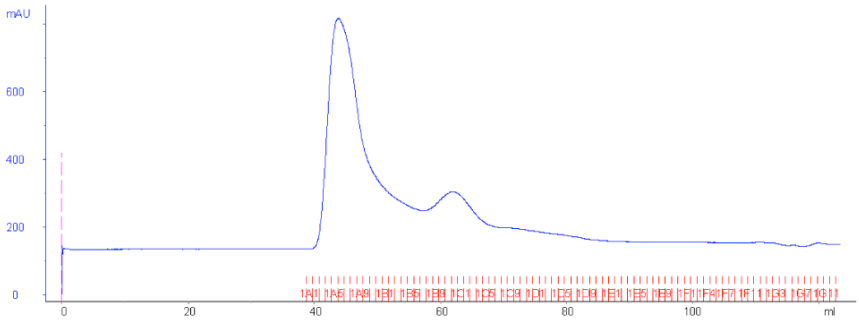

C

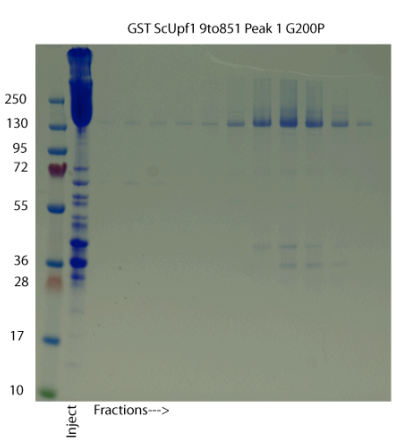

D

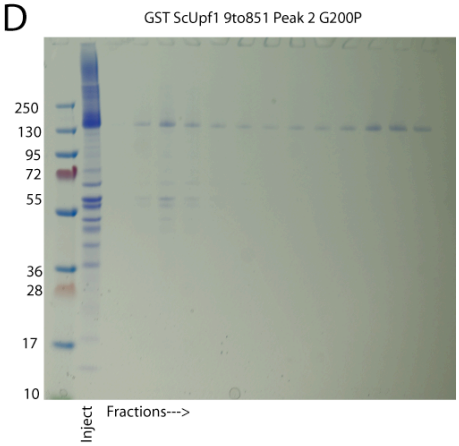

Figure 22: GST pulldown with longer Upf1 2-domain constructs and decapping complex. **(A)** Coomassie stained SDS page gel of 3 uM GST-Upf1 (9-851) and 60 uM Dcp1/2 (1-315) pulldown. **(B)** Coomassie stained SDS page gel of 3 uM GST-Upf1 (54-851) control. **(C)** Coomassie stained SDS page gel of 60 uM Dcp1/2 (1-315) control.

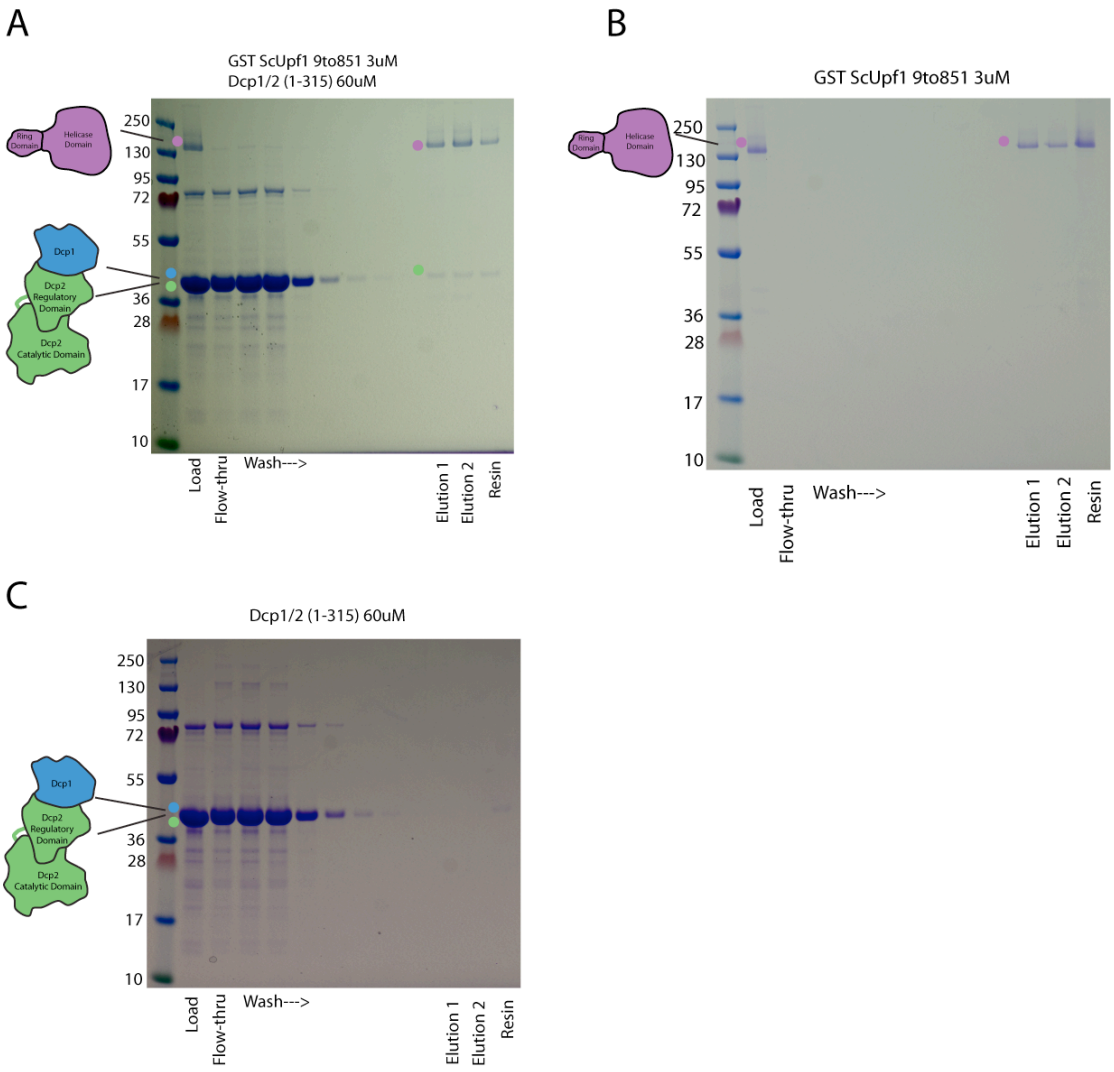

Figure 23: Anti-his western blot of GST-Upf1 pull-downs of Dcp1/2. **(A)** A 30 second exposure of 3 uM GST-Upf1 (9-851) with 60 uM Dcp1/2 (1-315). Dcp2 is eluted with Upf1. **(B)** A 30 second exposure of 3 uM GST-Upf1 (221-851) and 60 uM Dcp1/2 (1-315). Note that GST-Upf1 (221-851) has no His-tag. Dcp2 is observed in the elution, suggesting the pulldown result in (A) is non-specific. **(C)** A 60 second exposure of 60 uM Dcp1/2 (1-315) control.

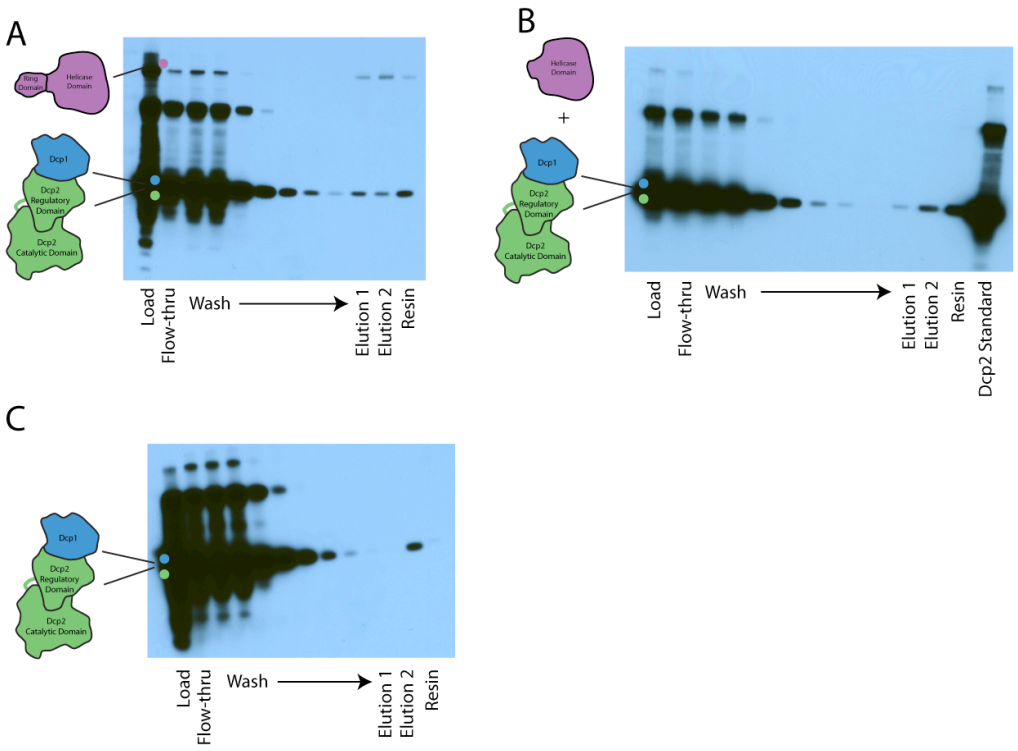

TABLES

Table 1: Solubility of yeast Upf1 ring domain constructs generated. "Pellet" denotes construct was located in the pellet fraction of expressions tests, while constructs at least partially in the supernate are labeled as "soluble". Constructs left blank were not tested for expression.

	Upf1 Boundary	GST	His	TRX
S pombe	31-204	Pellet	Pellet	
	31-212	Pellet		
	31-270	Pellet	Pellet	
	37-204	Pellet	Pellet	Pellet
	37-212	Pellet		
	37-270	Pellet	Pellet	
S cerevisiae	9-219	Soluble		
	9-223	Soluble		
	54-219	Pellet		Pellet
	54-223	Pellet		
	56-219	Pellet	Pellet	Pellet
	56-223	Pellet	Pellet	

Table 2: Co-expression tests of *S. pombe* Upf1 constructs with *S. pombe* Dcp2 constructs. Coexpression tests that resulted in insoluble Upf1 are marked "Pellet", and combinations not tested are left blank. None of the tested combinations yielded soluble Upf1.

Upf1 Boundary	Upf1 Tag	Dcp2 (1-243)	Dcp2 (1-266)
31-204	His	Pellet	
	GST	Pellet	
	TRX	Pellet	Pellet
31-212	His	Pellet	Pellet
	GST	Pellet	Pellet
31-270	His	Pellet	Pellet
37-204	His	Pellet	Pellet
	GST		Pellet
37-212	GST	Pellet	Pellet
	TRX	Pellet	Pellet
37-270	His	Pellet	Pellet
	GST	Pellet	Pellet

EXPERIMENTAL PROCEDURES

Upf1 Cloning: All ring domain sequences of Upf1 (both *S. cerevisiae* and *S. pombe*) were amplified via PCR using cDNA as a template. Constructs were inserted into pETDuet vector backbones using EcoR1 and Xho1, C-terminal to either a 6x-His, GST, or TRX tag. Constructs were then verified by sequencing before use.

Expression Tests: *E. coli* cultures were grown in 50 ml of LB media at 37 ˚C to an OD of 0.6. 1 ml of cell culture was then harvested via centrifugation, and the supernate and pellet fractions saved for SDS-page analysis as the uninduced samples. The remaining culture was split into two cultures. One culture was cooled induced with 0.5 mM IPTG for 3 hours at 37 ˚C, and the second culture was cooled to 15 ˚C for 30 minutes, and then induced with 0.5 mM IPTG for 18 hours for 16 ˚C. After induction, the cells were diluted with LB at the induction temperature to an OD of 0.6 and 1 ml of diluted cell culture was harvested by centrifugation. Pelleted cells were resuspended in 1 ml of lysis buffer, lysed via sonication and centrifuged at 13,000 rpm at 4 ˚C for 15 minutes to separate the supernate and pellet fractions. The pellet was then resuspended in 1 ml of lysis buffer. All samples were then assessed for protein expression by SDS-page analysis.

Protein Purification: Wild-type *S. cerevisiae* Dcp1/2 constructs were expressed and purified as described (Deshmukh et al., 2008) using a

hexahistidine affinity tag and Ni-NTA followed by size exclusion chromatography. Purified decapping complex was concentrated and flash frozen in decapping complex storage buffer (50 mM HEPES, 100 mM NaCl, 20 % glycerol, 5 mM DTT pH 7.5) and stored at -80 ˚C.

The ring domain of *S. cerevisiae* Upf1 was expressed with a GST solubility tag followed by a TEV protease site and the coding region of Upf1 residues 9-223 in *E. coli* Rosetta cells and induced for 18 hours at 16 ˚C. Cells were harvested at 5000g, resuspended in lysis buffer (20 mM HEPES, 300 mM NaCl, 10 mM BME, 0.5 % NP-40), lysed via sonication, clarified at 25,000 for 30 min, and purified by Ni-NTA affinity chromatography. Further purification via size exclusion chromatography was not successful, as the protein precipitated upon concentration prior to injection onto the column.

The longer constructs of Upf1 *(S. cerevisiae* GST- Upf1 54 – 851, 221-851 and 9-851) were expressed in BL21 (DE3) gold pLysS cells. Cultures were grown in 18 liters of Terrific Broth up to an OD of 3.0 at 37 ˚C, cooled for 1 hour at 4 ˚C, and then induced with 0.5 mM IPTG for 18 hours at 4 ˚C. Cells were then harvested at 5000g and resuspended in 1 L of lysis buffer (20 mM Tris pH 7.5, 1 M NaCl, 10% glycerol, 1 mM DTT, 1 mM $MgCl_2$, 1 μM $ZnCl_2$). The resuspended pellet was lysed via micro-fluidizer, and then clarified for 1 hour at 25,000 rpm at 4 ˚C. The resulting supernatant was briefly sonicated for 15 seconds to shear DNA, and then loaded onto 10 ml bed volume of packed glutathione-sepharose resin at a flow rate of 1 ml/min overnight. The resin was then washed with 80 ml of lysis buffer,

followed by 200 ml of Chaperone Wash Buffer (20 mM Tris pH 7.5, 1 M NaCl, 50 mM KCl, 10% glycerol, 10 mM DTT, 2 mM ATP, 10 mM $MgCl_2$, 1 μM $ZnCl_2$), 50 ml of Buffer A (20 mM Tris pH 7.5, 100 mM NaCl, 10% glycerol, 1 mM DTT, 1 mM $MgCl_2$, 1 μM $ZnCl_2$) and finally eluted in 1.1 column volumes of Buffer B (20 mM Tris pH 7.5, 100 mM NaCl, 10% glycerol, 1 mM DTT, 1 mM $MgCl_2$, 1 μM $ZnCl_2$, 20 mM reduced Glutathione). The sample was then diluted to 1.5mg/ml in Buffer A, incubated for 16-18 hours at 4˚C with TEV protease, spiked with 0.5X TEV protease and incubated at room temperature for 3 hours, and then loaded onto a 5 ml HiTrap Heparin HP column (GE Healthsciences). The column was washed with 30 ml of Buffer A1 (20 mM Tris pH 7.5, 100 mM NaCl, 10% glycerol, 1 mM DTT) and a gradient was run from 0-100% Buffer B1 (20 mM Tris pH 7.5, 1 M NaCl, 10% glycerol, 1 mM DTT) over 20 column volumes. Two peaks were observed during the heparin elution both comprised of Upf1. The first peak was collected and further purified via gel filtration chromatography using Buffer A1 and a Superdex 200 column. The second peak did not typically yield a monodispersed peak upon size exclusion chromatography and was discarded. This second heparin fraction typically co-eluted with a protein of approximately 70 kDa, consistent with a chaperone-Upf1 complex. Purified Upf1 after sizing was collected concentrated to 7-8 mg/ml, and flash frozen.

GST Pull-downs: Pull-downs were carried out by gravity flow with 250 ul bed-volume Glutathione Sepharose 4 Fast Flow resin purchased

from Amersham Biosciences. Proteins were mixed and pre-incubated for 30 minutes at 4 ˚C, loaded onto the column, washed with wash buffer (20 mM HEPES pH 7.5, 300 mM NaCl) and eluted with elution buffer (20 mM HEPES pH 7.5, 300 mM NaCl, 50 mM reduced glutathione). Samples were analyzed by SDS page. In some cases, samples were further analyzed by western blot using an anti-his primary antibody at 1:500, and an anti-mouse secondary at 1:5000.

Decapping Assays: Decapping reactions were carried out on ice as previously described (Jones et al., 2008) under single turnover conditions. For assays done with Upf1 constructs, stored protein was thawed on ice, and the decapping complex was allowed to pre-incubate on ice with Upf1 for 1 hour in 1X reaction buffer and at 3X final protein concentration. The decapping reaction was then initiated by adding the protein in a 1:2 ratio to 2X RNA substrate in 1X reaction buffer. Timecourses were then fit to a single exponential equation to calculate the fitted k_{obs} and endpoints.

REFERENCES

Amrani, N., Dong, S., He, F., Ganesan, R., Ghosh, S., Kervestin, S., Li, C., Mangus, D.A., Spatrick, P., and Jacobson, A. (2006). Aberrant termination triggers nonsense-mediated mRNA decay. Biochem Soc Trans *34*, 39-42.

Amrani, N., Ganesan, R., Kervestin, S., Mangus, D.A., Ghosh, S., and Jacobson, A. (2004). A faux 3'-UTR promotes aberrant termination and triggers nonsense-mediated mRNA decay. Nature *432*, 112-118.

Cao, D., and Parker, R. (2003). Computational modeling and experimental analysis of nonsense-mediated decay in yeast. Cell *113*, 533-545.

Chakrabarti, S., Jayachandran, U., Bonneau, F., Fiorini, F., Basquin, C., Domcke, S., Le Hir, H., and Conti, E. (2011). Molecular Mechanisms for the RNA-Dependent ATPase Activity of Upf1 and Its Regulation by Upf2. Molecular Cell *41*, 693-703.

Chamieh, H., Ballut, L., Bonneau, F., and Herve, L.H. (2008). NMD factors UPF2 and UPF3 bridge UPF1 to the exon junction complex and stimulate its RNA helicase activity. Nature Structural & Molecular Biology *15*, 85-93.

Cho, H., Kim, K.M., and Kim, Y.K. (2009). Human Proline-Rich Nuclear Receptor Coregulatory Protein 2 Mediates an Interaction between mRNA Surveillance Machinery and Decapping Complex. Molecular Cell *33*, 75-86.

Clerici, M., Mourao, A., Gutsche, I., Gehring, N.H., Hentze, M.W., Kulozik, A., Kadlec, J., Sattler, M., and Cusack, S. (2009). Unusual bipartite mode of interaction between the nonsense-mediated decay factors, UPF1 and UPF2. Embo Journal *28*, 2293-2306.

Colak, D., Ji, S.J., Porse, B.T., and Jaffrey, S.R. (2013). Regulation of Axon Guidance by Compartmentalized Nonsense-Mediated mRNA Decay. Cell *153*, 1252-1265.

Czaplinski, K., Ruiz-Echevarria, M.J., Paushkin, S.V., Han, X., Weng, Y.M., Perlick, H.A., Dietz, H.C., Ter-Avanesyan, M.D., and Peltz, S.W. (1998). The surveillance complex interacts with the translation release factors to enhance termination and degrade aberrant mRNAs. Genes & Development *12*, 1665-1677.

Czaplinski, K., Weng, Y., Hagan, K.W., and Peltz, S.W. (1995). Purification and Characterization of the Upf1 Protein - a Factor Involved in Translation and Messenger-Rna Degradation. Rna-a Publication of the Rna Society *1*, 610-623.

Deshmukh, M.V., Jones, B.N., Quang-Dang, D.U., Flinders, J., Floor, S.N., Kim, C., Jemielity, J., Kalek, M., Darzynkiewicz, E., and Gross, J.D. (2008). mRNA decapping is promoted by an RNA-binding channel in Dcp2. Mol Cell *29*, 324-336.

Fribourg, S., Gatfield, D., Izaurralde, E., and Conti, E. (2003). A novel mode of RBD-protein recognition in the Y14-Mago complex. Nature Structural Biology *10*, 433-439.

Gatfield, D., Unterholzner, L., Ciccarelli, F.D., Bork, P., and Izaurralde, E. (2003). Nonsense-mediated mRNA decay in Drosophila: at the intersection of the yeast and mammalian pathways. Embo Journal *22*, 3960-3970.

Gehring, N.H., Neu-Yilik, G., Schell, T., Hentze, M.W., and Kulozik, A.E. (2003). Y14 and hUpf3b form an NMD-activating complex. Molecular Cell *11*, 939-949.

Hagan, K.W., Ruizechevarria, M.J., Quan, Y., and Peltz, S.W. (1995). Characterization of Cis-Acting Sequences and Decay Intermediates Involved in Nonsense-Mediated Messenger-Rna Turnover. Molecular and Cellular Biology *15*, 809-823.

Harigaya, Y., Jones, B.N., Muhlrad, D., Gross, J.D., and Parker, R. (2010). Identification and analysis of the interaction between Edc3 and Dcp2 in Saccharomyces cerevisiae. Mol Cell Biol *30*, 1446-1456.

He, F., Brown, A.H., and Jacobson, A. (1997). Upf1p, Nmd2p, and Upf3p are interacting components of the yeast nonsense-mediated mRNA decay pathway. Molecular and Cellular Biology *17*, 1580-1594.

He, F., Peltz, S.W., Donahue, J.L., Rosbash, M., and Jacobson, A. (1993). Stabilization and Ribosome Association of Unspliced Premessenger Rnas in a Yeast Upfl- Mutant. Proceedings of the National Academy of Sciences of the United States of America *90*, 7034-7038.

Ishigaki, Y., Li, X.J., Serin, G., and Maquat, L.E. (2001). Evidence for a pioneer round of mRNA translation: mRNAs subject to nonsense-mediated decay in mammalian cells are bound by CBP80 and CBP20. Cell *106*, 607-617.

Ivanov, P.V., Gehring, N.H., Kunz, J.B., Hentze, M.W., and Kulozik, A.E. (2008). Interactions between UPF1, eRFs, PABP and the exon junction complex suggest an integrated model for mammalian NMD pathways. Embo Journal *27*, 736-747.

Jones, B.N., Quang-Dang, D.U., Oku, Y., and Gross, J.D. (2008). A kinetic assay to monitor RNA decapping under single- turnover conditions. Methods Enzymol *448*, 23-40.

Kadlec, J., Guilligay, D., Ravelli, R.B., and Cusack, S. (2006). Crystal structure of the UPF2-interacting domain of nonsense-mediated mRNA decay factor UPF1. Rna-a Publication of the Rna Society *12*, 1817-1824.

Kashima, I., Yamashita, A., Izumi, N., Kataoka, N., Morishita, R., Hoshino, S., Ohno, M., Dreyfuss, G., and Ohno, S. (2006). Binding of a novel SMG-1-Upf1-eRF1-eRF3 complex (SURF) to the exon junction

complex triggers Upf1 phosphorylation and nonsense-mediated mRNA decay. Genes & Development *20*, 355-367.

Kim, V.N., Kataoka, N., and Dreyfuss, G. (2001). Role of the nonsense-mediated decay factor hUpf3 in the splicing-dependent exon-exon junction complex. Science *293*, 1832-1836.

Kurosaki, T., and Maquat, L.E. (2013). Rules that govern UPF1 binding to mRNA 3 ' UTRs. Proceedings of the National Academy of Sciences of the United States of America *110*, 3357-3362.

Lai, T.F., Cho, H., Liu, Z., Bowler, M.W., Piao, S.F., Parker, R., Kim, Y.K., and Song, H.W. (2012). Structural Basis of the PNRC2-Mediated Link between mRNA Surveillance and Decapping. Structure *20*, 2025-2037.

Lejeune, F., Li, X.J., and Maquat, L.E. (2003). Nonsense-mediated mRNA decay in mammalian cells involves decapping, deadenylating, and exonucleolytic activities. Molecular Cell *12*, 675-687.

Lejeune, F., and Maquat, L.E. (2005). Mechanistic links between nonsense-mediated mRNA decay and pre-mRNA splicing in mammalian cells. Current Opinion in Cell Biology *17*, 309-315.

Longman, D., Plasterk, R.H.A., Johnstone, I.L., and Caceres, J.F. (2007). Mechanistic insights and identification of two novel factors in the C-elegans NMD pathway. Genes & Development *21*, 1075-1085.

Lykke-Andersen, J. (2002). Identification of a human decapping complex associated with hUpf proteins in nonsense-mediated decay. Mol Cell Biol *22*, 8114-8121.

Lykke-Andersen, J., Shu, M.D., and Steitz, J.A. (2001). Communication of the position of exon-exon junctions to the mRNA surveillance machinery by the protein RNPS1. Science *293*, 1836-1839.

Maquat, L.E. (2005). Nonsense-mediated mRNA decay in mammals. Journal of Cell Science *118*, 1773-1776.

Meaux, S., van Hoof, A., and Baker, K.E. (2008). Nonsense-mediated mRNA decay in yeast does not require PAB1 or a Poly(A) tail. Molecular Cell *29*, 134-140.

Mitchell, P., and Tollervey, D. (2003). An NMD pathway in yeast involving accelerated deadenylation and exosome-mediated 3 '-> 5 ' degradation. Molecular Cell *11*, 1405-1413.

Muhlrad, D., and Parker, R. (1994). Premature Translational Termination Triggers Messenger-Rna Decapping. Nature *370*, 578-581.

Muhlrad, D., and Parker, R. (1999). Aberrant mRNAs with extended 3 ' UTRs are substrates for rapid degradation by mRNA surveillance. Rna-a Publication of the Rna Society *5*, 1299-1307.

Rehwinkel, J., Raes, J., and Izaurralde, E. (2006). Nonsense-mediated mRNA decay: target genes and functional diversification of effectors. Trends in Biochemical Sciences *31*, 639-646.

Serin, G., Gersappe, A., Black, J.D., Aronoff, R., and Maquat, L.E. (2001). Identification and characterization of human orthologues to Saccharomyces cerevisiae Upf2 protein and Upf3 protein (Caenorhabditis elegans SMG-4). Molecular and Cellular Biology *21*, 209-223.

Singh, G., Jakob, S., Kleedehn, M.G., and Lykke-Andersen, J. (2007). Communication with the Exon-Junction complex and activation of nonsense-mediated decay by human Upf proteins occur in the cytoplasm. Molecular Cell *27*, 780-792.

Singh, G., Rebbapragada, I., and Lykke-Andersen, J. (2008). A competition between stimulators and antagonists of Upf complex recruitment governs human nonsense-mediated mRNA decay. Plos Biology *6*, 860-871.

Weng, Y.M., Czaplinski, K., and Peltz, S.W. (1996). Genetic and biochemical characterization of mutations in the ATPase and helicase regions of the Upf1 protein. Molecular and Cellular Biology *16*, 5477-5490.

CHAPTER 4

Investigating coactivation of Dcp2 by Xrn1 and the Pat1/Lsm1-7 complex

Robin Aglietti, Ashis Chowdhury, Tharun Sundaresan, John Gross

INTRODUCTION

A nexus of evidence suggests the possibility that an extended ribonucleoprotein (RNP) complex containing known mRNA decay factors Lsm1-7, Pat1, and/or Xrn1 (described below) may function in a concerted manner to directly affect the activity of the decapping enzyme Dcp2. Evidence for these interactions is scattered through various organisms, though conclusive proof of a direct mechanism of decapping activation remains to be found. Interestingly, however, the identification of short linear motifs with elevated conservation in both *S. cerevisiae* and *S. pombe* suggests the possibility that the decapping machinery exists in conserved complexes, even if the details of specific interactions change (Fromm et al., 2012; Gaudon et al., 1999; Neduva and Russell, 2005).

The Lsm (Like Sm) family of proteins is involved in numerous aspects of RNA biology within the cell, and is so named for its shared structural motif with the Sm family of proteins. Sm proteins have two unique motifs linked by a variable region (Hermann et al., 1995) and fold into a characteristic structure that is sufficient for binding RNA (Kambach et al., 1999; Khusial et al., 2005). The Lsm family of proteins typically exists as ring shaped complexes with 6-7 members, and Lsm proteins 1-8 are highly conserved members of the family (Beggs, 2005; Tharun, 2009; Wilusz and Wilusz, 2005). Lsm1-7 form a ringed cytoplasmic complex *in vivo*, with Lsm1 serving as the key factor that differentiates the cytoplasmic mRNA decay-associated

Lsm1-7 complex from the U6 snRNP-associated nuclear complex Lsm2-8 (Achsel et al., 1999; Bouveret et al., 2000; Ingelfinger et al., 2002; Mayes et al., 1999; Tharun, 2009; Tharun et al., 2000).

Pat1 is another mRNA decay factor (Bonnerot et al., 2000; Bouveret et al., 2000; Hatfield et al., 1996; Marnef and Standart, 2010) which was initially discovered in the nucleus as a protein associated with topoisomerase II (Wang et al., 1996). However, there has been much focus on its cytoplasmic role in mRNA decay, as it has been shown to bind the decapping complex Dcp1/Dcp2 (Braun et al., 2010; Nissan et al., 2010; Ozgur et al., 2010; Pilkington and Parker, 2008). In addition, disruption of the Pat1 gene in yeast results in deadenylated, capped RNA, further implicating Pat1 in decapping activity (Bouveret et al., 2000; Hatfield et al., 1996). Furthermore, Pat1 binds to another decapping activator Dhh1, and appears to be related to translational repression (Coller and Parker, 2005).

The Lsm1-7 complex binds to Pat1 *in vivo* to form a complex required for normal mRNA decapping rates in the 5'-3' mRNA decay pathway (Bouveret et al., 2000; Chowdhury and Tharun, 2009; Garneau et al., 2007; Sharif and Conti, 2013; Tharun et al., 2000). This complex preferentially binds to substrate RNA with an oligo(A) tail, and has been shown to protect the 3' end of mRNA *in vivo* (Boeck et al., 1998; Chowdhury et al., 2007; He and Parker, 2001; Tharun et al., 2005). The observation that Pat1 interacts with the decapping complex (Braun et al., 2010; Nissan et al., 2010; Ozgur et al., 2010; Pilkington and Parker, 2008) suggests that Pat1/Lsm1-7 could form a higher-order complex

with Dcp1/Dcp2 to promote the 5'-3' mRNA decay pathway through activation of Dcp2 activity.

Another possibility is that a complex of Dcp1/2 and Pat1/Lsm1-7 requires an additional factor to promote decapping, as suggested by the observation that the ability of the Pat1/Lsm1-7 complex to assemble onto an mRNA is necessary but not sufficient for decapping *in vivo* (Chowdhury and Tharun, 2009). In this case, a likely candidate is Xrn1, the 5'-3' exonuclease responsible for degradation of the RNA body following decapping in the 5'-3' mRNA decay pathway (Stevens and Maupin, 1987), as Xrn1 is reported to bind to the Pat1/Lsm1-7 complex as well as the decapping machinery (Bouveret et al., 2000; Braun et al., 2012; Nissan et al., 2010).

In this chapter, we set out to test these ideas by characterizing any effect of Pat1/Lsm1-7 and/or Xrn1 on Dcp2 activity. Through a collaboration with Dr. Tharun Sundaresan's lab, we obtained Pat1/Lsm1-7 complex purified from *S. cerevisiae*. We were able to demonstrate the RNA binding functionality of this complex, as well as *S. cerevisiae* Xrn1, using a gel shift assay. However, we did not observe any major changes in Dcp2 activity upon addition of either of these reagents in an *in vitro* decapping assay.

RESULTS AND DISCUSSION

Before beginning any biochemical studies, the purity of both the Xrn1 and Pat1/Lsm1-7 used in these studies was confirmed using a

silver-stained SDS-page gel (Figure 1). To assess the functionality of the reagents and ability of the Xrn1 and purified Pat1/Lsm1-7 complex to bind RNA, a gel shift assay was performed with Xrn1, Pat1/Lsm1-7, and Xrn1 + Pat1/Lsm1-7. The proteins were pre-annealed to yeast MFA2 RNA 100 nucleotides long with both a 5' cap and a short oligo-A 3' end (Figure 2) using a previously published annealing protocol (Chowdhury et al., 2007). Xrn1 bound the majority of the RNA as a single species, in contrast to the Pat1/Lsm1-7 complex, which only occupied a fraction of the RNA. Addition of both Xrn1 and Pat1/Lsm1-7 yielded an even slower migrating species, consistent with a large ribonucleoprotein (RNP) complex comprised of RNA, Xrn1, and Pat1/Lsm1-7. It should be noted that these results were not reproducible by another lab member, potentially due to differences in protein preparations.

To assess any effect addition of Xrn1 or Pat1/Lsm1-7 might have on decapping rates, a functional assay to measure *in vitro* decapping rates was used. Because the annealing protocol of binding Xrn1 or Pat1/Lsm1-7 to substrate RNA involves heating and cooling, it was first necessary to determine whether such a temperature cycle would have any effect on secondary structure of the substrate RNA, as such structures could affect the measured decapping rates even in the absence of any potential activators of the decapping complex. To this end, time-courses were taken for both wild-type and K135A variants of the decapping enzyme comparing decapping activity using a mock-annealed RNA (that was subjected to the annealing protocol, see

Experimental Procedures) and unannealed RNA (Figure 3, Table 1). In all cases tested, the annealing protocol had no effect on measured Dcp2 activity.

We next asked whether addition of Xrn1 or Pat1/Lsm1-7 have any effect on decapping rates in our *in vitro* decapping assay. As observed with the annealing controls, there was a slight biphasic quality to even the wild-type Dcp1/Dcp2 activity, most likely due to secondary structure of the RNA (Figure 4A, see Experimental Procedures). Addition of either Xrn1 or Xrn1 + Pat1/Lsm1-7 resulted in a slight decrease in decapping rate and observed endpoint (Figure 4B-D, Table 2) as compared to Dcp1/Dcp2 alone. However, this effect was small and probably a non-specific artifact of RNA-binding proteins, as it was also observed with addition of Upf1 (see Chapter 3).

To rule out a lack of effect due to slow binding kinetics of Xrn1 to the decapping complex, Dcp1/Dcp2 was pre-incubated with Xrn1 and RNA, and then the decapping reaction was initiated by addition of magnesium. Wild-type Dcp1/Dcp2 pre-annealed to RNA in this manner shows an even stronger biphasic behavior (Figure 5) than when the RNA was subjected to a mock-annealing (Figure 5, Table 3). Addition of Xrn1 does not change k_{obs} appreciably, while the endpoint is only slightly decreased (Figure 5, Table 3). This biphasic behavior is possibly due to some population equilibrium between two different states of the enzyme, but further characterization is needed before any definitive statements can be made.

FIGURES

Figure 1: Silver stain of the purified reagents used in gel shift and kinetic assays reported here.

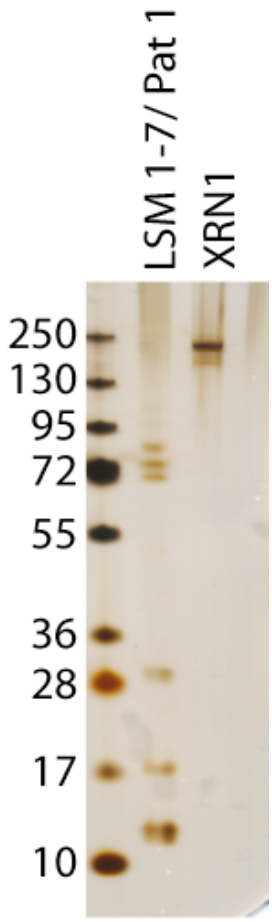

Figure 2: Gel shift binding assay. Xrn1 binds to the RNA completely, while the Pat1/Lsm1-7 complex does not completely shift the RNA alone. However, addition of both Xrn1 and Pat1/Lsm1-7 shows a complete shift of the RNA to a slowly migrating RNP complex. GST-Upf1 (9-851) is shown as a positive RNA-binding control, which probably is partially oligomerized as a large RNP complex (see Chapter 3).

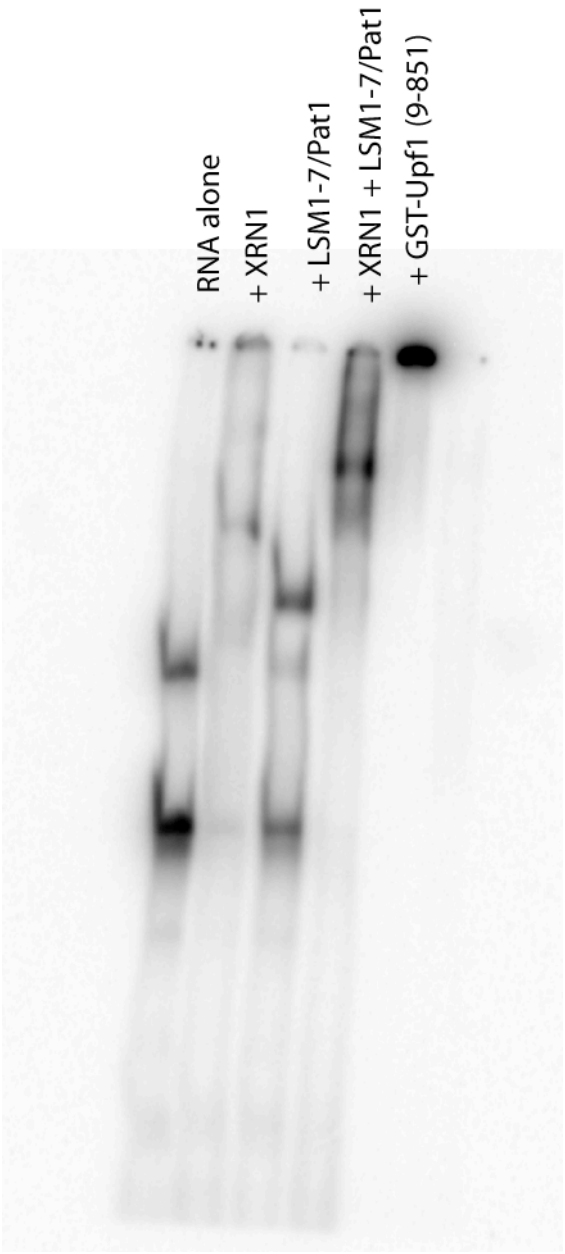

Figure 3: Annealing controls for wild-type and K135A Dcp1/2. **(A)** Time-courses of wild-type Dcp1/Dcp2 (1-245) with and without a mock annealing step for the RNA substrate. Fit lines shown are single exponential fits. **(B)** Time-courses of the Dcp1/Dcp2 K135A mutant with and without a mock annealing step for the substrate RNA. Fit lines shown are single exponential fits.

A

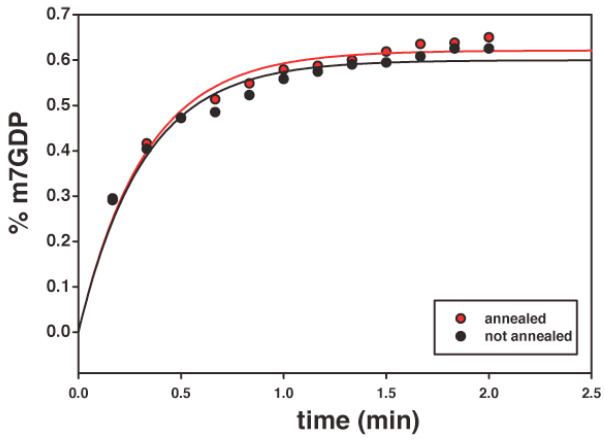

B

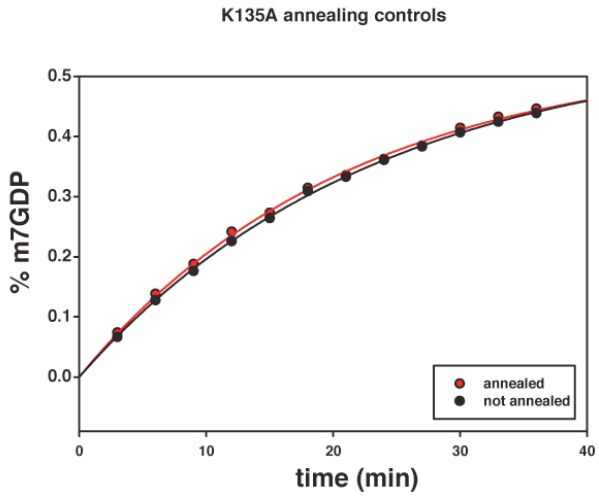

Figure 4: Comparison of decapping activity with Dcp1/2 and Xrn1 and Pat1/Lsm1-7. **(A)** Data plotted is a time course of % m7GDP released by 12.5 uM Dcp1/2. The red line is a single exponential fit used to calculate the endpoint and k_{obs}, and the blue line is a double exponential fit. **(B)** Time-course of m7GDP released by 12.5 uM Dcp1/2 in the presence of 100 nM Xrn1. Colored fit lines shown are the same as (A). **(C)** Time course of m7GDP released by 12.5 uM Dcp1/2 in the presence of 100 nM Xrn1 and 100 nM Pat1/Lsm1-7. Colored fit lines are the same as in (A). **(D)** Overlay comparison of the data points from A-C. Addition of either Xrn1 or Xrn1+ Pat1/Lsm1-7 lowers the observed endpoint of the decapping reaction. See Table 2.

A

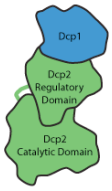
Dcp1
Dcp2
Regulatory
Domain
Dcp2
Catalytic Domain

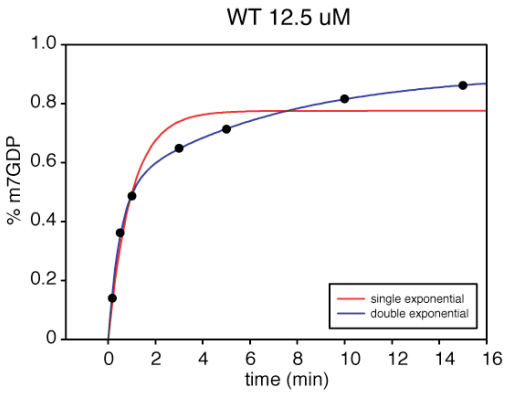
WT 12.5 uM
% m7GDP
time (min)
single exponential
double exponential

B

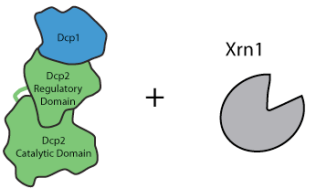
Dcp1
Dcp2
Regulatory
Domain
Dcp2
Catalytic Domain
Xrn1

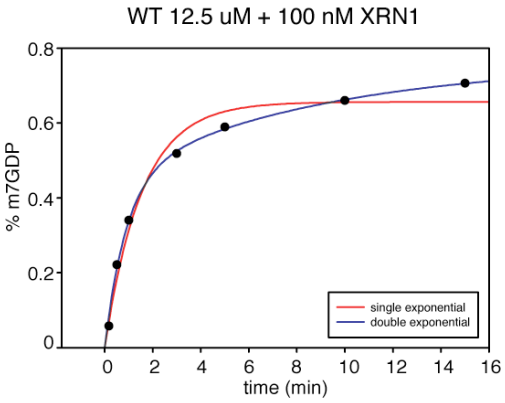
WT 12.5 uM + 100 nM XRN1
% m7GDP
time (min)
single exponential
double exponential

C

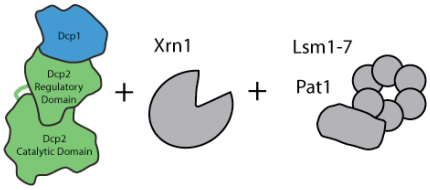
Dcp1
Dcp2
Regulatory
Domain
Dcp2
Catalytic Domain
Xrn1
Lsm1-7
Pat1

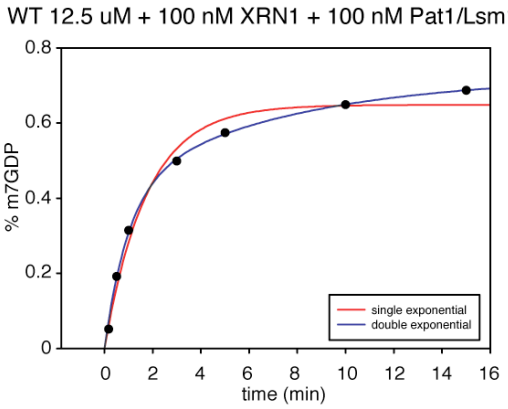
WT 12.5 uM + 100 nM XRN1 + 100 nM Pat1/Lsm1-7
% m7GDP
time (min)
single exponential
double exponential

D

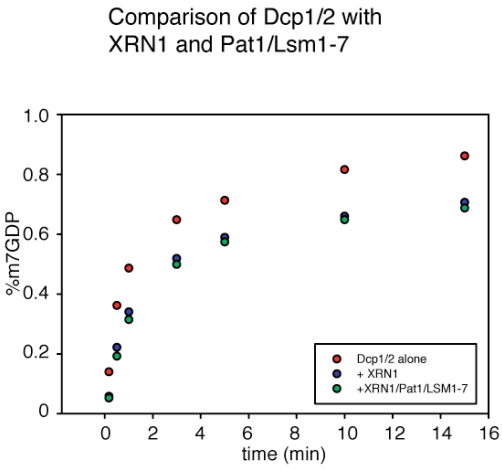
Comparison of Dcp1/2 with
XRN1 and Pat1/Lsm1-7
%m7GDP
time (min)
Dcp1/2 alone
+ XRN1
+XRN1/Pat1/LSM1-7

Figure 5: Comparison of decapping activity with Dcp1/2 and Xrn1 when the decapping reaction is initiated with magnesium. **(A)** Time-course of 12.5 uM wild-type Dcp1/2 (1-245), initiated by addition of magnesium. The blue line is a single exponential fit, and the green line is a double exponential fit. **(B)** Comparison time-courses of wild-type Dcp1/2 with and without Xrn1. Fit lines shown are double exponential fits. See Table 3.

A

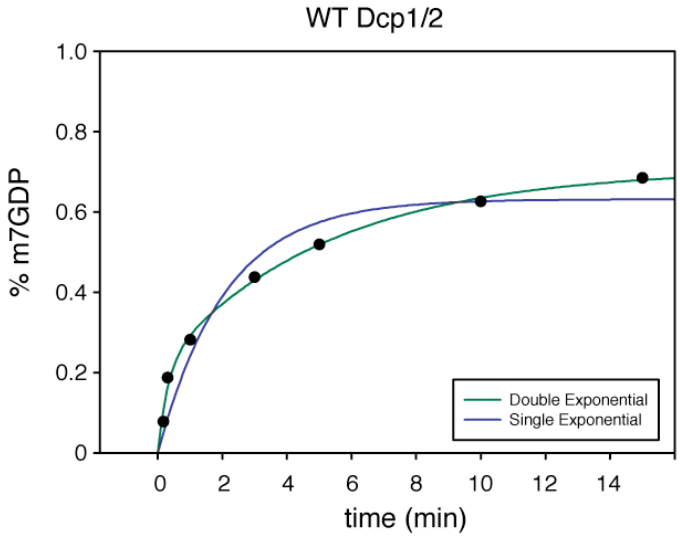

B

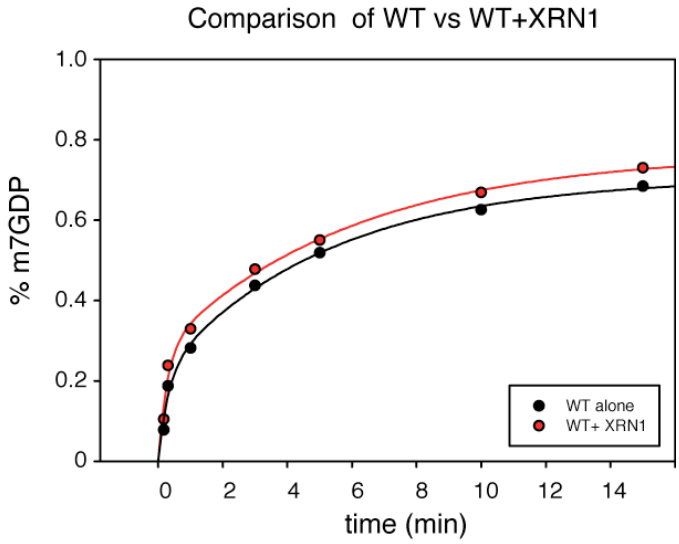

TABLES

Table 1: Annealing controls for wild-type and K135A Dcp1/2. A comparison of the observed k_{obs} on substrate RNA that has or has not been annealed shows the annealing protocol has no effect on decapping rates.

	k_{obs} (min^{-1})	Endpoint
WT annealed	3.08	0.62
WT not annealed	3.15	0.60
K135A annealed	0.05	0.54
K135A not annealed	0.05	0.54

Table 2: Comparison of decapping rates and endpoints for Dcp1/2 in the presence of Xrn1 and Pat1/Lsm1-7.

	Fit	k_{obs} (min^{-1})	Endpoint
Wild-type Dcp1/2	Double A	2.02	0.50
	Double B	0.15	0.40
	Single	1.02	0.78
WT + Xrn1	Double A	1.12	0.45
	Double B	0.11	0.31
	Single	0.65	0.66
WT + Xrn1 +Pat1/Lsm1-7	Double A	1.01	0.42
	Double B	0.14	0.30
	Single	0.57	0.65

Table 3: Comparison of decapping rates and endpoints for Dcp1/2 in the presence of Xrn1 when the decapping reaction is initiated with magnesium.

	Fit	Endpoint	k_{obs} (min^{-1})
Wild-type Dcp1/2	Double A	0.21	3.25
	Double B	0.49	0.19
	Single	0.63	0.48
WT + Xrn1	Double A	0.27	3.63
	Double B	0.49	0.17
	Single	0.65	0.64

EXPERIMENTAL PROCEDURES

Protein Purification: *S. cerevisiae* Dcp1/2 constructs were expressed and purified as described (Deshmukh et al., 2008). Briefly, constructs were purified using a hexahistadine affinity tag and Ni-NTA resin followed by size exclusion chromatography into Dcp2 storage buffer (50 mM HEPES pH 7.5, 100 mM NaCl, 5 % glycerol, 5 mM DTT), flash frozen and stored at -80 ˚C. The *S. cerevisiae* Xrn1 was purchased from New England Biolabs, Inc and stored at -20 ˚C. The Pat1/Lsm1-7 complex used in these studies was supplied by Tharun Sundaresan's lab and purified as described previously (Tharun, 2008).

RNA Transcription and Preparation: Transcription of the MFA 100-A5 RNA was done using T7 polymerase in a 1 ml reaction consisting of 40 mM HEPES KOH pH 8.1, 2 mM spermidine, 0.01 % Triton X-100, 50 mg/ml PEG 8000, 20 mM DTT, 8 mM GTP, 5 mM each UTP, ATP and CTP, 40 mM $MgCl_2$, 2 U/ml thermostable inorganic pyrophosphatase (TIPP), 0.1 mg T7 RNA polymerase and 500 nM template DNA. Reaction was incubated at 37 ˚C for 3 hours and then treated with RNase-free DNase for 30 minutes to remove the template DNA, and then the reaction was quenched by addition of EDTA to a final concentration of 50 mM. The quenched reaction was mixed with 1 ml of formamide, heated to 85 ˚C for 10 min and gel purified using UV shadowing followed by a phenol-chloroform extraction and ethanol precipitation. Purified RNA was diluted to 20 uM and stored at -20 ˚C

for capping reactions. Incorporation of alpha-^{32}P GTP as the 5' cap was carried out as described previously (Jones et al., 2008).

Gel Shift Assay: Proteins for the gel shift assay were pre-annealed to the ^{32}P-capped MFA2 100-A5 RNA in gel shift buffer (10 mM HEPES-KOH pH 7.5, 100 mM KCl, 0.5 mM EDTA, 1 mM DTT, 10 % glycerol, and 50 ug/ml yeast tRNA from Life Technologies) by heating to 30 ˚C for 45 minutes, and then cooling to 4 ˚C for 15 minutes. The non-denaturing acrylaminde gel was run at 4 ˚C in TBE running buffer, dried at 85 ˚C, and visualized using a phosphorus sensor screen. Protein concentrations were as follows: 100 nM Xrn1, 100 nM Pat1/Lsm1-7, 25 uM Upf1.

Decapping Assay: Dcp1/Dcp2 (1-315) was diluted to 1X reaction buffer (50 mM NH_4Cl, 0.01% NP-40, 1 mM DTT, 5 mM $MgCl_2$ and 50 mM Tris-HCl pH 8.0) and 3X final protein concentration, and added to the substrate RNA mixture to initiate the reaction. Substrate RNA was pre-annealed to potential decapping effectors (Xrn1 or Pat1/Lsm1-7) at 2X final protein concentration in 1X reaction buffer by heating to 30 ˚C for 45 minutes, and then allowed to cool to the assay temperature of 4 ˚C for 15 minutes before the reaction was initiated (Chowdhury et al., 2007). Protein concentrations were as follows: 12.5 uM Dcp1/Dcp2, 100 nM Xrn1, 100 nM Pat1/Lsm1-7. Decapping reactions were analyzed as previously described (Jones et al., 2008). In the case of initiation by magnesium, all proteins and RNA were annealed as above

but in 1X reaction buffer without $MgCl_2$, and the reaction was started by addition of 15 mM $MgCl_2$ in 50 mM NH_4Cl, 0.01% NP-40, 1 mM DTT, and 50 mM Tris-HCl pH 8.0, yielding a final magnesium concentration of 5 mM.

REFERENCES

Achsel, T., Brahms, H., Kastner, B., Bachi, A., Wilm, M., and Luhrmann, R. (1999). A doughnut-shaped heteromer of human Sm-like proteins binds to the 3 '-end of U6 snRNA, thereby facilitating U4/U6 duplex formation in vitro. Embo Journal *18*, 5789-5802.

Beggs, J.D. (2005). Lsm proteins and RNA processing. Biochemical Society Transactions *33*, 433-438.

Boeck, R., Lapeyre, B., Brown, C.E., and Sachs, A.B. (1998). Capped mRNA degradation intermediates accumulate in the yeast spb8-2 mutant. Molecular and Cellular Biology *18*, 5062-5072.

Bonnerot, C., Boeck, R., and Lapeyre, B. (2000). The two proteins Pat1p (Mrt1p) and Spb8p interact in vivo, are required for mRNA decay, and are functionally linked to Pab1p. Molecular and Cellular Biology *20*, 5939-5946.

Bouveret, E., Rigaut, G., Shevchenko, A., Wilm, M., and Seraphin, B. (2000). A Sm-like protein complex that participates in mRNA degradation. Embo Journal *19*, 1661-1671.

Braun, J.E., Tritschler, F., Haas, G., Igreja, C., Truffault, V., Weichenrieder, O., and Izaurralde, E. (2010). The C-terminal alpha-alpha superhelix of Pat is required for mRNA decapping in metazoa. Embo Journal *29*, 2368-2380.

Braun, J.E., Truffault, V., Boland, A., Huntzinger, E., Chang, C.T., Haas, G., Weichenrieder, O., Coles, M., and Izaurralde, E. (2012). A direct interaction between DCP1 and XRN1 couples mRNA decapping to 5' exonucleolytic degradation. Nat Struct Mol Biol *19*, 1324-1331.

Chowdhury, A., Mukhopadhyay, J., and Tharun, S. (2007). The decapping activator Lsm1p-7p-Pat1p complex has the intrinsic ability to distinguish between oligoadenylated and polyadenylated RNAs. Rna-a Publication of the Rna Society *13*, 998-1016.

Chowdhury, A., and Tharun, S. (2009). Activation of decapping involves binding of the mRNA and facilitation of the post-binding steps by the Lsm1-7-Pat1 complex. Rna-a Publication of the Rna Society *15*, 1837-1848.

Coller, J., and Parker, R. (2005). General translational repression by activators of mRNA decapping. Cell *122*, 875-886.

Deshmukh, M.V., Jones, B.N., Quang-Dang, D.U., Flinders, J., Floor, S.N., Kim, C., Jemielity, J., Kalek, M., Darzynkiewicz, E., and Gross, J.D. (2008). mRNA decapping is promoted by an RNA-binding channel in Dcp2. Mol Cell *29*, 324-336.

Fromm, S.A., Truffault, V., Kamenz, J., Braun, J.E., Hoffmann, N.A., Izaurralde, E., and Sprangers, R. (2012). The structural basis of Edc3- and Scd6-mediated activation of the Dcp1:Dcp2 mRNA decapping complex. EMBO J *31*, 279-290.

Garneau, N.L., Wilusz, J., and Wilusz, C.J. (2007). The highways and byways of mRNA decay. Nature Reviews Molecular Cell Biology *8*, 113-126.

Gaudon, C., Chambon, P., and Losson, R. (1999). Role of the essential yeast protein PSU1 in transcriptional enhancement by the ligand-dependent activation function AF-2 of nuclear receptors. Embo Journal *18*, 2229-2240.

Hatfield, L., Beelman, C.A., Stevens, A., and Parker, R. (1996). Mutations in trans-acting factors affecting mRNA decapping in Saccharomyces cerevisiae. Molecular and Cellular Biology *16*, 5830-5838.

He, W.H., and Parker, R. (2001). The yeast cytoplasmic LsmI/Pat1p complex protects mRNA 3 ' termini from partial degradation. Genetics *158*, 1445-1455.

Hermann, H., Fabrizio, P., Raker, V.A., Foulaki, K., Hornig, H., Brahms, H., and Luhrmann, R. (1995). Snrnp Sm Proteins Share 2 Evolutionarily Conserved Sequence Motifs Which Are Involved in Sm Protein-Protein Interactions. Embo Journal *14*, 2076-2088.

Ingelfinger, D., Arndt-Jovin, D.J., Luhrmann, R., and Achsel, T. (2002). The human LSm1-7 proteins colocalize with the mRNA-degrading enzymes Dcp1/2 and Xrn1 in distinct cytoplasmic foci. Rna-a Publication of the Rna Society *8*, 1489-1501.

Jones, B.N., Quang-Dang, D.U., Oku, Y., and Gross, J.D. (2008). A kinetic assay to monitor RNA decapping under single- turnover conditions. Methods Enzymol *448*, 23-40.

Kambach, C., Walke, S., Young, R., Avis, J.M., de la Fortelle, E., Raker, V.A., Luhrmann, R., Li, J., and Nagai, K. (1999). Crystal structures of two Sm protein complexes and their implications for the assembly of the spliceosomal snRNPs. Cell *96*, 375-387.

Khusial, P., Plaag, R., and Zieve, G.W. (2005). LSm proteins form heptameric rings that bind to RNA via repeating motifs. Trends in Biochemical Sciences *30*, 522-528.

Marnef, A., and Standart, N. (2010). Pat1 proteins: a life in translation, translation repression and mRNA decay. Biochemical Society Transactions *38*, 1602-1607.

Mayes, A.E., Verdone, L., Legrain, P., and Beggs, J.D. (1999). Characterization of Sm-like proteins in yeast and their association with U6 snRNA. Embo Journal *18*, 4321-4331.

Neduva, V., and Russell, R.B. (2005). Linear motifs: Evolutionary interaction switches. Febs Letters *579*, 3342-3345.

Nissan, T., Rajyaguru, P., She, M.P., Song, H.W., and Parker, R. (2010). Decapping Activators in Saccharomyces cerevisiae Act by Multiple Mechanisms. Molecular Cell *39*, 773-783.

Ozgur, S., Chekulaeva, M., and Stoecklin, G. (2010). Human Pat1b Connects Deadenylation with mRNA Decapping and Controls the Assembly of Processing Bodies. Molecular and Cellular Biology *30*, 4308-4323.

Pilkington, G.R., and Parker, R. (2008). Pat1 contains distinct functional domains that promote P-body assembly and activation of decapping. Molecular and Cellular Biology *28*, 1298-1312.

Sharif, H., and Conti, E. (2013). Architecture of the Lsm1-7-Pat1 complex: a conserved assembly in eukaryotic mRNA turnover. Cell Rep *5*, 283-291.

Stevens, A., and Maupin, M.K. (1987). A 5'----3' exoribonuclease of Saccharomyces cerevisiae: size and novel substrate specificity. Arch Biochem Biophys *252*, 339-347.

Tharun, S. (2008). Purification and Analysis of the Decapping Activator Lsm1p-7p-Pat1p Complex from Yeast. Rna Turnover in Eukaryotes: Nucleases, Pathways and Anaylsis of Mrna Decay *448*, 41-55.

Tharun, S. (2009). Roles of Eukaryotic Lsm Proteins in the Regulation of Mrna Function. International Review of Cell and Molecular Biology, Vol 272 *272*, 149-+.

Tharun, S., He, W.H., Mayes, A.E., Lennertz, P., Beggs, J.D., and Parker, R. (2000). Yeast Sm-like proteins function in mRNA decapping and decay. Nature *404*, 515-518.

Tharun, S., Muhlrad, D., Chowdhury, A., and Parker, R. (2005). Mutations in the Saccharomyces cerevisiae LSM1 gene that affect mRNA decapping and 3 ' end protection. Genetics *170*, 33-46.

Wang, X.Q., Watt, P.M., Louis, E.J., Borts, R.H., and Hickson, I.D. (1996). Pat1: A topoisomerase II-associated protein required for faithful chromosome transmission in Saccharomyces cerevisiae. Nucleic Acids Research *24*, 4791-4797.

Wilusz, C.J., and Wilusz, J. (2005). Eukaryotic Lsm proteins: lessons from bacteria. Nature Structural & Molecular Biology *12*, 1031-1036.

Publishing Agreement:

It is the policy of the University to encourage the distribution of all theses, dissertations, and manuscripts. Copies of all UCSF theses, dissertations, and manuscripts will be routed to the library via the Graduate Division. The library will make all theses, dissertations, and manuscripts accessible to the public and will preserve these to the best of their abilities, in perpetuity.

I hereby grant permission to the Graduate Division of the University of California, San Francisco to release copies of my thesis, dissertation, or manuscript to the Campus Library to provide access and preservation, in whole or in part, in perpetuity.

Author Signature  Date 1.8.14